THE EFFECT OF ENGINEERING PARAMETERS ON THE FRETTING BEHAVIOUR OF MORSE TAPERS UNDER CYCLIC LOAD

Debra L. Young
Department of Mechanical Engineering
McGill University
Montreal, Quebec, Canada

January 1997

A Thesis submitted to the
Faculty of Graduate Studies and Research
in partial fulfillment of the requirements
of the degree of
Master of Engineering (MEng)

THE EFFECT OF ENGINEERING PARAMETERS ON THE FRETTING BEHAVIOUR OF MORSE TAPERS UNDER CYCLIC LOAD

Debra L. Young

In recent years the advantages provided by modular hip implants have been overshadowed by reports suggesting that the junction between modular components is susceptible to fretting wear and fretting corrosion. Although the fracture resistance and locking strength of the junction do not appear to be at risk, the particulate debris generated and released into the joint space may elicit adverse biologic reactions that could eventually compromise fixation of the implant in the bone. It is hypothesized that improving the mechanical linkage between modular hip implant components connected via a Morse taper may mitigate the adverse effects of fretting. Three design parameters, surface finish, taper mismatch, and taper size, were examined in a simplified model of a Morse taper femoral head/neck connection to evaluate their effect on fretting damage at the junction under cyclic load. Microscopic and profilometric methods were used to assess fretting damage on the male tapers qualitatively and quantitatively after 2 or 5 million cycles. Fretting wear was evidenced by damage to the peaks of the machining marks on all taper surfaces. A smooth surface finish of 0.2 μm RMS on the male taper contained less volume of material in the machining marks compared with a rough surface finish of 1.6 μm RMS, and thus had the potential to generate less particulate debris. Taper mismatches of ±8' appeared to have no significant effect on the overall fretting wear compared to a 0 taper mismatch. Large tapers with a two-fold increase in surface area and a four-fold increase in flexural rigidity compared to small tapers significantly reduced fretting wear, presumably because of lower shear forces at the taper interfaces.

L'EFFET DES PARAMETRES DE DESIGN SUR LE FROTTEMENT A L'INTERFACE DES CONES MORSE SOUS CHARGEMENT CYCLIQUE

Debra L. Young

Récemment, les avantages qu'offrent les implants artificiels de la hanche du type modulaire ont été obscurcis par des études montrant que la jonction entre les composantes modulaires est susceptible à la dégradation due au frottement et à la corrosion. Bien que la résistance du joint à la fracture et sa force de jonction ne semblent pas être compromises, les débris produits peuvent causer des réactions biologiques néfastes et ainsi compromettre la stabilité de l'implant dans l'os. Il a été suggeré qu'une amélioration de l'interface méchanique entre les composantes du joint modulaire connectées via un cône du type Morse pourrait réduire les effets néfastes causés par la dégradation. Trois paramètres de design du cône Morse, l'état de surface, l'angle, et la taille, ont été étudiés à l'aide d'un modèle simplifié de la connection tête/cou du joint afin d'évaluer leurs effets sur l'usure lorsque le modèle est soumis à des chargements cycliques. Des analyses microscopiques et profilométriques quantitatives de même que qualitatives ont été utilisées pour évaluer le degré de détérioration/dégradation sur les parties mâles après 2 ou 5 millions de cycles. Sur toutes les surfaces du cône Morse, des dommages ont pu être observés sur les sommets des marques de machinages mettant en évidence la dégradation due au frottement. Les surfaces avec une finition lisse de 0.2 μm RMS sur la partie mâle contenaient au total un volume moindre de matière dans les marques de machinages que les surfaces avec une finition plus corsée de 1.6 μm RMS, et, de ce fait, peuvent probablement produire moins de débris. Les mauvais alignements du cône de l'ordre de ±8° ne semblaient pas avoir d'effets sur l'usure. Les cônes Morse avec deux fois la surface et quatre fois la rigidité flexurale ont démontré moins de dommage d'usure, probablement à cause d'une diminution des forces de cisaillement aux interfaces coniques.

ACKNOWLEDGMENTS

A project of this magnitude obviously cannot be undertaken by one individual alone, and the author is greatly indebted to many for all the help and support received throughout the course of this thesis.

First and foremost, the author wishes to thank Dr. Dennis Bobyn, her thesis advisor, for sharing his wisdom and knowledge, and for his moral support and understanding during a particularly difficult four years. His infectious enthusiasm for research has been an inspiration.

The author wishes to extend her sincere gratitude to all her colleagues, past and present, who she has had the pleasure of working with in the Jo Miller Orthopaedic Research Laboratory; Ariel Dujovne for his help during the initial planning stage of the project, Jan Krygier whose technical knowledge and skills have been invaluable time and again, Frank Chan who has been available unfailingly for discussing ideas and offering sound advise, and Adam Hacking for his diligent assistance when it came to the final crunch. Additionally, the author is extremely grateful for all their moral support and encouragement when it was greatly needed.

The author wishes to express appreciation to the staff at Brimfield Inc., particularly Dan Szall and Glen Ruprecht, for their cooperation in manufacturing and measuring the test specimens. Also, thanks are owing to the staff at the McGill Machine Tool Lab, especially Fernand Picard and Jack Kelley, who were responsible for fabricating the holding devices used for testing. The author would like to acknowledge Jacques Lajoie and Gianni Farrari from the Modern Fabrication Lab at the Ecole Polythechnique for their cooperation and assistance with the profilometry. Gratitude is expressed to Helen Campbell from the Metallurgy Lab at McGill for performing some of the x-ray analysis. Finally, the author wishes to thank Dr. Nigel Shrive and Dan Tilleman from the Civil Engineering Department at the University of Calgary for accommodating her in

their lab, Manfred Herefort and Michael Schoel from the Calgary Foothills Hospital for helping out with the SEM and photomicroscopy, and Rob Scorry from the U of C Engineering Machine Shop for machining specialized stages for the SEM.

Last but not least, the author would like to express a heartfelt thanks to her family and her friends who have provided her with the strength and encouragement to fulfill this goal.

TABLE OF CONTENTS

LIST OF FIGURES

LIST OF TABLES

to Charles, without his support this thesis would not have reached fruition

1 INTRODUCTION

Hip implants are simple mechanical devices used by orthopaedic surgeons to replace the skeletal structure of a hip joint whose function has been compromised by disease or injury. Since the first successful total hip replacement (THR) performed in the late 1950's, hip implants have evolved from simple one-piece or monobodied devices to more complex ones comprised of two or more components. This evolution has resulted, to a great extent, from increased knowledge of the properties of bone and of the biomechanics of the hip joint and the surrounding musculoskeletal system. The following overview of relevant hip joint anatomy and biomechanics is provided for better comprehension of contemporary implant designs and the current issues surrounding them.

1.1 ANATOMY AND BIOMECHANICS OF THE HIP

1.1.1 Anatomy of the Hip Joint and Proximal Femur

The hip joint is the articulation of the proximal femur and the innominate bone (hip bone) (Figure 1.1). Extending from the femoral shaft, at about 125° of inclination and 10° of anteversion, are the neck and head of the femur. Apposition of the latter with the acetabulum (the cup-like recess in the innominate bone) is maintained by a cylindrical encasement of multi-directional fibres and intrinsic ligaments called the articular capsule. The head, neck, and acetabulum are all composed of a very porous trabecular network of bone mass referred to as cancellous or spongy bone, strengthened by a thin, hard shell of compact or cortical bone. Smooth motion of the joint is facilitated by the low frictional properties of hyaline cartilage (coefficient of friction [μ] = 0.002)[1] which partially covers the surfaces of the apposing bone segments. The medullary canal refers to the hollow cavity of the tubular femoral shaft which consists primarily of compact bone.[2,3,4]

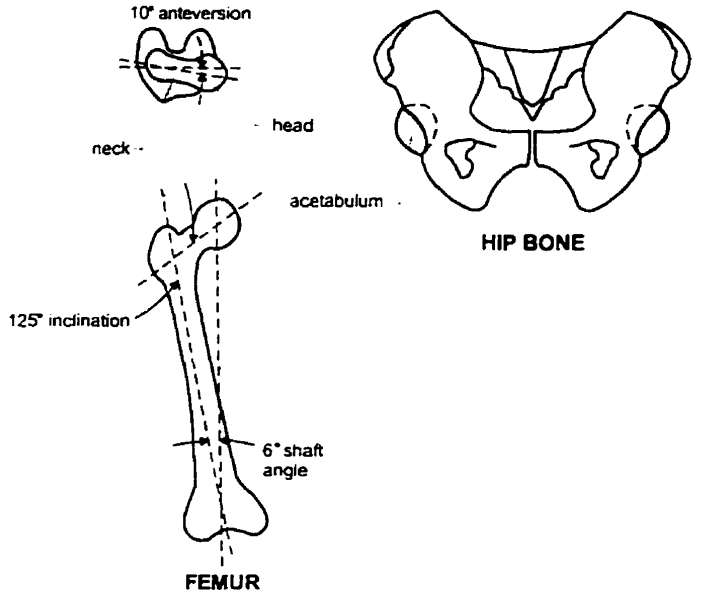

FIGURE 1.1 Schematic of the femur and hip bone. The hip joint is the articulation of the head of the femur and the acetabulum of the hip bone.

Approximately 26 musculotendinous units act at and about the articulation, functioning to passively and actively stabilize the joint and permit wide ranging motion during everyday activities.

1.1.2 Biomechanics of the Hip Joint

The hip is a synovial joint, and thus has two important characteristics: low friction between the articulating components, and high load transfer capabilities.[5] As will be seen in subsequent sections, both of these factors have had considerable impact on the design of THR implants. Since bone is a dynamic material which constantly adapts to functional demands, long term decreases in applied mechanical stresses can result in localized degeneration and resorption of bone mass.[6]

The hip joint is also categorized under the broader classification of spherical, or ball and socket joints because it possesses three degrees of rotational freedom.[5] Activation of various periarticular muscles and ligaments produces a broad range of motion including flexion-extension, abduction-adduction, medial-lateral rotation, as well as circumduction. In the absence of a physical connection between the innominate bone and the femur, joint movement is restricted only by geometric interference between anatomical structures (e.g. flexion is limited by contact of the thigh with the anterior abdominal wall), or by finite tension in the muscles and ligaments.

In view of the motional freedom of the hip joint and the absence of a physical connection between the articulating surfaces, the responsibility of other anatomical or geometric features to provide stability of the joint is of considerable importance, especially with artificial hip replacement implants. These include the shape of the constituent bones, the strong reinforced articular capsule, and the periarticular muscles. In the anatomical position the orientation of the neck results in about a 6° angle between the femoral shaft and the vertical axis; an orientation which maintains the femoral head within the physical confines of the acetabulum for the full normal range of motion. Gross deviations in the angles of inclination (greater than 130°) and anteversion (greater than 15°) of the neck, which are sometimes caused by disease or injury, can significantly decrease the stability of the joint.[2,3] Close apposition of the joint components is further enhanced by the strong multi-directional reinforcing fibres of the articular capsule which resist tensile stresses, and the numerous muscles acting in the region of articulation.

In addition to providing stability the numerous periarticular muscles also contribute significantly to the high loads transferred across the articulation during regular daily activity. Although precise information regarding hip joint reaction forces would be extremely beneficial for optimizing implant designs, as well as

for assessing pathological changes in the hip, a method for accurately quantifying these forces has still not been established despite considerable efforts. Determining hip joint loading conditions involves analysing a statically indeterminate system since muscle forces are immeasurable by direct means, and since there are no constitutive equations defining their behaviour (such as Hooke's law relating stress and strain of engineering materials). This problem has been circumvented in analytical approaches that apply experimentally obtained kinetic and kinematic data to a biomechanical model of the lower limb, by either combining muscles into functional groups (reduction method),[7,8] or by using linear programming techniques to optimize a physiologic or anatomic condition such as maximum joint compression or total muscle force (optimization method)[9,10,11] Discrepant results reported in the literature arise due to variations in methods used for acquiring data, and in how the data are applied to the models, which, themselves, vary between researchers.[9] Differences in assumptions regarding muscle activity, or in constraints used in the optimization analyses also add to variable results. Direct measurements of the joint reaction forces using instrumented implants have been attempted,[12,13] but the applicability of these results is limited because of the anomalous nature of the subjects' joints. Furthermore, it has also been shown that the reaction force is influenced by subject variables such as spinal posture, limb placement, pelvic tilt,[7] and gait.[8,13] At best, the data reported in the literature, which are summarized in Table 1.1, provide a range within which the magnitude of forces transferred across the hip joint can be expected to fall.

Since the human body is a dynamic system that not only changes with time, but which also adapts in response to changes introduced into the system, the challenge of THR surgery is to reconstruct the joint with a mechanical device that in addition to restoring joint function and alleviating pain, also maintains the natural operating conditions existing in the normal joint.

TABLE 1.1 Estimated Reaction Force at the Hip Joint

Investigators	Test Method	Activity	Hip Reaction Force (X BW)
McLeish & Charnley	Modelling and reduction	Single limb stance	1.8 - 2.7
Paul	Modelling and reduction	Level walking - slow	4.9
		- fast	7.6
		Stair climbing	7.2
		Ascending ramp	5.9
Crowninshield *et al.*	Modelling and optimization	Level walking	3.3 - 5.0
Seireg & Arvikar	Modelling and optimization	Level walking - slow	5.4
Davy *et al.*	Telemetric measurement	Single limb stance	2.1
		Level walking	2.6 - 2.8
		Stair climbing	2.6
English & Kilvington	Telemetric measurement	Level walking	2.7

1.2 TOTAL HIP REPLACEMENT (THR)

Total hip replacement (THR), or total hip arthroplasty* (THA) is a common surgical procedure for restoring the function of hip joints afflicted by degenerative disease or injury. As the name implies, it involves replacing the entire joint, including both the femoral head and the acetabulum, with artificial components (Figure 1.2).

1.2.1 Indications for THR

THR is most commonly performed on the relatively aged (60% on persons over 65 years)[14] as the only effective relief of symptoms of advanced osteoarthritis, a degenerative disease which afflicts 75% of the population by the time they reach the age of 75.[15] The disease, which has no known cause

* Arthroplasty is a word with Greek origin meaning formation of an artificial joint.

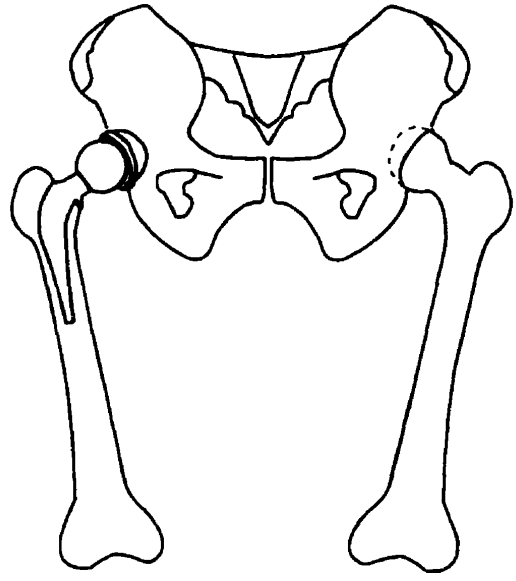

FIGURE 1.2 Schematic of an implanted total hip replacement on the left and a natural hip on the right.

progressively destroys the articular cartilage and, in advanced cases, causes pain and stiffness of the joint coupled with decreased mobility.

In addition to osteoarthritis other indications include fracture and dislocation of the hip, especially congenital dislocation; rheumatoid arthritis which is a chronic systemic inflammation of the joint;[15] aseptic bone necrosis which deteriorates bone in the absence of infection; and revision of previous hip operations.[14]

Today THR boasts very low morbidity and mortality rates, however, during the developmental stages many major obstacles were encountered. A brief look at the evolution of total hip implants shows how these obstacles were overcome largely due to increased knowledge of the dynamics of the human body and of the biomechanics of the hip joint.

1.2.2 Evolution of Total Hip Implants

Although the idea of reconstructing the entire joint was born more than 100 years ago, THR has only been widely accepted and practiced in the last half century.

The first documented THR, in which the articulating surfaces were replaced with an ivory ball and socket secured to the bone with a form of cement, was performed by T. Gluck in Germany in 1890. Subsequent attempts were not recorded until 1938 when an English surgeon by the name of P.W. Wiles implanted the first stainless steel prosthesis which had the form of an acetabular socket screwed to a buttressed plate and a congruent ball which was bolted into the residual femoral neck.[16,17,18] Neither of these procedures appear to have been particularly successful.

During the 1940's hip replacement surgery was dominated by the development of hemiarthroplasty prostheses to replace one or the other articulating surface (Figure 1.3a). In 1951 another attempt at total hip arthroplasty using a device similar to that of Wiles was performed by G.K. McKee but it wasn't until the femoral component was modified to incorporate the articulating head onto an intramedullary stem a couple of years later that encouraging results were obtained (Figure 1.3b). Instead of stainless steel a more durable cobalt-chrome (Co-Cr) alloy was used for the femoral component; a design which provided greater implant stability but which frequently required revision due to eventual implant loosening.[16,17,18]

The most monumental contributions leading to the ultimate success of THR were made by Sir John Charnley, an English surgeon whose initiatives were strongly based on knowledge of hip biomechanics. Between 1956 and 1958 Charnley investigated the lubricity and friction of human joints surmising that implant loosening, which had heretofore hampered the success of hip replacement surgery, was associated with frictional resistance generated by the

artificial components. He attempted to replicate the joint's natural low frictional properties by covering damaged femoral and acetabular articulating surfaces with cups of polytetrafluoroethylene (PTFE), or Teflon. The Teflon femoral cups, however, had a tendency to induce avascular necrosis* of the residual femoral heads, and were later replaced by stainless steel intramedullary head/stems similar to that developed by McKee. Short term results were phenomenal, but within a few years wear of the Teflon acetabular components reached catastrophic proportions (Figure 1.4). Finally, in 1962 Teflon was replaced by high molecular weight polyethylene (HMWPE) which had low frictional properties and, as well, was self-lubricating.[17] A derivative of this plastic (ultra high molecular weight polyethylene (UHMWPE)) is still widely used for the acetabular sockets of contemporary implants.

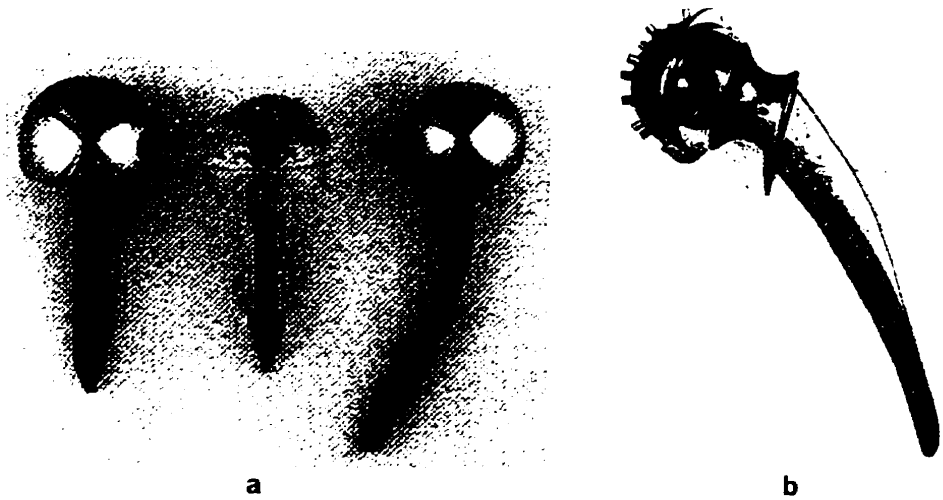

FIGURE 1.3 **a** Intramedullary hemiarthroplasty components to replace the femoral head. **b** McKee-Farrar total hip implant with intramedullary femoral stem. (Reproduced from reference 19)

* Avascular necrosis results in the loss or death of tissue due to inadequate blood flow.

FIGURE 1.4 Catastrophic wear of the Charnley Teflon acetabular cup. (Reproduced from reference17)

Another significant contribution made by Charnley in approximately 1960 was the use of self-curing acrylic cement, or polymethylmethacrylate (PMMA), as a mode of fixation. Other surgeons had previously used this material as an adhesive for tight fitting stemmed femoral components, but results were poor because bone resorption eventually left the implants inadequately supported. Charnley, speculating that this deleterious change was evoked by insufficient load transmission from the implant to surrounding bone, started implanting loose fitting stems into a generous bed of cement which infiltrated the cancellous bone of the medullary canal. This produced a mechanical interlock which dispersed loads over a larger bone area.[17] Again, Charnley's application of the principles of biomechanics vastly improved the results of the surgery.

Although grouting with PMMA became a popular technique for mechanically attaching implants, and is still commonly practiced today, it was eventually discovered that the bone cement had a tendency to craze and microfracture, releasing small fragments into the joint space which wore the bearing surfaces and induced bone resorption leading to eventual loosening of the components.

Concern for these problems likely prompted the development in the late 1960's of alternate modes of fixation without bone cement.

The first comprehensive cementless prosthesis, which was developed by P.A. Ring, had a femoral component that was press-fit into the medullary canal and a cup which was screwed into the acetabulum (Figure 1.5a). In 1969 yet another mode of fixation was introduced by R.G. Tronzo, an American surgeon, who implanted a press-fit system which had a unique surface coating of stainless-steel particles (Figure 1.5b). The purpose of the coating was to allow bone to grow into the interstices between particles establishing biological fixation.[16,17,18] Porous coated implants are currently very popular, but cemented and press-fit implants are also still widely used.

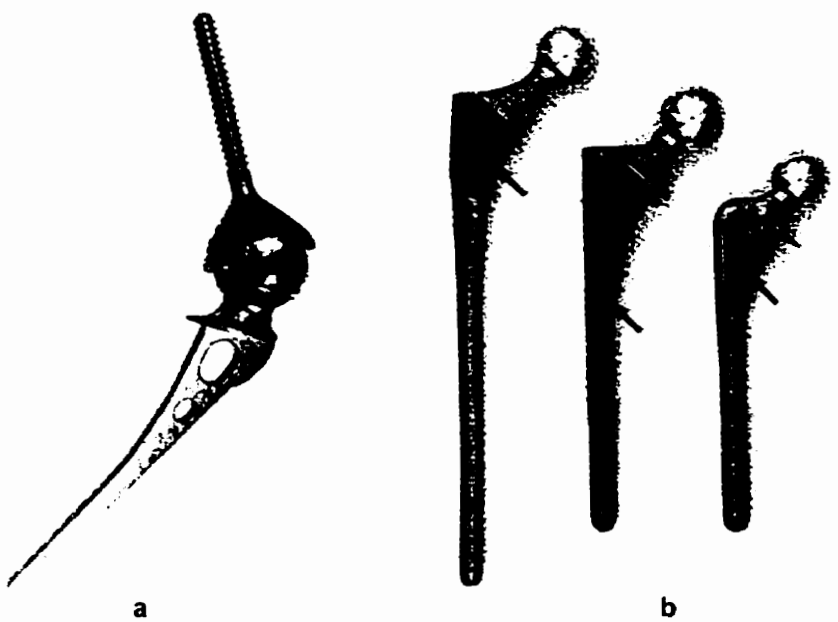

FIGURE 1.5 **a** Ring prosthesis with press fit femoral stem and screwed acetabular cup. **b** Various porous coated femoral stems for biological fixation. Arrows indicate area with porous coating. (Reproduced from reference 19)

Concurrent with the development of alternative modes of implant fixation in the late 1960's was the introduction of multi-component devices with the advent of the trunnion bearing total hip prosthesis (Figure 1.6). This implant, designed to address the issue of extensive wear of bearing surfaces, consisted of a separate head which rotated on an integral trunnion of the femoral stem, and articulated with the acetabular cup. The intention of the two sites of mobility within the joint was to reduce wear of the articulating components by transferring some of the motion of the joint to the secondary junction between the head and trunnion. Furthermore, in the event of wear the design also facilitated replacement of the head while obviating disruption of the well fixed femoral and acetabular components during revision surgery. Additionally, modular heads and stems of various sizes were interchangeable, allowing the surgeon to assemble a prosthesis most suitable for the anatomical situation of different patients.[20,21,22,23]

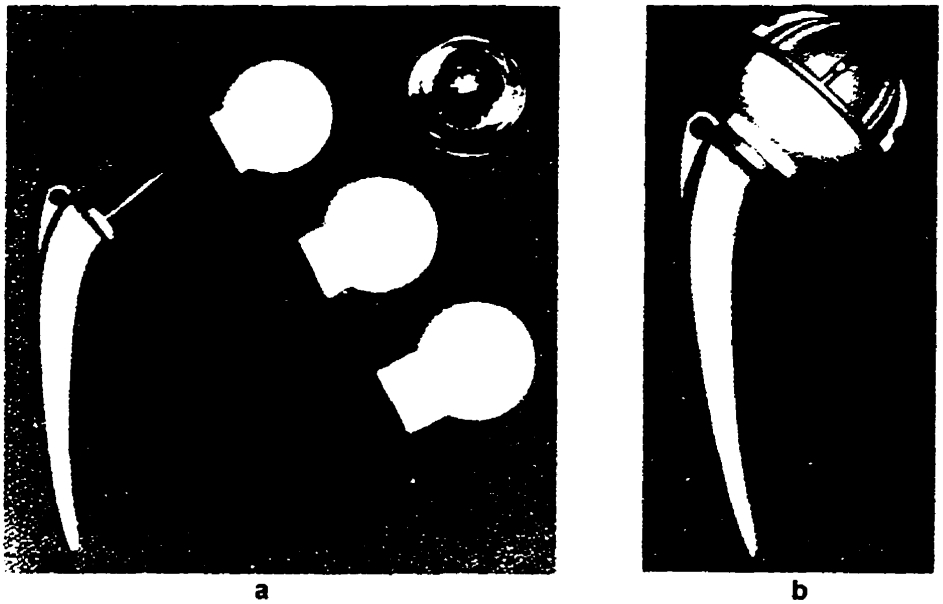

FIGURE 1.6 Trunnion bearing total hip prosthesis. **a** Co-Cr femoral stem and acetabular cup, and three polyester heads with different neck lengths. **b** The assembled prosthesis. (Reproduced from reference 20)

In the early 1970's the concept of modularity was applied to the acetabular component with the invention of a replaceable insert for the acetabular cup.[24]

Today modular implants are a popular commodity in the field of orthopaedics. Many contemporary modular hip implants closely resemble the original trunnion bearing design except the secondary site of mobility between the head and trunnion has been replaced by a self-holding taper junction, a connection mechanism borrowed from the machine tool industry. Self-holding tapers are so called because the small taper angle (between ½ inch and ¾ inch per foot (2.38° and 3.57° per side)) provides sufficient friction between well seated components to hold them in place without additional locking mechanisms.[25] The most common taper used for modular hip implants is the Morse taper which typically has a nominal taper angle of approximately ⅝ inch per foot (2.98° per taper side) (Figure 1.7).

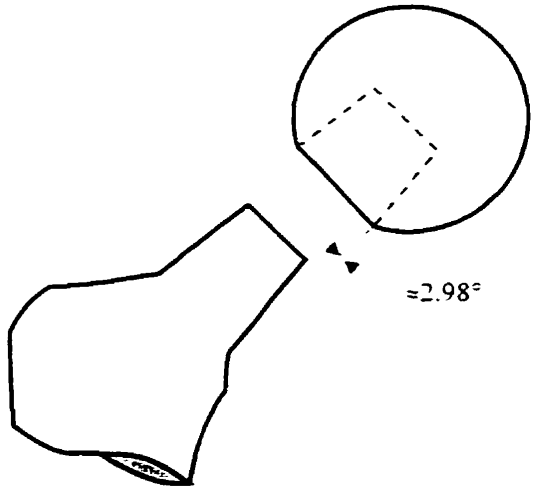

FIGURE 1.7 Schematic of a Morse taper connection.

Due to the advantages afforded by modularity, THR implants are becoming increasingly complex with additional sites of modularity, especially in the proximal region (Figure 1.8). Although the head remains the most common modular component of the femoral stem, others include stem extensions, proximal sleeves, or proximal pads. Various methods are used for connecting additional components such as dovetails, snap fits, screws, and tapers; the Morse taper is the most common since it is used universally at the head/neck junction.

The following literature review elaborates on the advantages and disadvantages of modular femoral implants and summarizes current research in this area.

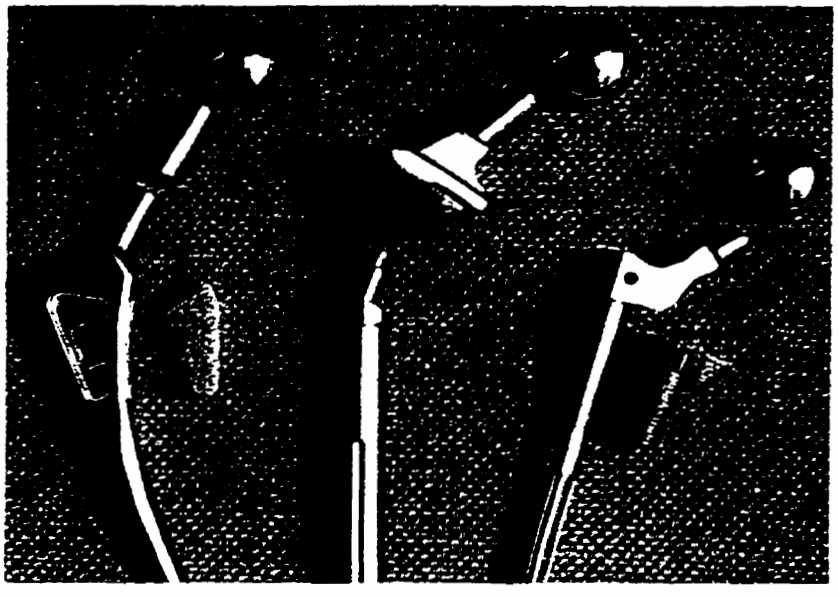

FIGURE 1.8 Contemporary modular femoral stems with multiple sites of modularity.

2 LITERATURE REVIEW

In the past two decades modular hip implants have become increasingly popular because they provide greater design flexibility and surgical latitude, thus improving the effectiveness of THR surgery. Recent reports, however, suggest that the junction of modular components is susceptible to wear and corrosion, generating particulate debris that is released into the joint space. Concern over the potential deleterious effects this may have on implant longevity and over elicited adverse biologic reactions has stimulated debate over whether the known advantages of implant modularity outweigh these potential risks.

2.1 ADVANTAGES OF FEMORAL IMPLANT MODULARITY

Among the numerous advantages afforded by the "building block" system of modular implants is that patient anatomical variability is routinely handled without expensive implant customization. The availability of heads with various neck lengths allows optimal adjustment of the patient's leg length and femur offset yielding higher periarticular muscle and ligament tension that improve biomechanics and joint stability. Furthermore, the advent of additional sites of modularity in recent years (Figure 1.8 in section 1.2.2), particularly in the proximal region, provides optimal fit and fill of the proximal femur which enhances implant stability.

As alluded to in section 1.2.2, in many cases the exchangeability of modular components considerably facilitates revision surgery by eliminating the need to remove well fixed primary components. For example, if loosening of the acetabular component necessitates replacement with a cup having a larger internal diameter, modularity enables the exchange of the femoral head for one of an appropriate size without removing the entire stem.

Finally, component interchangeability yields a greater range of implant sizes with less inventory, which correspondingly reduces inventory costs.[26]

From a mechanical point of view, modularity allows implant designers to select materials possessing optimum mechanical properties for the disparate functional requirements of each component. For instance, a femoral stem made of a titanium alloy (Ti6-Al4-V) is often preferred because it has a relatively low modulus of elasticity, and therefore improves stress transfer to the femur. For best wear performance, a cobalt-chrome alloy (Co-Cr) is preferable because its greater hardness results in less wear of the polyethylene insert of the acetabular cup. Thus, modularity allows the optimum matching of these two material properties.

2.2 COMPLICATIONS RELATED TO FEMORAL IMPLANT MODULARITY

2.2.1 Component Dissociation and Mechanical Failure

One potential complication associated with head/neck modularity is the separation of components. A few cases of head/neck dissociation have been reported,[27,28,29] most of which have resulted from extreme forces required to reduce dislocated hips. It has been suggested that such incidents may be prevented by administering a regional or general anesthetic to adequately relax the muscles and minimize the force required to achieve reduction. In other cases head/neck separation has been the result of sudden impact such as during a fall or a motor vehicle accident.[29]

Reports of component separation have fostered concern over whether intraoperative component assembly achieves sufficient locking; a concern that seems justified considering detachment of the femoral head has occurred during the simple action of rising from a chair.[29] Although the assembly conditions in this particular case were not discussed, it is common practice during surgery to impact the head onto the stem after the latter has been implanted in the femur. Under simulated operative assembly conditions it has been demonstrated that this practice results in significantly lower assembly forces and, consequently,

lower axial forces required to distract the heads, even after being subjected to repetitive compressive loading, than if the implants are assembled externally with specialized instrumentation.[30]

While these findings may emphasize a need to establish an effective assembly protocol to ensure sufficient locking, the low incidence of component dissociation (roughly estimated at less than 0.2% of all THR surgeries performed)[29] does not alone provide sufficient rationale for abandoning the concept of modular implants.

A rarer complication is fracture of the femoral implant neck.[29,31] *In-vitro* fatigue testing of modular head/neck junctions under harsh loading conditions has shown them to be acceptably fatigue resistant.[32] Thus it is believed that the rare reported cases of mechanical failure *in-vivo* are likely symptomatic of the more serious complication of corrosion, probably the most serious concern with regard to femoral stem modularity.

2.2.2 Corrosion at the Component Interface of Modular Femoral Stems

Attention was first drawn to the problem of corrosion of modular hip implants by *in-vivo* findings of accumulated black deposits in the tissue immediately surrounding the head/neck junction.[33,34] Examination of the retrieved implants' taper surfaces revealed ostensible etching of the interdendritic phase of the implant alloy, leading the authors to conclude that crevice corrosion had been facilitated by these metallurgical imperfections. Imperfections such as interdendritic regions of carbides and shrinkage pores, as well as large grains and course dendrites were typical characteristics of the cast Co-Cr alloy that was commonly used at the time for manufacturing implants.

More recently Gilbert et. al.[31] reported on two retrieved modular prostheses with failed femoral necks that had been manufactured from a wrought or forged Co-Cr alloy. The fractures that occurred along grain boundaries just distal to the

head/neck junction were attributed to intergranular corrosion that likely precipitated fatigue failure. In this case metallurgical degradation of the implant alloy, manifested by intergranular porosities, was likely the result of sintering heat treatments that were used to apply porous coatings to cementless femoral stems. As in the studies by Svensson et al.[33] and Mathiesen et al.,[34] the presence of these imperfections was believed to have facilitated the corrosion process.

Inferior metallurgical properties of Co-Cr alloys have been implicated in only a limited number of cases of crevice corrosion reported with modular implants. Special attention to material processing and implant manufacturing techniques can greatly improve material properties, and current surgical grade Co-Cr-Mo alloys possess excellent corrosion resistance.[35] Despite this, however, corrosive attack of modular implants still occurs indicating that factors other than the inherent material properties are responsible.

Galvanic corrosion caused by the coupling of components fabricated from two dissimilar metals was considered by Collier et al.[36] who reported on 139 retrieved modular implants of which 48 consisted of mixed alloy couples; Co-Cr alloy heads on Ti alloy stems. Corrosion was observed on more than half (52%) of the mixed alloy couples, whereas none of the similar alloy couples showed any evidence of attack. Greater material loss and deeper pitting occurred on the more anodic Co-Cr heads than on the Ti necks, suggesting that the attack was chemically, rather than mechanically, induced. The authors therefore concluded that the mode of corrosion was likely galvanic. In contradiction, *in-vitro* electrochemical studies have demonstrated that the Co-Cr alloy/Ti alloy couple is stable owing to the protective oxide layer (passive layer) that forms on both these metals.[37] Collier et al.[36] addressed this point by suggesting that the passive film may have been disrupted during assembly of the modular

components, however, it has also been demonstrated that this interface has a rapid repassivation rate.[38] Although some electrochemical investigations have shown the interface between Co-Cr alloy/Ti alloy components to be slightly susceptible to localized corrosion under static conditions,[39,40] there has been no strong evidence supporting the theory of galvanically accelerated corrosive attack.

Furthermore, the theory of galvanic corrosion has also been refuted by several retrieval studies that reported findings of corrosion on similar, as well as mixed, alloy couplings.[26,41,42,43,44] It is of value to note, however, that corrosion of all Co alloy modular implants is consistently less frequent,[26,43,45] and often less severe[41,44] than that observed with mixed Co-Cr alloy/Ti alloy couplings, suggesting that the presence of Ti may be an enhancing factor in the corrosion process.

Currently the prevailing theory is that crevice corrosion at the interface of modular connections is mechanically induced by fretting* .

2.2.3 Fretting Wear Between Modular Components

It has been hypothesized that constant fretting between modular components causes repetitive disruption of the protective oxide layer on the interface surfaces of the implants creating a propensity for corrosion.[40,42,44,45] A direct link between fretting and corrosion has been established *in-vitro* by Gilbert et al.[40] who reported significant increases in fretting corrosion currents when cyclic mechanical loads were applied to simulated head/neck taper connections. Concomitant changes in pH and chlorine (Cl) concentration within the junction creating an environment conducive to crevice corrosion were also observed.

---

* Fretting is defined as small amplitude (between 125 nm and 100 μm) oscillatory relative motion between two solid surfaces in contact.[50]

In recent years evidence of *in-vivo* fretting causing wear and corrosion at the connection sites of modular hip implants has been mounting.[32,41,43,44,46,47,48,49] Although there have been no reported failures of modular implants as a direct result of fretting wear, and only rare cases linked to corrosion as previously discussed, both processes generate debris which gives rise to other concerns.

In-vitro wear studies have shown that fretting wear of modular components could potentially release hundreds of thousands to millions of micron and sub-micron sized particles into the joint space.[32,45,51] Furthermore, corrosion within the modular junction is believed to account for the solid corrosion products observed in retrieved periprosthetic tissue[33,34,52] that have recently been identified as oxides and chlorides constituted primarily of mixed elements from the implant alloys, and a chromium orthophosphate hydrate-rich product.[52,53] The highly crystalline oxides and chlorides form a friable plate-like layer, up to 20 μm thick, within the taper junction with a propensity to delaminate from the surface. The chromium orthophosphate products have been typically observed loosely adhered to the edge of the taper junction making them more susceptible to release into the joint space.

In addition to accumulating in periprosthetic tissue, the potential for systemic dissemination of metal particulate to remote areas in the body has also been demonstrated. Patients with THR implants have been found to have elevated levels of metal elements consistent with the implant alloys in their serum, urine,[53] spleen, liver, and para-aortic lymph nodes.[54]

2.2.4 Biological Response to Particulate Debris

Several cases have been reported in which loose modular implants have been surrounded with fibrous tissue containing macrophages and giant cells.[33,34] Since the role of macrophages and giant cells is typically associated with defense against foreign substances in the body, such findings have prompted

numerous studies to elucidate the potential role of particulate debris in bone resorption and implant loosening; a prevalent problem of THR.

The propensity of loose implants and implants releasing metallic particulate debris to evoke the formation of a highly cellular periprosthetic membrane similar to that observed in failed human THR has been demonstrated *in-vivo* using a canine model.[55] Analysis of the generated canine tissue revealed elevated levels of biochemical factors known to cause osteolysis or bone resorption. The secretion of similar bone resorbing mediators in response to common implant alloy particulates injected directly into the tissue of rats has also been reported.[56]

In-vitro studies have also demonstrated the capacity of common implant alloy particulate materials and metal corrosion products to activate various human cell types (including macrophages, monocytes, and osteoblasts) to secrete proinflammatory and bone resorbing mediators[57,58,59,60] in a dose and composition dependent manner. This response can be evoked via two mechanisms; either directly in response to challenge by particulate debris, or indirectly through exposure to other media that have been conditioned with metallic particles.[59,60]

Although a definitive link between metallic debris or corrosion products, and bone resorption has yet to be established *in-vivo* in humans, findings of giant cells surrounding metal particles contained in periprosthetic osteolytic lesions provides strong evidence of this causal relationship.

2.2.5 Other Adversities Associated With Particulate Debris

Particulate debris that migrates and becomes entrapped between the articulating components of the implant can act as an abrasive contributing to third body wear of these surfaces. Jasty et al.[61] examined retrieved Co-Cr heads, which have superior wear resistance to other metal materials used for this purpose, and reported frequent occurrences of multi-directional scratches

that morphologically appeared to be caused by extraneous particles. Although fragmented bone cement has previously been implicated as a source of accelerated wear of the articulating components,[62] this study revealed that damage was less extensive and less frequent with cemented implants than with cementless or hybrid (cemented femoral component with cementless acetabular component) implants, establishing the significance of other potential sources of debris such as modular connections. In this study the potential sources of metallic debris common to all the cementless and hybrid implants were identified as modular femoral heads, metal acetabular backings, and porous coatings.

Confirming the ability of extraneous particles to migrate to, and permeate the articulation, Urban et al.[52] reported findings of orthophosphate hydrate-rich corrosion products, various particles of the implant materials, bone cement, and bone fragments embedded in the polyethylene bearing surface of total hip implants.

In addition to compromising the integrity of the implant, excessive wear of the articulating materials adds to the load of particulate debris on periarticular tissue thereby increasing the risk of adverse biological reactions as previously discussed (polyethylene debris induced peri-implant granulomas and bone resorption).

In view of the potential problems associated with wear debris and corrosion products, and the role of fretting in the generation of debris either directly through wear or indirectly through corrosion, modular connections have been subject to numerous investigations attempting to identify design modifications that may minimize or eliminate fretting. The following summary focuses on studies involving the most common modular connection, the Morse taper type head/neck junction.

2.3 EFFECTS OF MODULAR INTERFACE DESIGN MODIFICATIONS ON FRETTING DAMAGE - PREVIOUS *IN-VITRO* INVESTIGATIONS

Barrack and Jani[63] examined fretting behaviour of two distinctly different modular femoral head/stem taper assemblies *in-vitro* under simulated physiologic loading conditions. In addition to a visible difference in taper diameter, the two Co-Cr head/Ti6Al4V stem designs also had statistically significant differences in conicity, surface roughness and taper angle mismatch. The results indicated that the smaller tapers that had greater deviations in conicity, a smoother surface finish, and greater taper mismatches than the larger tapers released significantly higher levels of metal particulate debris, and exhibited visible fretting scars and dark deposits on the medial aspect of the tapers. Larger tapers had minimal fretting scars and no deposits. Although this study did not determine the relative influences of each of the design variables independently, it successfully demonstrated the influence of design modifications on fretting behaviour at the interface of tapered modular components.

Cook et al.[45] investigated the effects of surface finish, neck extensions, and different material couplings on the total generation of particulate debris from fretting wear and corrosion by applying physiologic loading conditions to a model of the head/neck taper junction. The results showed that for both Co-Cr alloy and Ti alloy male tapers those with a rough surface finish (>2.50 μm), or those that had been treated with nitrogen ion implantation generated less debris than those with a smooth surface finish (<0.50 μm) when coupled with Co-Cr alloy heads. The authors also stated that Co-Cr alloy heads with a +10 mm neck extension coupled with either Ti alloy or Co-Cr alloy male tapers produced more debris than regular heads coupled with the same materials. The data tabulated in their paper, however, did not seem to support this conclusion. In the case of Ti alloy male tapers there was a slight increase in debris generation of approximately 5%, however, when heads with the extension were coupled with

Co-Cr male tapers the data actually indicated a decrease in debris generation of almost 22%. Equally confounding was the authors' statement that Co-Cr alloy male tapers, in general, produced a greater number of particles regardless of surface finish, head material, or neck extension length. While this appeared to hold true for all surface finishes investigated, the data seemed to indicate that Co-Cr male tapers coupled with zirconium heads produced approximately 20% less debris than Ti alloy male tapers coupled with the same heads. Furthermore, when neck extensions were applied, Co-Cr alloy male tapers also produced approximately 18% less debris than Ti alloy male tapers.

As an incidental finding Cook et al.[45] also reported that the number of particles produced generally increased with increasing taper mismatch, however, given the randomness of this uncontrolled variable the data presented did not clearly reveal the significance of this effect. For example, for the test group of Co-Cr alloy head/Co-Cr alloy smooth male taper couples the greatest measured mismatch of +0.170° (male taper angle < female taper angle) produced a particle count of 8.4 million compared to 7.97 million produced from the smallest mismatch of -0.001° ; a decrease in particulate debris of only approximately 5%. On the other hand, for the same material coupling with a rough male taper, a slight decrease in mismatch from -0.018° to -0.015° produced a decrease in particle generation of approximately 38% (6.68 million vs 4.12 million). Although the data did suggest that taper mismatch may have some effect, it did not appear to be the predominant factor with regard to debris generation. Further investigation with taper mismatch as a controlled variable is necessary to ascertain its effect on fretting damage.

The effects of neck extensions and material couplings was also studied by Brown et al.[44] by measuring fretting corrosion currents. They reported that when Co-Cr-Mo head/Ti6Al4V alloy stem couples were subjected to cyclic loading

conditions, couples incorporating a 10 mm neck extension produced a significant increase in fretting corrosion currents. These results corroborate the findings by Cook et al. that neck extensions increase the effects of fretting, at least for Co-Cr alloy/Ti alloy head/neck couples, most likely because of increased bending moments and micromotion at the taper interfaces.

In the same study different material combinations were investigated under fretting and static conditions employing two-hole plate/screw methods. The plate/screw material combinations used for fretting corrosion tests were Ti6Al4V/commercially pure titanium (CPTi), Ti6Al4V/wrought Co-Cr alloy (MP35N), MP35N/CPTi, and MP35N/MP35N. The results revealed that the Ti6Al4V/CPTi couple produced significantly higher fretting corrosion currents than any of the other material combinations, all of which produced comparable results. Static corrosion tests on Ti6Al4V/as cast CoCrMo, Ti6Al4V/wrought CoCrMo, and wrought CoCrMo/as-cast CoCrMo plate/screw couples produced no evidence of susceptibility to localized crevice corrosion for any of the material combinations, lending support to the hypothesis that fretting is a necessary antecedent for the initiation of crevice corrosion.

In a separate study Brown et al.[38] investigated the effects of various modifications to the head/neck taper junction including increasing neck extensions (0, +5 mm, +10 mm), decreasing neck surface coverage (25%, 50% reductions), reducing penetration of the neck in the head, and varying taper mismatch (-2', -1', 0, +1', +2'). The effects of these modifications on interface stability, as well as on fretting, under *in-vitro* physiologic loading conditions were monitored. The results indicated that longer neck extensions contributed to a more unstable interface and to higher fretting currents. Reducing cone coverage produced no noticeable effect on interface stability but was found to significantly decrease fretting currents. It was reported that reducing cone penetration

resulted in a very unstable interface and very high spiked fretting currents under physiologic loads. Taper couples with a positive mismatch (base engaged) had greater interface instability, but in general had lower fretting currents than the negative mismatched (tip engaged) taper couples. The authors also reported the effect of taper mismatch on the location of fretting, with base engaged taper couples exhibiting fretting only at the initial contact area, whereas tip engaged couples appeared to fret over the entire potential contact surface. Although the highest fretting currents observed in this study were produced by tip engaged taper couples, the results did not indicate that fretting was necessarily worse with increasing taper mismatch. In fact, higher fretting currents were produced by taper couples with a -1' mismatch than by those with -2' or 0' mismatches, and lower fretting currents were produced by +1' mismatched taper pairs than either +2' or 0' mismatched pairs. In this study all design modifications were tested using 10 mm neck extensions, with the exception of the neck extension study. It has clearly been demonstrated that neck extensions significantly influence interface stability and fretting, and therefore, it cannot be ascertained from these results that the observed effects were strictly due to the modifications being examined.

The studies that have been conducted to date have clearly demonstrated that fretting of modular connections is, in part, a function of design, however, effective isolation of different design parameters to determine their contribution to fretting wear and corrosion has not been accomplished.

2.4 PURPOSE AND SCOPE OF CURRENT STUDY

It is hypothesized that the mechanical linkage of two modular components connected via a Morse taper can be improved, thus reducing the adverse effects of fretting, by modifying the design parameters of the taper.

The purpose of this study was to determine the effects of modifying three design parameters of the Morse taper head/neck connection on fretting wear; namely taper size, taper mismatch, and surface finish. A simplified model of the head/neck taper junction was designed and fabricated for this study so that the parameters under investigation could be strictly controlled. The taper pairs were subjected to simulated physiologic loading conditions, and the damage due to fretting was assessed qualitatively and quantitatively using microscopic and profilometric methods.

3 MATERIALS AND METHODS

3.1 TEST SPECIMEN DESIGN

The test specimens used for this study were custom manufactured so that the parameters to be investigated could be strictly controlled. In order to eliminate the high cost associated with manufacturing entire femoral stems and heads, a simplified model of the head/neck Morse taper junction was designed.

The test specimen male component representing the neck of the femoral stem (Figure 3.1a) consisted of a cylindrical base incorporating a tapered shank at one end (Figure 3.1b). A flat was machined on one side of the base for securing the specimen into the testing apparatus. All male components were fabricated from a surgical grade titanium alloy, Ti-6Al-4V (ASTM 136-84). The tapers were machined to a specified surface finish. The engineering drawing for this component is included in Appendix 2.

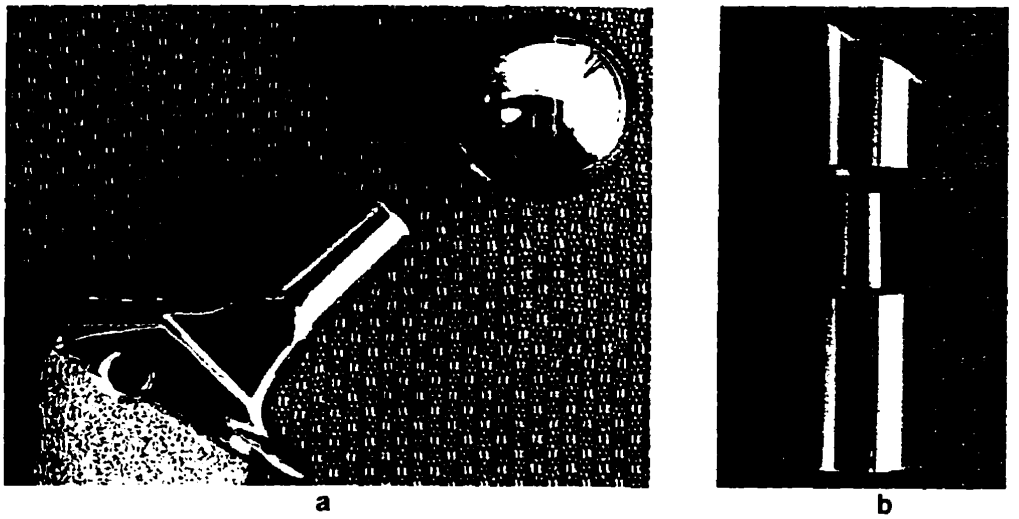

FIGURE 3.1 **a** Modular femoral neck and head with Morse taper connection. **b** Test specimen male and female components.

The test specimen female component was modelled to represent a regular 28 mm implant femoral head (Figure 3.1a) and consisted of a cylindrical bar comprising a tapered socket in one end (Figure 3.1b). A loading surface oriented 30° from the horizontal plane was machined from the top of the component. This angle was consistent with the orientation of resultant forces acting at the hip as measured *in-vivo* by Davy et al.[12] All female components were machined from a surgical grade cobalt-chromium alloy, Co-Cr (ASTM F799-87). Subsequent to machining, the tapers were precision ground to a specified surface finish. The engineering drawing for this component is included in Appendix 2.

A total of thirty test specimens, five for each of six test groups, were produced for this study. The taper specifications for each component, which are listed in Table 3.1, were chosen from the wide range of modular implant designs existing in industry. Table 3.2 summarizes the test groups involved in each part of the study.

The large and small taper sizes (Figure 3.2) investigated had approximate nominal surface areas of 1054 mm^2 (1.6 in^2) and 560 mm^2 (0.9 in^2) , respectively, resulting in an approximately two-fold difference. Furthermore, the diameter of the large tapers compared to the small ones resulted in an approximately four-fold increase in flexural rigidity as calculated at the base of the tapers (Appendix 1). Taper mismatches of +8' and -8' (Figure 3.3) were chosen to represent the two worst case scenarios given a realistic taper included angle specification of 6° ±4'. To accurately achieve these mismatches the actual test specimens were machined with tight angular tolerances of +30" and ±30" for the male and female tapers, respectively. The two surface finishes specified for the male tapers, 0.2 μm and 1.6 μm RMS, roughly represented the upper and lower limits of those

TABLE 3.1 Test Specimen Taper Specifications

	Test Group Designation†	Specimen Control Numbers	Major Diameter mm ±0.03 mm (in.± 0.001 in.)	Height mm ±0.25mm (in.±0.010 in.)	Included Angle	Surface Finish (RMS) µm (µin)
Female	L-8R	1 - 5	16.05 (0.632)	16.61 (0.654)	5°56'±30"	0.20 (8)
	L0R & L0S	6 - 15	16.05 (0.632)	16.61 (0.654)	6°0'±30"	0.20 (8)
	S-8R	16 - 20	11.46 (0.451)	10.87 (0.428)	5°56'±30"	0.20 (8)
	S0R	21 - 25	11.46 (0.451)	10.87 (0.428)	6°0'±30"	0.20 (8)
	S+8R	26 - 30	11.46 (0.451)	10.87 (0.428)	6°4'±30"	0.20 (8)
Male	L-8R	1 - 5	16.59 (0.653)	21.69 (0.854)	6°4'+30"	1.6 (63)
	L0R	6 - 10	16.59 (0.653)	21.69 (0.854)	6°0'+30"	1.6 (63)
	L0S	11 - 15	16.59 (0.653)	21.69 (0.854)	6°0'+30"	0.20 (8)
	S0R	16 - 20	11.99 (0.472)	15.95 (0.628)	6°0'+30"	1.6 (63)
	S-8R	21 - 25	11.99 (0.472)	15.95 (0.628)	6°4'+30"	1.6 (63)
	S+8R	26 - 30	11.99 (0.472)	15.95 (0.628)	5°56'+30"	1.6 (63)

† Identifies condition of three investigated design parameters; taper size, mismatch, and surface finish. L = large, S = small; -8 = -8' mismatch, 0 = 0 mismatch, +8 = +8' mismatch; R = rough, S = smooth.

TABLE 3.2 Test Groups Used to Investigate Each Design Parameter

Taper Size	**Large** L0R†	vs	**Small** S0R
Taper Mismatch	**-8'** L-8R S-8R	vs	**0** L0R S0R
	+8' S+8R	vs	**0** S0R
Surface Finish	**Rough** L0R	vs	**Smooth** L0S

† Identifies condition of three investigated design parameters; taper size, mismatch, and surface finish. L = large, S = small; -8 = -8' mismatch, 0 = 0 mismatch, +8 = +8' mismatch; R = rough, S = smooth.

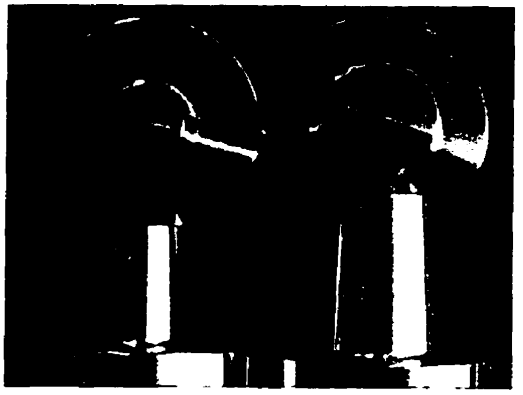

FIGURE 3.2 Male taper test specimen showing small and large taper size.

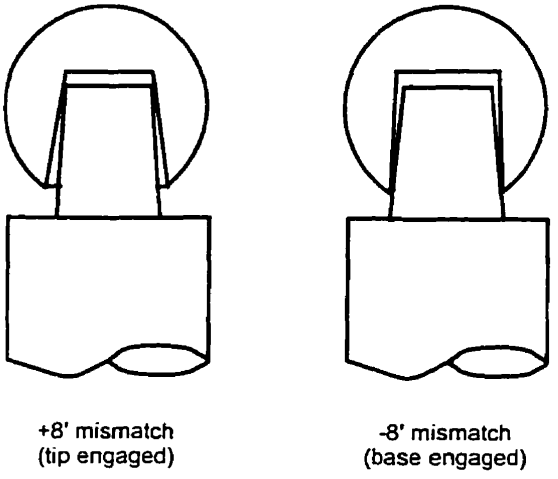

FIGURE 3.3 Schematic of +8' and -8' taper mismatches.

used in industry. The rough surface finish resulted in distinct machining peaks with an average height of approximately 7 μm as shown in the profilometric scan in Figure 3.4. The machining peaks of the smooth surface profiles were obscured by random surface fluctuations presumed to be caused by irregularities

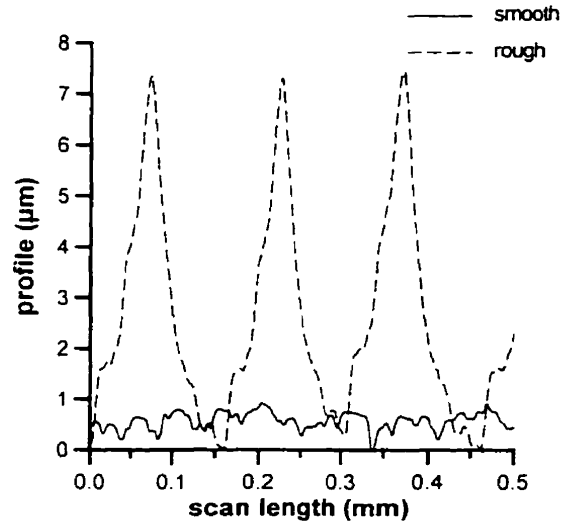

FIGURE 3.4 Graph of rough surface profile vs smooth surface profile.

in the flank of the cutting tool. The maximum deviation between the lowest and highest point on these profiles was approximately 1 µm, seven times less than the average peak height of the rough tapers (Figure 3.4). The female test specimen tapers were ground to a surface finish of 0.2 µm RMS consistent with a typical femoral head taper design.

3.2 TEST SPECIMEN MANUFACTURING AND QUALITY CONTROL

Machining of all test specimens was done by Brimfield Precision Incorporated (Brimfield, MA), a manufacturing company that specializes in medical implants and devices. After fabrication the specimens were subjected to the same standard procedures for quality control, cleaning, and passivation as is required for medical implants.

In addition to the standard quality control inspection, additional measurement of the tapers was performed using a Mitutoyo AE112 coordinate measuring machine (CMM)(MTI Corp., Paramus, NJ). Eight circumferential

measurements were taken at three different vertical positions (drawings included in Appendix 3) using a 3 mm probe on the male tapers and a 2 mm stylus on the female tapers. For each vertical position the software GeoPak 1000 (IBM) incorporated in the CMM processed the eight data points to output the taper deviation from centrality in the x and y directions with respect to the base, taper diameter, and roundness. These data were used to randomly verify that tapers met specifications and to determine if there were any statistically significant differences in roundness between the test groups.

3.3 TESTING HARDWARE

3.3.1 Specimen Holding Fixture

A specialized fixture for holding the test specimens during the cyclic testing was designed to meet the following criteria:

- The fixture had to be mountable on the two servo-hydraulic testing apparatuses available; an Instron (Model 1310, Instron Corp., Canton, MA) and a Shore Western (Shore Western Mfg., Inc., Monrovia, CA).
- Test specimens had to be rigidly secured at an angle of 30° from the vertical while subjected to high cyclic loads.
- Positioning of the test specimens in the fixture had to be adjustable to allow for alignment with the load applicator.
- The fixture had to support a fluid chamber that was to surround the taper junction during testing.

The first generation holding fixture is shown in Figure 3.5a (engineering drawings are provided in Appendix 4). This fixture consisted of a right angle triangular frame and a specimen holding plate, both made of cold rolled steel.

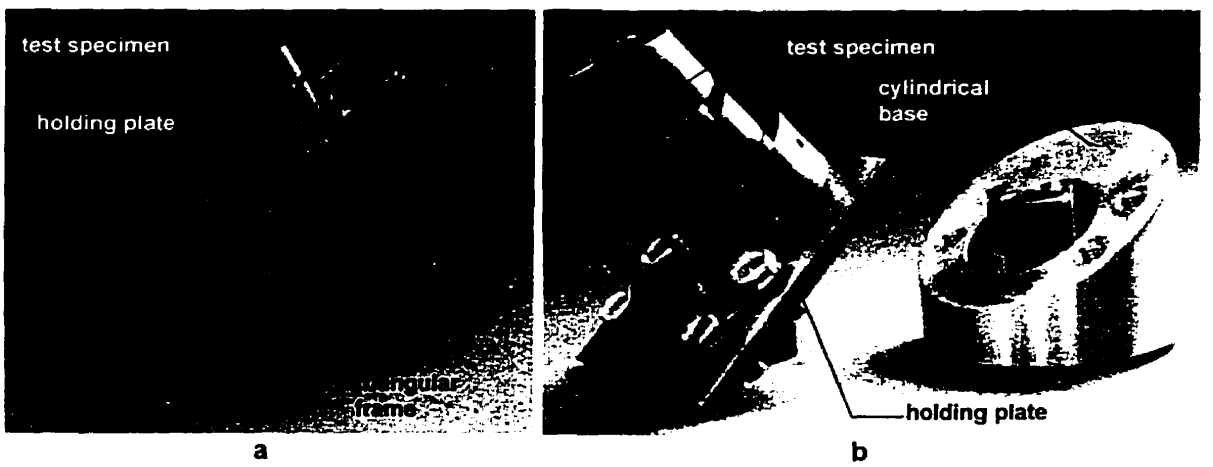

FIGURE 3.5 **a** First generation specimen holding fixture. **b** Second generation specimen holding fixture.

The frame could be bolted to the load cell of either testing apparatus via the holes on the base. The holding plate, which comprised a cylindrical receptacle with three set screws for securing the test specimen, was bolted to the 30° inclined ramp of the frame. Positioning adjustment was provided by edgewise and lengthwise slots in the holding plate and ramp, respectively.

A second generation holding fixture had to be designed for the lighter weight, bench top Shore Western testing apparatus since the size and weight of the first one caused the system to reach unstable conditions during testing. This holding device, shown in Figure 3.5b (engineering drawings are included in Appendix 5), comprised a cylindrical base and a specimen holding plate machined from aluminum. The base was attached to the load cell of the Shore Western via a bolt that passed through a counterbored hole through its centre. The slightly oversized hole allowed for limited positioning of the fixture on the load cell. Additional positioning of the test specimen was made possible by the four slots on the specimen holding plate that was bolted to the 30° inclined

surface of the base. The test specimen was secured in the receptacle of the holding plate with three set screws.

3.3.2 Fluid Chamber

During testing the taper junction was to be immersed in a solution simulating synovial fluid. A fluid chamber was designed to satisfy the following conditions:

- Contain approximately 20 cm^3 of fluid to immerse the taper junction.
- Prevent particulate contamination of the testing fluid from the testing apparatus.
- Withstand rapid vibrations of high cyclic loading conditions.

Figure 3.6a shows the first generation fluid chamber (engineering drawings included in Appendix 6) which was constructed from cast acrylic. The lid was tightly secured to the body of the chamber with machine screws, and the

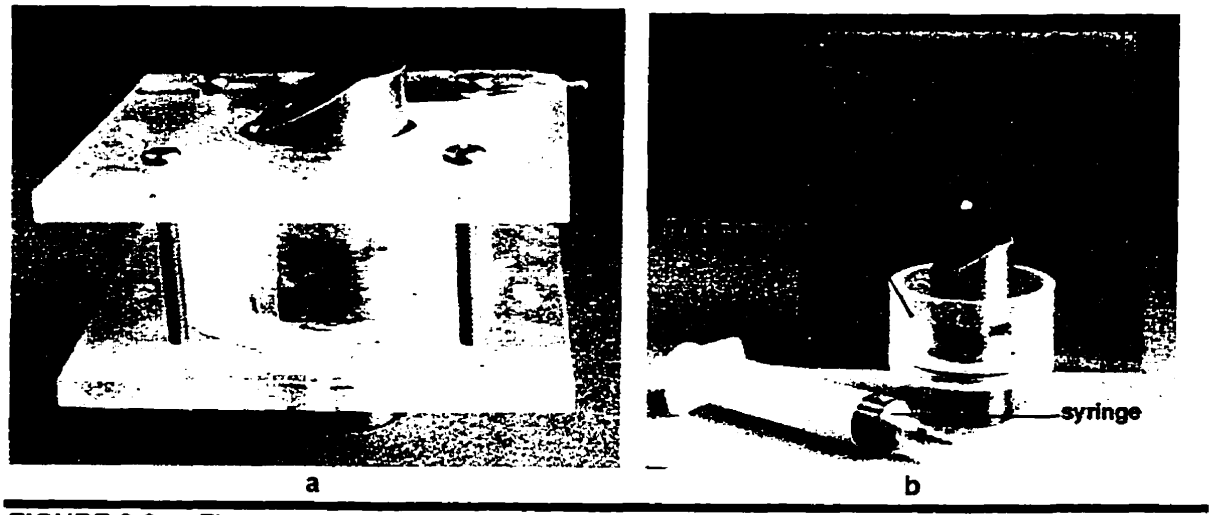

FIGURE 3.6 **a** First generation fluid chamber. **b** Second generation fluid chamber with syringe for filling chamber.

entire assembly was sealed around the test specimen using rubber O-rings inset into the floor and lid.

This chamber, which began to deteriorate and leak after several tests, was replaced by the fluid chamber shown in Figure 3.6b (engineering drawings in Appendix 6). The structure of this second generation chamber was improved by machining the wall and floor as one integral part and replacing the lid with a flexible latex sheet that had a small central hole that was expanded over the top of the test specimen. This flexible cover was secured to the body of the fluid chamber with two thin rubber straps.

3.4 TESTING PROTOCOL

3.4.1 Pre-Test Specimen Preparation and Set-Up

To ensure consistent positioning, and to prevent drifting of the load applicator during testing, a conical indentation was made on the loading surface of the female components. Its location was such that the line of action of the applied load was consistent with that of *in-vivo* reaction forces passing through the centre of an implant head during the load bearing portion of level gait.[12] The appropriate location of the indentation on the test specimen was established by superimposing a drawing of a regular 28 mm implant head on a true-view drawing of the female component. The drawing was then transformed into a parallel line development that was used for constructing a three-dimensional cellophane template. With the template tightly fitted over the female component a notch was made with a steel punch at the desired location to guide a conical tipped dental drill that was subsequently used to make the final indentation.

Immediately prior to assembly male and female tapers were cleaned of dust particles using pressurized nitrogen gas. The taper pair was then loosely assembled manually and, in the inverted position, was securely fastened into a holding plate (similar to the specimen holding plate described in section 3.3.1) by

a point contact on the long side of the female component and a surface contact on its short side. This was done to prevent the components from skewing during the final assembly, which consisted of impacting the base of the male component with a 0.5 kg weight dropped three times from a height of 40 cm along a vertical steel rod that acted as a guide (Figure 3.7). The weight and dropping distance used in this final seating procedure approximated the weight and distance travelled of a surgical mallet during intraoperative assembly of modular hip implants.

Following assembly the fluid chamber was positioned on the specimen, and the entire interior of the chamber was cleaned of dust particles using pressurized nitrogen gas before installing the cover.

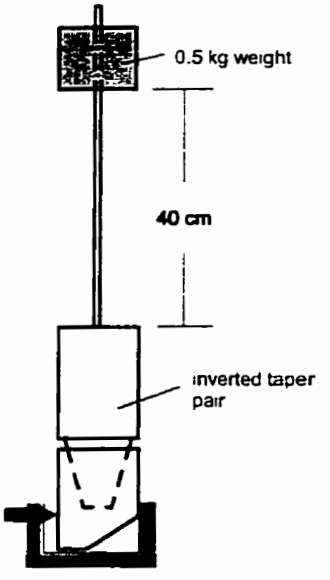

Figure 3.7 Schematic of component assembly set-up.

With the specimen holding fixture mounted on the testing apparatus, the test specimen/fluid chamber assembly was carefully installed so that its loading surface was level with respect to the base of the apparatus. The position of the specimen holding plate was finally adjusted to achieve perfect alignment of the load applicator with the indentation on the load surface of the specimen.

In the final stage of the test set-up the fluid chamber was filled with a solution of 90% physiologic saline and 10% bovine serum,[64] which had been pre-mixed in a sterile container and stored at a temperature of approximately 8°C until the time of testing. The fluid was injected through a small opening in the fluid chamber cover using a syringe equipped with a flexible extension tube. After filling the chamber, the syringe and tubing were thoroughly flushed out with saline solution to prevent contamination of subsequent tests. Figure 3.8 shows the final test set-up on the Shore Western testing apparatus.

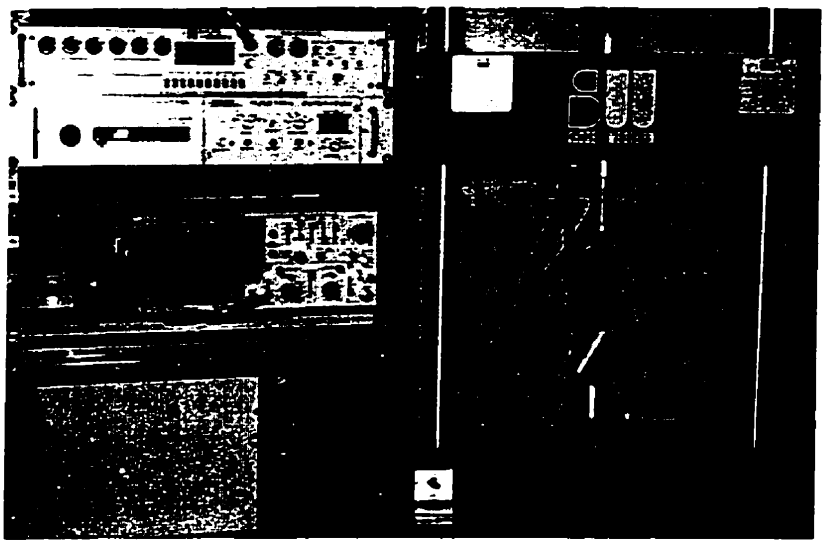

FIGURE 3.8 Test set-up on Shore Western servo-hydraulic testing apparatus.

3.4.2 Loading Conditions

The loading conditions used in this study are shown in Table 3.3. Preliminary testing on the first ten specimens was necessary to establish the most appropriate testing conditions for the given time constraints. The initial load range of 220 N to 2200 N (approximately 3 X bodyweight (BW) based on an average weight of 75 kg) was increased to a range of 400 N to 4000 N (approximately 5.5 X BW) to maximize the opportunity of detecting differences in results between test groups with the methods of analysis employed. Since the time required for testing at 5 Hz for 5 million cycles was excessive, two tests were run at 10 Hz to examine this effect on the results. Finally, however, since the majority of fretting damage is believed to occur within the first million cycles,[50] it was decided that running the tests to 2 million cycles at 5 Hz would be preferable to testing at higher frequencies. Under these conditions each test ran for 4.6 days.

TABLE 3.3 Loading Conditions

Number of Tests	Test Groups	Load Range (N)	Frequency (Hz)	Number of Cycles ($\times 10^6$)
2	1 x L0R† 1 x L-8R	220 - 2200	5	5
2	S-8R	400 - 4000	10	5
4	1 x L-8R 3 x S-8R	400 - 4000	5	5
22	4 x L0R 3 x L-8R 5 x L0S 5 x S+8R 5 x S0R	400 - 4000	5	2

† Identifies condition of three investigated design parameters; taper size, mismatch, and surface finish. L = large, S = small; -8 = -8' mismatch, 0 = 0 mismatch, +8 = +8' mismatch; R = rough, S = smooth.

The two tapers tested at the lower loads and the two tested at the higher frequency were ultimately excluded from this study because of uncertainty about the possible effects of these different parameters on the results.

3.4.3 Post-Testing Procedures

After testing, the load applicator was retracted and the test specimen/fluid chamber assembly was removed from the holding fixture and oscillated manually to suspend all particulate debris in the testing fluid. Using the syringe the fluid was immediately transferred to a sterile vial so it could be analysed for particle counts in a separate study. Residual particles in the fluid chamber and syringe were retrieved by rinsing them with saline that was added to the testing fluid. In preparation for subsequent tests, the fluid chamber and syringe were thoroughly rinsed with regular water, and finally with saline.

To disassemble the test specimen with minimal extraneous damage to the tapers, a dual-pronged, wedge shaped steel fork was placed in the clearance between components so that the prongs straddled, but did not come in contact with, the male taper. The handle of the steel fork was impacted until the components separated.

Prior to cleaning, the male tapers were examined for evidence of fluid ingress into the taper junction using a stereomicroscope (20X magnification), and photographed in four circumferential quadrants. After cleaning the male components in acetone in an ultrasonic cleaning apparatus for a minimum of 20 minutes, each quadrant of the male tapers was photographed again.

3.4.4 Procedure for Examining Assembly Damage

An additional test was conducted on one specimen to assess the damage to the male taper surface caused by assembly of the components. The test specimen used for the procedure was a small taper with a rough surface finish

(taper mismatch was unknown). Prior to assembly images were taken of the male taper surface from the tip, mid, and base of two opposing quadrants on the taper using a scanning electron microscope (SEM) (JEOL JSM840A, JEOL Ltd., Tokyo, Japan). The male and female components were cleaned with pressurized nitrogen gas and immediately assembled using the same protocol as described above in section 3.4.1, and disassembled with a dual pronged fork as described in section 3.4.3. SEM images were taken of the damage on the male surface caused by the assembly procedure.

3.5 ANALYSIS

Damage on the male tapers was analysed both qualitatively and quantitatively. The methods employed were not able to differentiate between damage due to assembly, and wear caused by fretting, therefore, subsequent reference to wear on the surfaces refers to damage which may have been caused by one or both processes.

3.5.1 Qualitative Analysis

After cleaning, the male tapers were examined in detail using a high powered (maximum magnification of 70X) stereomicroscope (Bausch and Lomb). For this purpose each taper was visually divided into 12 zones; three longitudinal divisions in each of four circumferential quadrants (Figure 3.9). Wear on the tapers with a rough surface finish appeared as distinct circumferential bands of variable widths depending on the amount of material removed from the original machining peaks. Four classifications of wear were derived based on the width of the wear bands relative to the original inter-machining peak spacing. These are described in Table 3.4, and shown photographically in Figure 3.10. Modifications to these classifications were necessary for the smooth tapers (Table 3.4) since the original machining peaks

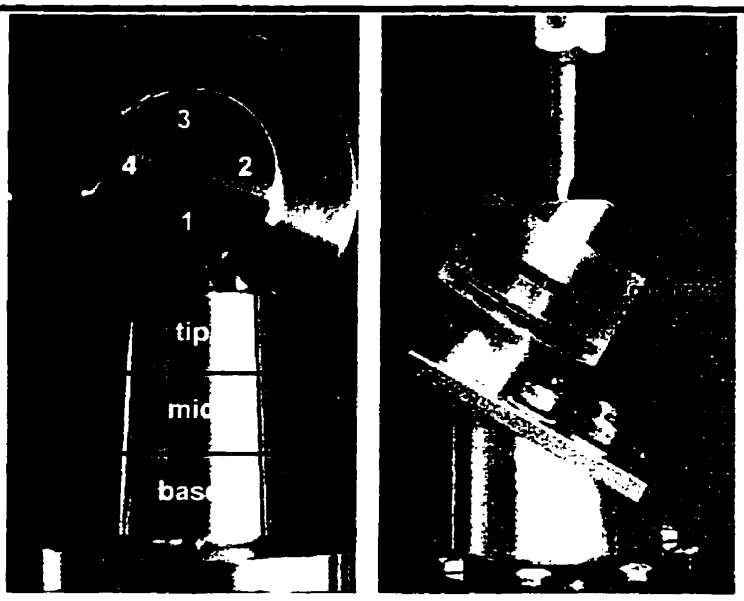

FIGURE 3.9 Twelve zones of analysis on the male tapers; four circumferential quadrants with three longitudinal divisions. Quadrant 1 corresponds to the load, and quadrant 3 is opposite the load.

TABLE 3.4 Qualitative Wear Classifications

Wear Classification	Appearance	
	Rough Surface Finish	Smooth Surface Finish
Negligible	- tiny specks - random distribution within zone	- same
Mild	- thin continuous circumferential bands - maximum width: ¼ original inter-peak spacing	- patches spanning several machining marks - original machined surface still visible within patches
Moderate	- continuous circumferential bands - width range: ¼ to ½ original inter-peak spacing	- continuous circumferential bands spanning several machining marks - original machined surface still visible within patches
Severe	- continuous circumferential bands - width: >½ original inter-peak spacing	- continuous circumferential bands spanning several machining marks - original machining marks totally obliterated

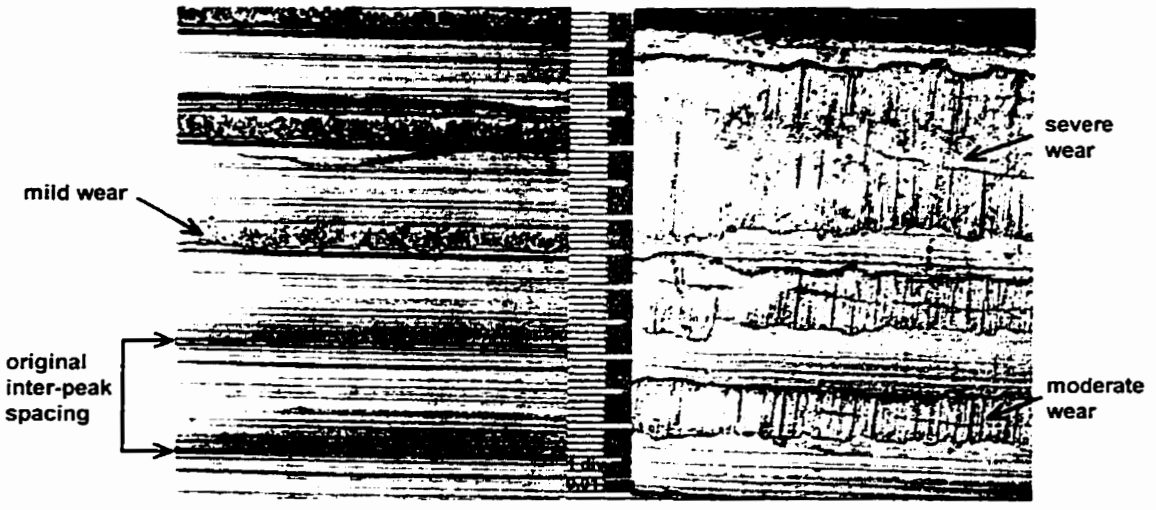

FIGURE 3.10 Photomicrograph of different wear classifications on male tapers with rough surface finish.

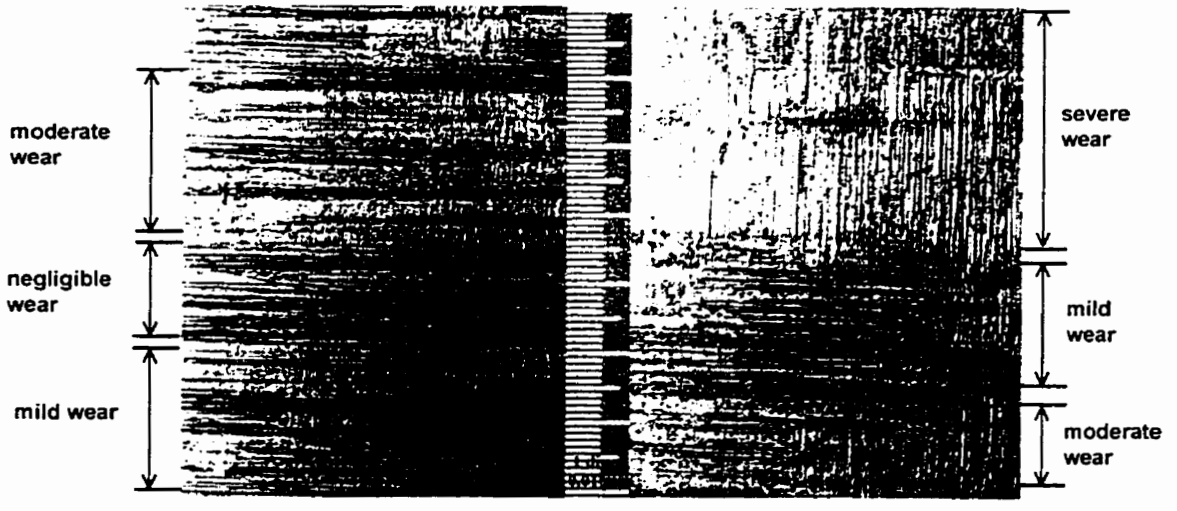

FIGURE 3.11 Photomicrograph of different wear classifications on male tapers with smooth surface finish.

were obscured by cutting marks caused by irregularities on the flank of the cutting tool. These classifications are illustrated in Figure 3.11.

Each zone on the taper was classified according to the highest degree of wear observed regardless of the size of area it covered. In borderline cases a conservative classification was given. The degree of wear affecting the majority of the surface area in each zone was also documented. The classification procedure was repeated twice for each test group, and any zones given disparate classifications were analysed a third time. There was an interval of at least 24 hours between analyses. Chi-squared tests for comparing proportions were performed on the data to determine whether there were statistically significant differences in the number of regions given a specific classification between test groups.

In addition to the microscopic classification analysis, selected tapers were examined by SEM to further characterize the wear, and a limited number of energy dispersive x-ray (EDX) (Tracor Northern, Tracor Northern Inc., Middleton, WI) spectra were obtained to roughly identify debris observed on the surface of the tapers.

3.5.2 Quantitative Analysis

Linear wear measurements were calculated from surface profiles of the male tapers obtained using a Dektak (3030 Series, Veeco Instruments Inc., Santa Barbara, CA) surface texture analysis system that was located in a strictly controlled class 2000 HEPA filtered clean room with laminar flow. To prevent particulate contaminants from entering the clean room a static resistant jumpsuit with a hood and shoe covers had to be worn while operating the instrument.

A specimen holder with course levelling capabilities had to be fabricated for the tapered components since the Dektak system was equipped to measure flat surfaces only. This device is shown in Figure 3.12. The tapered surface to

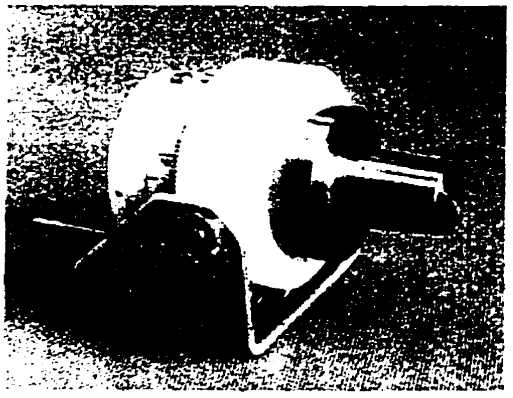

FIGURE 3.12 Specimen holder used to level tapers for profilometric measurements.

be scanned was levelled by adjusting the screw mounted to the base of the aluminum frame, and abutted against the spring loaded outer thermoplastic cylinder. The nested cylinders allowed the specimen to be rotated for subsequent scans without having to make major readjustments for levelling .

To obtain the profiles five parameters were required by the Dektak scan program; speed (slow, medium, large), stylus force (range 1 - 40 mg), vertical measurement range (65 kÅ , 655 kÅ, 1355 kÅ), resolution (low: 2000 data points, medium: 4000 points, high: 8000 points), and scan length. A medium speed was selected so the scans could be obtained in a reasonable length of time while minimizing the risk of the stylus bouncing off the surface. A 5 mg stylus force was selected based on a compromise between the risk of scratching the specimen surface and the potential for the stylus to bounce. The vertical measurement range was necessarily set at 655 kÅ given the height of the machining peaks. Again, time was a factor in selecting a medium resolution since this affected the speed at which the profiles were obtained, and finally, a

scan length of 2 mm was chosen to minimize the effects on accuracy associated with malpositioning and misalignment of the tapers.

The vertical and horizontal resolution of the Dektak, which are functions of the selected input parameters, were as follows. The vertical resolution corresponding to a vertical measurement range of 655 kÅ was 10 Å, and the horizontal resolution, calculated by dividing the scan length by the number of data points corresponding to the medium resolution input, was 0.5 μm.

The holding device was carefully positioned on the sample stage of the Dektak to ensure the stylus obtained the surface profile from the apex of the taper in a direction perpendicular to the machining marks. Positioning and alignment was done visually. The cathode ray tube (CRT) equipped on the Dektak, which displayed the surface profile as the scan was being performed, was used for the purpose of levelling the tapers. The angle of the specimen holder was adjusted for course levelling until the displayed profile appeared approximately horizontal, at which point fine adjustments were made by tilting the Dektak specimen stage. The surface was considered level when the angle between two cursors positioned in separate inter-peak recesses selected as representative of the profile was less than 0.01°.

Between one and five scans (average of three) were taken from non-contact locations (i.e. below the contact area) on the male tapers to represent surface profiles prior to wear. These data were not obtained prior to testing to avoid the risk of scratching the taper surface with the stylus. Between two and nine scans (average of five) were taken from various regions within the contact area on the tapers for quantifying wear. A hard copy of each profile was produced, and the data collected were downloaded as an ASCII file to a diskette for subsequent analysis. The process of positioning and levelling the taper,

obtaining the scan, and downloading the data proved to be arduous, and required approximately 10 to 15 minutes per scan.

Quantitative data analysis was performed using MATLAB 4.0, a data analysis software. Three programs and two user defined functions (included as Appendix 7) were written to perform various tasks of the analysis as described below.

The MAIN.M program called upon the user defined function DATARRAY.M to rearrange the data from each scan into a single row array, and to shift the array so the approximate mid-point of each profile occurred at a zero reference level. The user defined function PKVALLEY.M calculated the height of each machining peak by identifying each point where the profile crossed the reference axis, splitting the data into complete cycles (corresponding to one machining peak) spanning three consecutive reference crossings, and subtracting the minimum value for each cycle from the maximum. Reference crossings caused by small perturbations occurring in the profile at the reference axis were identified and eliminated by this function. For consistency, each complete cycle started with a positive slope so that each peak height was measured on the descending side of the machining mark.

All the peak heights measured from non-contact profiles were accumulated for each specimen, and the mean and standard deviation were calculated by the program PRETST.M to represent the average peak height before wear occurred.

In the program WEAR.M, the following simple formula was used to obtain linear wear (LW) measurements for each peak from each of the contact profiles.

$$LW = \frac{(mean\ non-contact\ peak\ height)-(worn\ peak\ height)}{(mean\ non-contact\ peak\ height)} \times 100\%$$

Two-tailed student t-tests for two independent samples with unequal variances were performed on the data to determine the significance of differences in wear between test groups. For the purpose of these computations, since the wear of subsequent machining peaks in each scan was not strictly independent of the others, the mean wear measurement for each scan was considered as one data point, and the sample size used for determining the degrees of freedom for the t-test was a function of the number of scans included in each test group as opposed to the number of worn machining peak height measurements.

4 RESULTS

4.1 QUALITATIVE RESULTS

4.1.1 Assembly Damage

The assembly experiment revealed deformation to the original machining peaks that varied circumferentially and longitudinally on the taper, probably due to out-of-roundness and waviness of the surface. These two parameters were not controlled in this study, but CMM measurements indicated an average roundness of 0.3/1000 inches (6.7 μm) for the male tapers and 0.4/1000 inches (10.4 μm) for the female tapers. There were no statistically significant differences in roundness between test groups. The image in Figure 4.1 taken from the base of the contact area, shows undamaged machining marks that were below the contact junction on the left, and damaged machining peaks on the right. Images taken from the mid-taper zone showed very little deformation of the machining marks indicating minimal contact in this area. In contrast, damage at the tip of the taper as shown in Figure 4.2a was considerably greater. This image shows the generation of metal fragments on the surface of the machining peaks (top view) as well as hanging from the edges (side view). Machining peaks with less deformation appeared to generate less fragments as Figure 4.2b illustrates. This image was taken from the base zone of the taper.

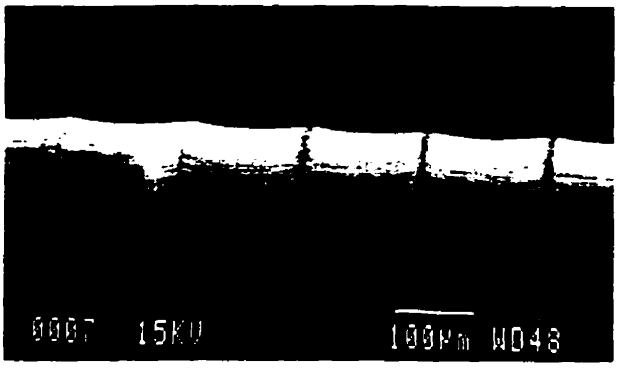

FIGURE 4.1 SEM image of assembly control test specimen showing undamaged machining marks on the left and damaged peaks on the right.

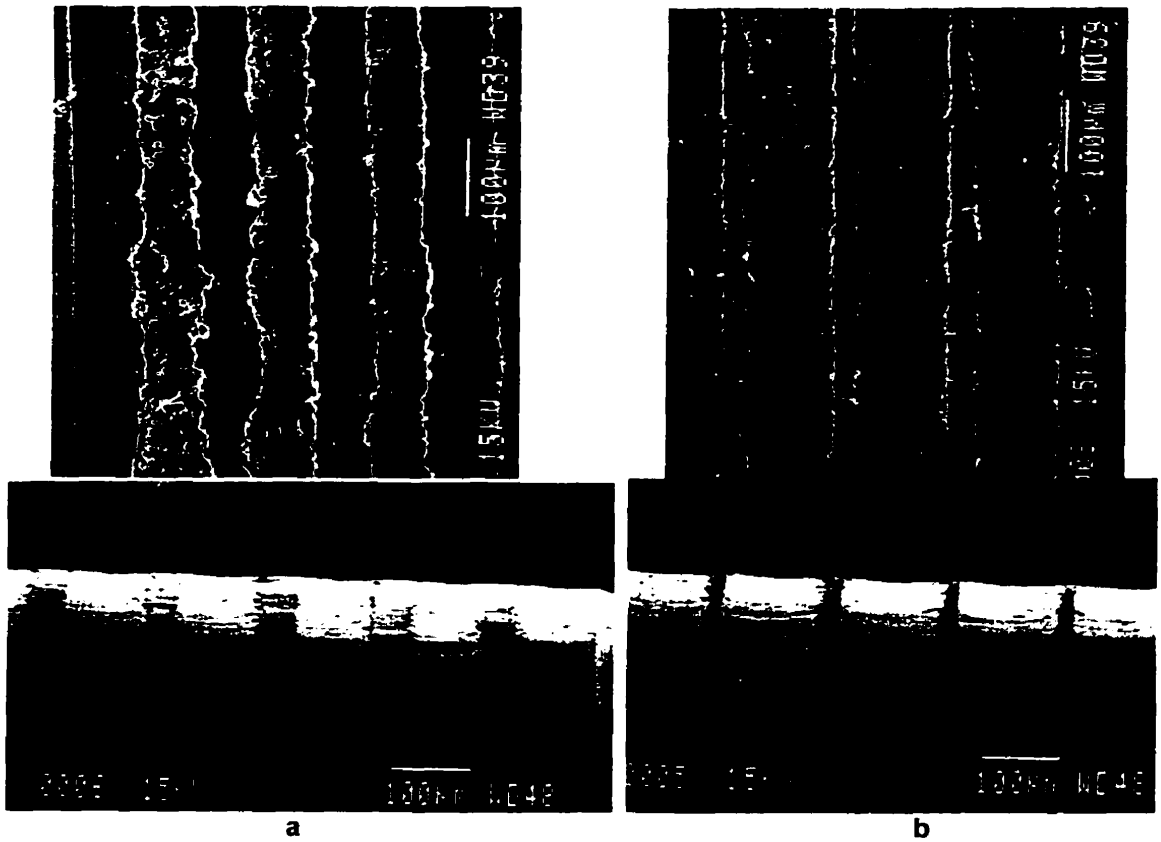

FIGURE 4.2 **a** Assembly damage at the tip of the male assembly control test specimen. **b** Damage at the base of the same male taper.

4.1.2 Initial Observations Before Specimen Cleaning

Fluid ingress into the taper junction was observed on the majority of test specimens, manifesting as a dried film on the male taper surfaces. The appearance, extent, and location of this film varied between test groups.

L0R (large, 0 mismatch, rough surface)

Permeation of fluid into the taper junction of L0R tapers was evidenced by a white flaky coating extending from the base of the contact area to approximately the mid-taper region. This was not unique to any particular quadrant of the specimen. Typical findings from this test group are illustrated in Figure 4.3a.

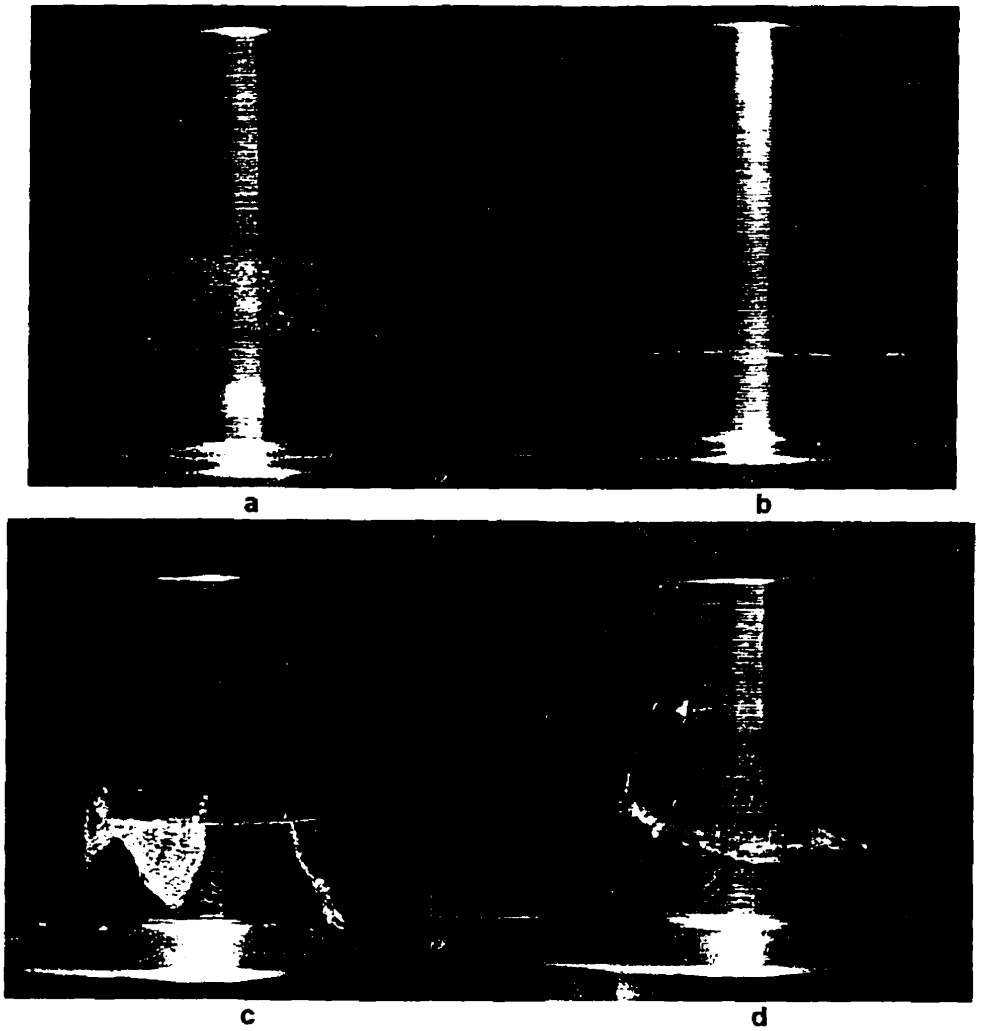

FIGURE 4.3 Evidence of fluid ingress into the taper junction. **a** Taper from the L0R test group showing fluid ingress extending from the base to the mid-taper region. **b** Taper from L-8R test group showing a typically clean surface with thin flaky band delineating the base of the contact junction. **c** Quadrant 3 of an S0R taper with a more continuous film covering two thirds of the taper. Large thick white flakes with undulated topography seen protruding from taper at base of contact junction (solid arrow), and greyish-brown patch in the same region (broken arrow). **d** Taper from S+8R test group with large white undulated flakes at taper junction (solid arrow), and greyish-brown discoloration (broken arrow) similar to that observed on all small tapers.

L-8R (large, -8' mismatch, rough surface)

In contrast, the surfaces of L-8R tapers, which had maximal engagement at the taper base, generally appeared clean with only a very mild or no film within the contact area (Figure 4.3b). The most noticeable feature on the majority of these tapers was the delineation of the contact junction at the taper base by a narrow white flaky band of dried fluid.

L0S (large, 0 mismatch, smooth surface)

The surface film on the L0S tapers was similar in appearance and location to the L0R tapers but was markedly less extensive. On one of the tapers a small patch of greyish-brown discoloration was observed in quadrant 3 near the base of the contact area.

S0R (small, 0 mismatch, rough surface)

S0R tapers showed a thicker, and often more continuous (as opposed to flaky) film which covered as much as two thirds of the surface in quadrant 3 of all tapers, and receded in the lateral quadrants. Two of the tapers were virtually devoid of any surface film in quadrant 1, the side corresponding to the load. The most striking observation was the adherence of large, thick, white flakes which protruded from the edge of the junction in quadrant 3 of the tapers. The progressive formation of these flakes, which had an undulated topography, was observed during testing. Also of interest was the formation of conspicuous greyish-brown patches in the same region at the base of the contact area in quadrant 3 of the tapers (Figure 4.3c).

S-8R (small, -8' mismatch, rough surface)

Tapers from the S-8R test group (base engaged) appeared cleaner than the S0R tapers with very little evidence of fluid ingress into the taper junction except one taper which had a very noticeable continuous thin film extending to the tip region in quadrant 3. The contact junction on all tapers in this group was delineated by a narrow flaky band at the taper base similar to that observed with

the L-8R tapers except it was most prominent in quadrant 3. Greyish-brown discoloration was observed in the base region in quadrant 3 of all tapers except one which had an extensive patch covering the basal third of the taper (not the same taper showing extensive fluid ingress).

S+8R (small, +8' mismatch, rough surface)

All S+8R tapers, which engaged more toward the tip, had evidence of fluid ingress; either a flaky coating or a thin continuous film covering almost the entire contact area. All but one of the tapers had patches of greyish-brown discoloration which occurred at the base of the contact area in quadrant 3, with the exception of one taper on which the discoloration was observed in the lower tip region. Large white undulated flakes were observed in juxtaposition with the discoloration in the base region. Figure 4.3d is an example of a taper showing the greyish-brown discoloration and the large undulated flake which had protruded from the taper junction.

4.1.3 Microscopic Wear Classification

Microscopically, all zones of all tapers showed some evidence of contact and wear of varying degrees depending on the amount of material removed. Typically, the contact between male and female components occurred at the peaks of the regularly spaced machining marks on the male tapers. The surface of the female tapers was ground as opposed to machined, and was not easily examined without sectioning, therefore, all data on microscopic wear classifications pertain to examination of the male tapers. Furthermore, this analysis does not differentiate between initial assembly damage and fretting wear.

With the exception of the smooth (L0S) tapers, there were no obvious differences observed in the gross appearance of the taper surfaces between groups, the bulk of which showed mild wear with limited areas of higher degrees

of wear particularly at the extreme tip and base of the contact area. The graph in Figure 4.4, which shows the percentage of total zones given a specific classification, indicates that the smooth tapers (L0S) had a greater number of zones exhibiting moderate and severe wear compared to all other test groups, and that the small tapers (S0R, S-8R, S+8R) had slightly more zones in which moderate and severe wear were observed compared to the large tapers (L0R and L-8R). Chi-squared tests for comparing proportions were performed on the data for each wear classification, excluding data for the smooth tapers since their classifications were not equivalent to those for rough tapers. There was no statistically significant difference between 0 mismatched versus ±8' mismatched tapers, or between large versus small tapers, for any of the wear classifications.

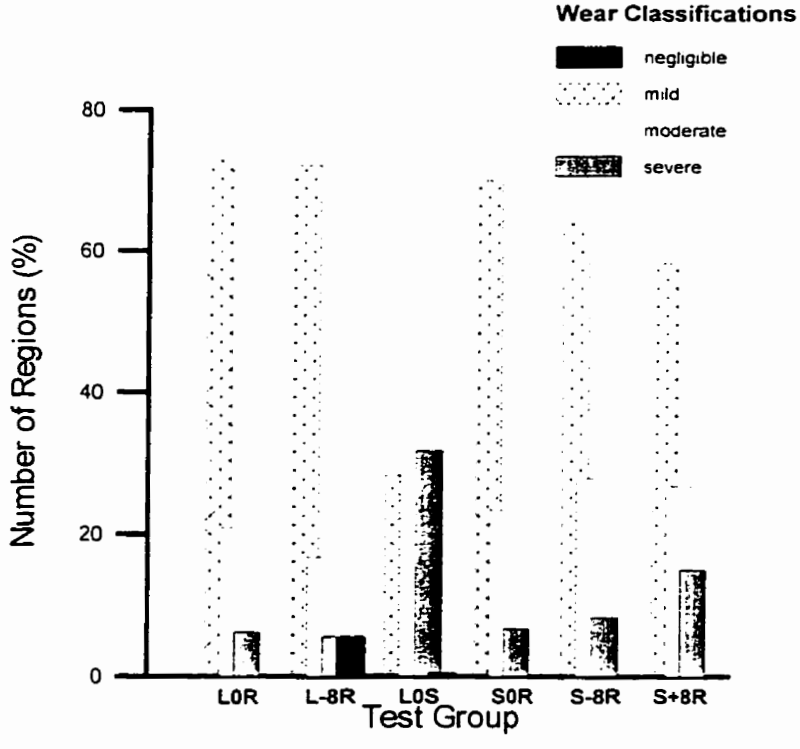

FIGURE 4.4 Results of qualitative analysis. Each bar represents the total number of zones given a specific wear classification for the particular test group.

Analysing the results for each of the 12 zones of analysis (the base, mid taper, and tip divisions for each of the four quadrants) revealed subtle differences between test groups with regard to location of damage. The data in Table 4.1 summarizes these results for each of the three longitudinal divisions. In general, higher degrees of wear (i.e. moderate and severe) were observed only in the tip and base zones, except on smooth (L0S) tapers which exhibited moderate wear in the mid taper zones as well. Additionally, it was noted that moderate and severe wear were generally limited to only 2 or 3 machining peaks, and at the most 6 or 7 peaks (comprising a distance of approximately 1 mm), located at the extreme limits of the overall contact area. Severe wear occurred almost exclusively in the tip zones.

The following observations are based on the complete breakdown of the results into the 12 zones of analysis.

L0R (large, 0 mismatch, rough surface)

The frequency of moderate and severe wear on L0R tapers was higher at the tip than at the base. The moderate wear was observed in all quadrants, whereas severe wear occurred only in quadrants 1 and 3. At the base there was basically no difference in wear between quadrants.

L-8R (large, -8' mismatch, rough surface)

These tapers had a higher frequency of moderate and severe wear at the base than at the tip. Two zones in particular consistently exhibited higher degrees of wear; the base in quadrant 3 which sustained moderate wear on all tapers, and the tip in quadrant 1 which accounted for all the severe wear observed in this group.

L0S (large, 0 mismatch, smooth surface)

The L0S tapers had a higher frequency of moderate and severe wear than any other test group. Moderate wear affecting the mid and base zones generally occurred in all quadrants, and, similarly, severe wear was observed in

TABLE 4.1 Breakdown of Wear Classification Results

		Zones Given Specific Wear Classification (%)			
		Negligible	Mild	Moderate	Severe
L0R†	tip	0	37.5	43.8	18.8
	mid	0	100.0	0	0
	base	0	81.3	18.8	0
L-8R	tip	0	75.0	8.3	16.7
	mid	16.7	83.3	0	0
	base	0	58.3	41.7	0
L0S	tip	0	0	10.0	90.0
	mid	5.0	50.0	45.0	0
	base	0	35.0	60.0	5.0
S0R	tip	0	30.0	50.0	20.0
	mid	0	100.0	0	0
	base	0	80.0	20.0	0
S-8R	tip	0	50.0	25.0	25.0
	mid	0	100.0	0	0
	base	0	41.7	58.3	0
S+8R	tip	0	5.0	50.0	45.0
	mid	0	100.0	0	0
	base	0	70.0	30.0	0

† Identifies condition of three investigated design parameters; taper size, mismatch, and surface finish. L = large, S = small; -8 = -8° mismatch, 0 = 0 mismatch, +8 = +8° mismatch; R = rough, S = smooth.

all quadrants in the tip zone.

S0R (smooth, 0 mismatch, rough surface)

The locality of wear on the S0R tapers was quite similar to the L0R tapers. The frequency of moderate and severe wear was higher at the tip than at the base. The moderate wear was observed in all quadrants but was more frequent in quadrants 3 and 4, and the severe wear occurred only in quadrant 1. Moderate wear in the base zones occurred slightly more frequently in quadrant 3 of the tapers.

S-8R (smooth, -8' mismatch, rough surface)

Moderate and severe wear at the tip of these tapers was observed almost as frequently as moderate wear at the base, and was widely distributed to all quadrants. The majority of moderate wear observed in the base zones occurred in quadrant 1.

S+8R (smooth, +8' mismatch, rough surface)

Similar to the 0 mismatch tapers (L0R, S0R), moderate and severe wear occurred more frequently at the tip than at the base on the S+8R tapers, and was generally distributed to all quadrants. Relative to the other test groups, excluding that which had smooth tapers (L0S), the frequency of severe wear observed at the tip was high. Moderate wear was observed in all quadrants in the base zones, but was slightly more frequent in quadrants 1 and 3.

4.1.4 Scanning Electron Microscopy and Energy Dispersive X-Ray Analysis

Under the SEM, damage to the machining peaks had three characteristic appearances. Some modified machining peaks were marked by definite striations running perpendicular to the original machining marks (Figure 4.5a). Burr formation on both the upper and lower edges of these damaged machining peaks were noted. On the other hand, several of the flattened peaks appeared

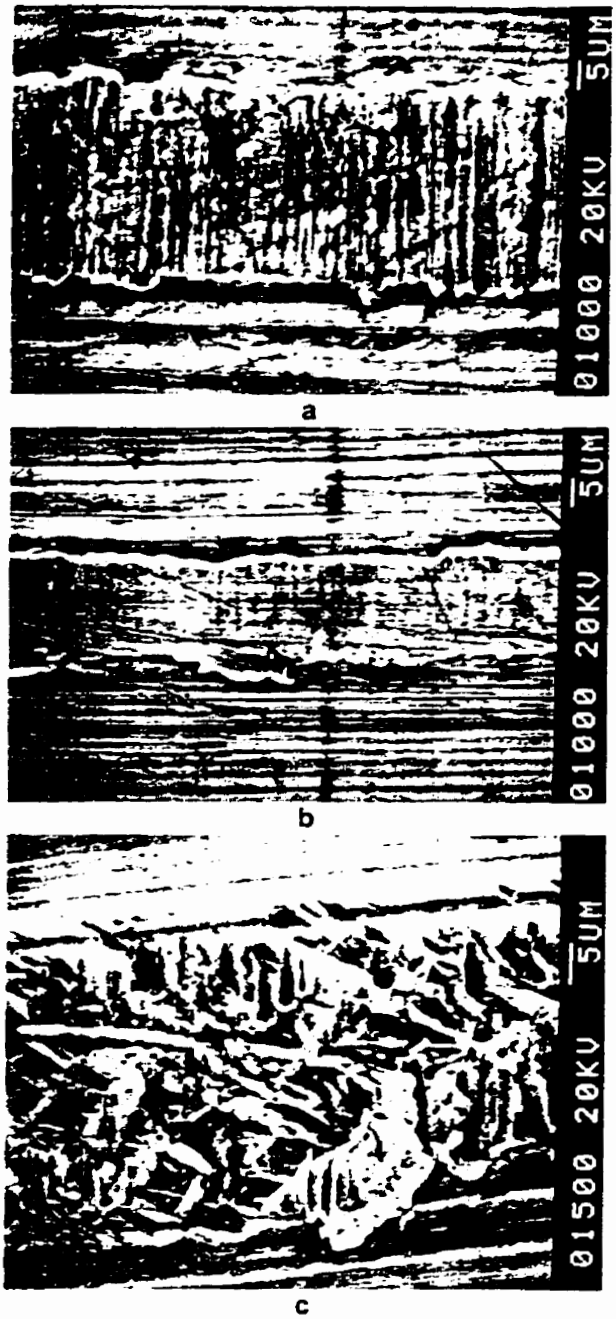

FIGURE 4.5 Three characteristic appearances of damage to the machining peaks seen under SEM. **a** Marked striations running perpendicular to machining mark. **b** Flattened machining peak with smooth appearance. **c** Damaged machining peak with multidirectional scoring.

smooth with very faint or no apparent longitudinal striations (Figure 4.5b). Less frequently observed was damage with the appearance of multidirectional scoring (Figure 4.5c).

Besides mechanical damage, SEM also revealed possible evidence of corrosive activity. The greyish-brown patches initially observed under the light microscope, which were not removed by ultrasonic cleaning, appeared as dark cracked laminae adhered to the taper surface immediately adjacent to the damaged machining peaks (Figure 4.6) and seemed to be indicative of oxidized particulate debris, a product of fretting corrosion. Energy dispersive x-ray spectra obtained from these laminae were high in Ti and Cr, with discernible peaks of Co, Al, and Mo (Figure 4.7). Using the ultra thin window (UTW) on the electron microscope, which allows low energy x-rays to be detected, it was possible to discern peaks of O that were not apparent in spectra taken from outside the contact area on the tapers.

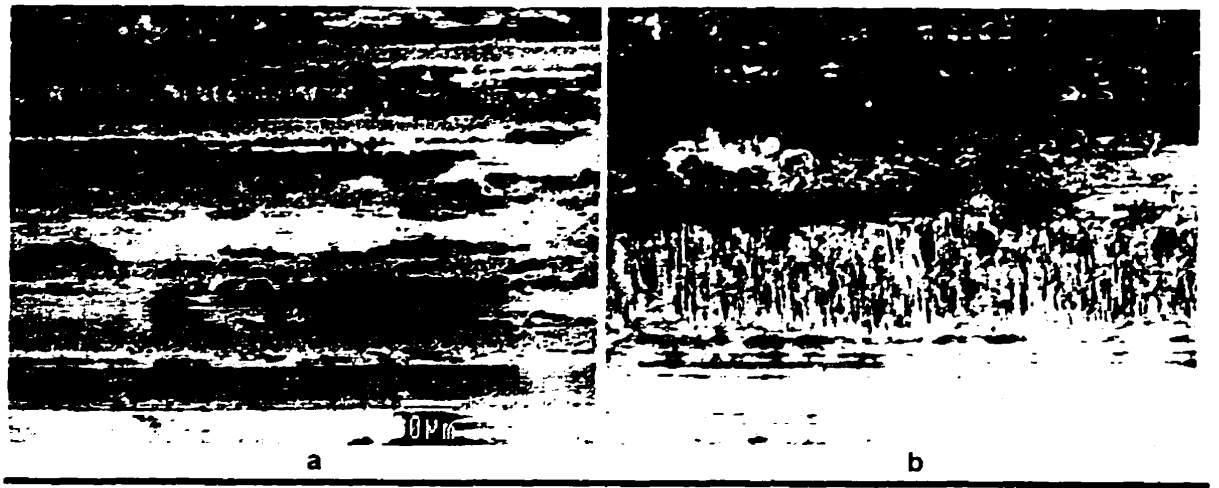

FIGURE 4.6 **a** SEM image showing copious black deposits adjacent to damaged machining peaks on an S+8R taper. **b** One of the machining peaks seen at higher magnification (600X) revealing elongated pits.

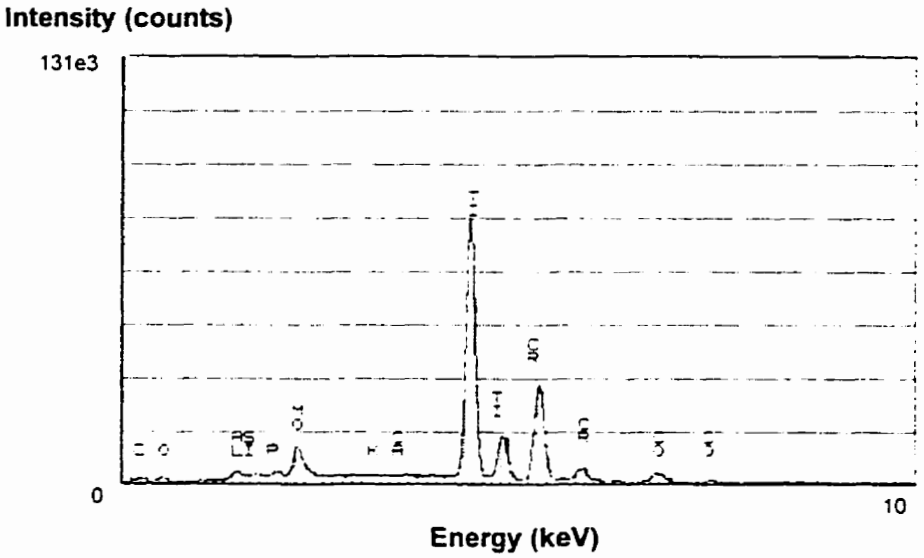

FIGURE 4.7 X-ray spectrum taken from black deposits observed on S+8R male taper.

Also observed, particularly in juxtaposition with regions of copious black deposits, were areas of possible pitting (Figure 4.8). This damage, was limited almost exclusively to the worn machining peaks with the exception of heavily scarred areas where it appeared to have spread into the otherwise undamaged recesses between peaks. It was also noted that the machining peaks in these areas often appeared amorphous as opposed to having distinct striations. Energy spectra from these apparent pits contained the same metal elements as spectra from the dark laminae but with different peak height ratios (Figure 4.9).

The black deposits and ostensible pitting described above were apparent on all small tapers examined under the SEM, particularly in quadrant 3 in the base region. Small localized areas of similar damage were observed on a few large tapers (at least one from each group; L-8R, L0R, L0S) but these were only detectable at very high magnifications (>600X). This damage, which was unlike that observed on the specimen from the assembly test, provided evidence that fretting had occurred.

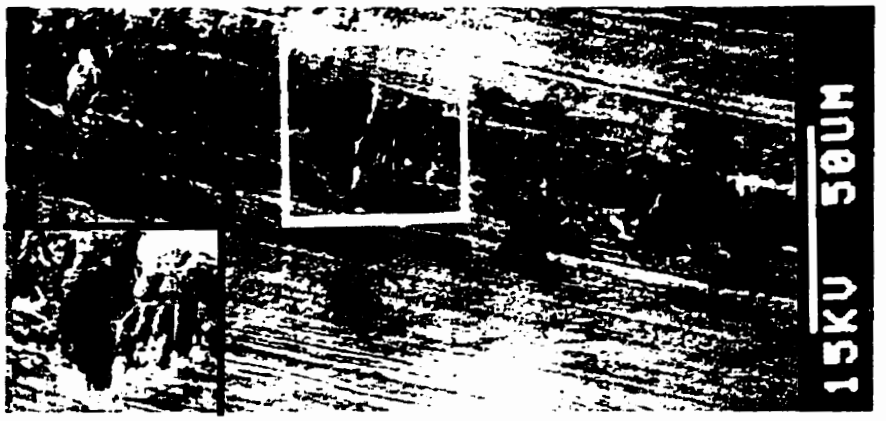

FIGURE 4.8 SEM image of pit observed on the damaged machining peak of an S0R male taper. Inset is 1000X magnification.

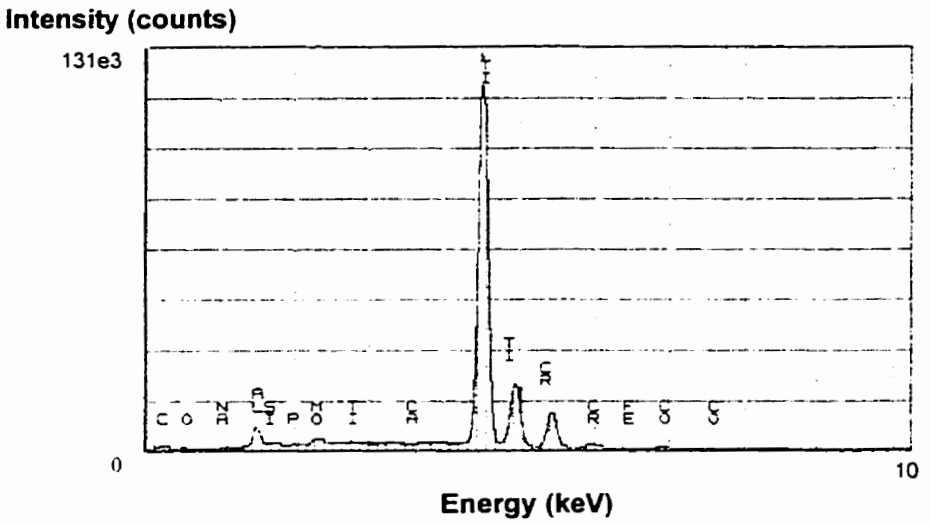

FIGURE 4.9 X-ray spectrum taken from pit observed on S+8R male taper.

Finally, EDXA was performed on some of the large undulated flakes that had been removed from the opening of the taper junction. In the majority of spectra obtained the most prominent peak was Cl, likely from the sodium chloride (NaCl) used in the testing fluid. Other elements consistently detected in the spectra were Cr, Co, Ti, Al, V, Si, Zn, S, P, C and O.

4.2 QUANTITATIVE RESULTS

As stated previously, it was not possible to differentiate between damage caused by assembly and that caused by fretting, and therefore the following wear measurements assess the combined effect of both processes.

4.2.1 Linear Wear Based on Profilometric Measurements

Linear wear measurements were calculated for all but the smooth (L0S) tapers. Non-contact surface profiles taken from L0S tapers contained high frequency noise which obscured the actual surface roughness profiles (Figure 4.10a). This noise was believed to represent measurements of the microscopic grooves left on the taper surface by irregularities in the flank of the cutting tool. Profiles of the worn surfaces taken after testing had a similar appearance (Figure 4.10b) and, consequently, linear wear of smooth tapers could not be determined with this procedure.

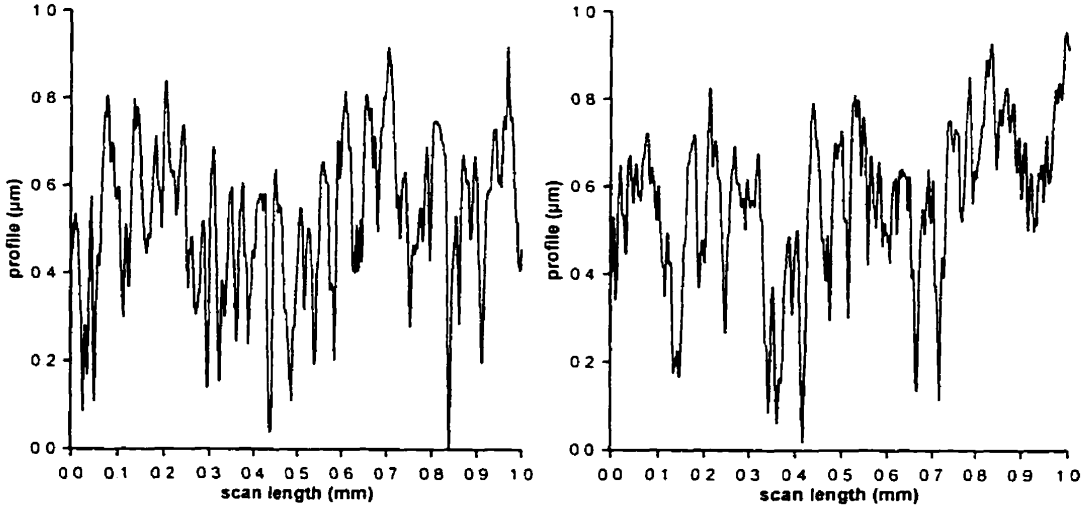

FIGURE 4.10 **a** Non-contact surface profile from a taper with a smooth surface finish. **b** Profile taken from contact area on same taper after testing. Lack of distinction between non-contact and contact surface profiles precluded quantification of wear using profilometric method.

In lieu of wear measurements, a non-contact surface profile from a smooth taper was plotted against one from a rough taper (Figure 4.11) for a relative comparison of the potential debris that could be generated from the two surfaces. From this comparison it was apparent that even if complete wear of the machining marks on the smooth surface down to the substrate material were to occur, this would only represent a fraction of the height of the machining marks on the rough tapers. Despite the high number of zones classified with severe wear on these tapers observations of large areas in which the original machined surface was still apparent (Figure 4.12) indicated that widespread obliteration of the machining peaks did not occur.

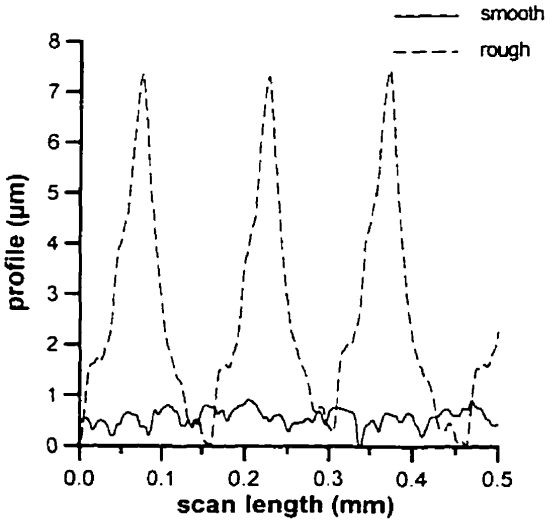

FIGURE 4.11 Graph of rough surface profile vs smooth surface profile.

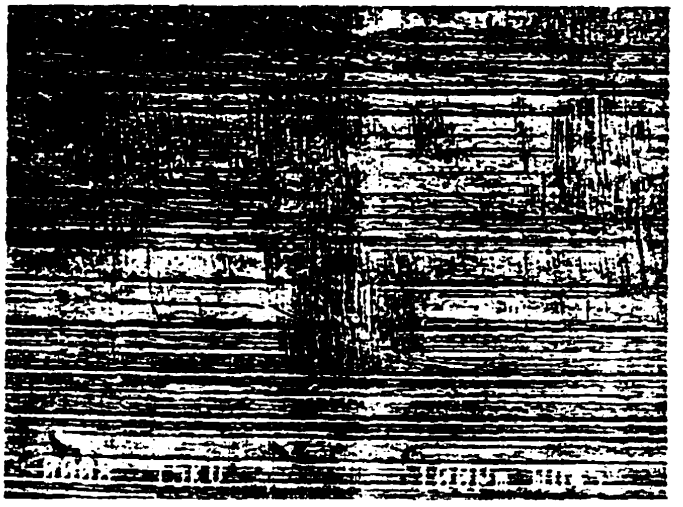

FIGURE 4.12 SEM image showing wear on an L0S (smooth) taper with a large area where the original machined surface is still visible.

Profiles taken from non-contact areas on tapers with a rough surface finish showed distinct machining marks whose heights were easily measured. After testing, the machining peaks were noticeably flattened but there was no other deformation to their form making it possible to compare their heights with the average original machining peak height. Profiles taken from non-contact and contact areas of tapers from different test groups with a rough surface finish are shown in Figures 4.13 - 4.16 No obvious differences were seen from the profiles for different test groups.

Results of the linear wear measurements are tabulated in Table 4.2. Each value calculated for the base and tip zones was based on an average of nine profiles, each profile providing approximately 11 peak height measurements. Since mid-taper wear appeared more homogeneous, only two or three profiles were obtained for computing these values. Minimum and maximum wear measurements exemplify the wide range of wear occurring within a particular zone. In all test groups except the small -8' mismatch (S-8R) test group, the greatest material removal occurred in the tip zone, with as much as

approximately 60% of the original machining marks worn in some areas. The measurements taken from the tip zones are considered slightly conservative since the greatest wear occurred at the extreme limit of the taper which was difficult to obtain profiles from due to complications caused when the stylus dropped off the end of the taper.

Similar to observations made from the qualitative analysis, the mean values calculated for each longitudinal division shown in Table 4.2 revealed differences in the locality of wear between groups.

L0R (large, 0 mismatch, rough surface

Greater wear occurred at the tip of the L0R tapers than at the base, and very little wear occurred in the mid-taper zones.

L-8R (large, -8' mismatch, rough surface

Contrary to observations made from the L0R tapers, L-8R (base engaged) tapers had higher wear measurements at the base than at the tip. The overall mean wear for this test group was not significantly higher than that of the L0R test group. No measurements were available from the mid-taper zone which would likely lower the overall mean wear value for this test group.

S0R (small, 0 mismatch, rough surface)

Similar to the L0R tapers, greater wear measurements were obtained from the tip of the S0R tapers than from the base. The least wear was measured in the mid-taper zones. In all three of the longitudinal divisions the wear measurements on these tapers were higher than those for the corresponding division on the L0R tapers (tip: $p=.009$, base: $p=0.03$), and thus the overall mean wear was significantly higher ($p=0.002$).

S-8R (small, -8' mismatch, rough surface)

On the S-8R (base engaged) tapers wear was approximately equivalent at the tip and at the base. Compared to the S0R tapers, wear at the tip was slightly lower, whereas wear at the base was slightly higher. Neither of these differences were

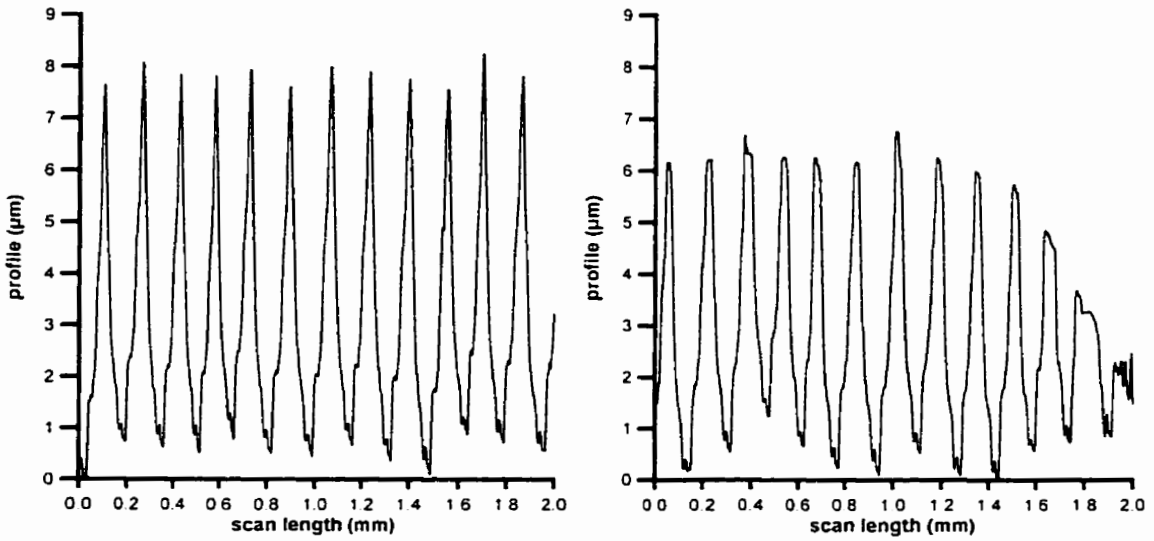

FIGURE 4.13 **a** Non-contact surface profile taken from a large taper with 0 mismatch. **b** Surface profile taken from the extreme tip of the same taper after testing. Between 12% and 60% of the original machining peaks have been removed.

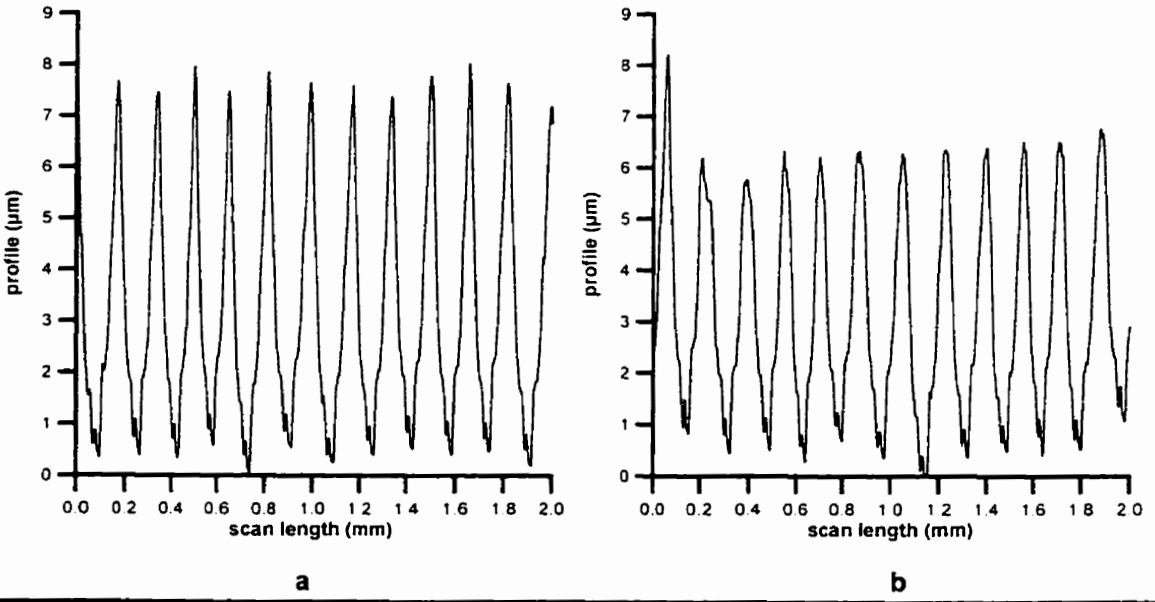

FIGURE 4.14 **a** Non-contact surface profile taken from a large taper with -8' mismatch. **b** Surface profile taken from the extreme base of same taper after testing. The first machining peak in this profile was below the contact junction. Between 15% and 28% of the tips of the original machining peaks have been removed.

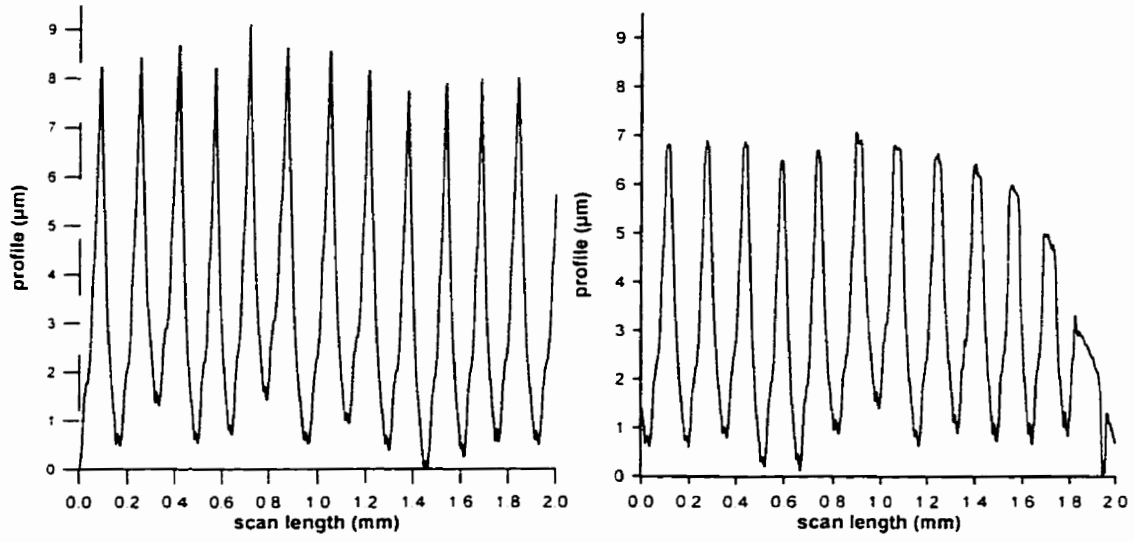

FIGURE 4.15 **a** Non-contact surface profile from a small taper with 0 mismatch. **b** Profile taken from extreme tip of contact area on same taper after testing. Between 12% and 57% of the original machining peaks have been removed.

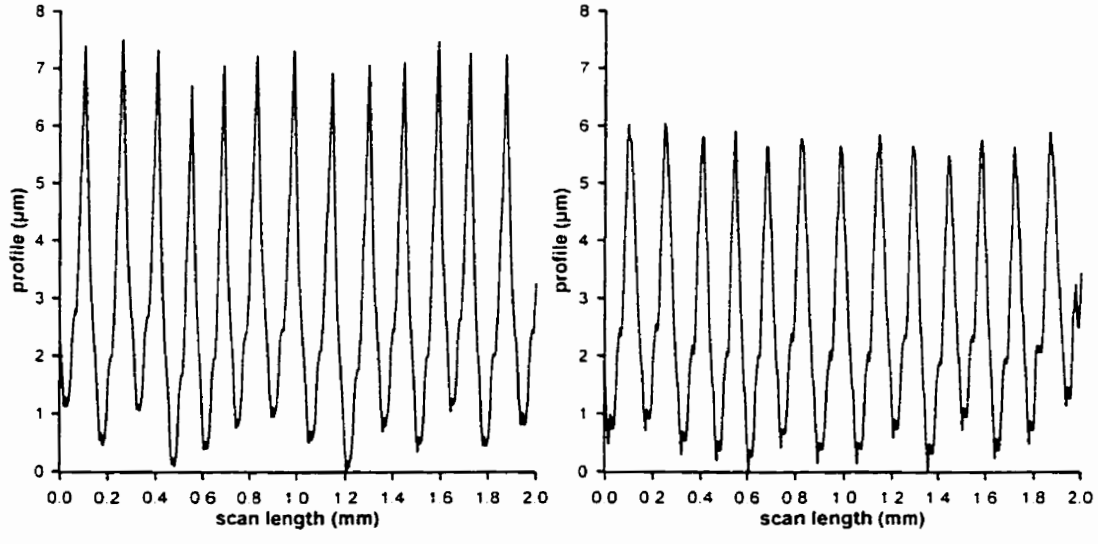

FIGURE 4.16 **a** Non-contact surface profile taken from a small taper with +8' mismatch. **b** Profile taken from mid-taper shows decreases in the height of the original machining peaks ranging from 12% to 29%

TABLE 4.2 Profilometric Wear Measurement Results

Test Group and Taper Region		Linear Wear Measurements (% of original machining peak height)			
		Minimum	Maximum	Mean ± standard deviation	Overall Mean ± standard deviation
L0R[†]	tip	0	59.80	15.94 ± 10.96	8.75 ± 11.22
	mid	0	10.90	0 ± 5.37	
	base	0	39.34	4.63 ± 8.56	
L-8R	tip	0	45.30	8.79 ± 9.18	10.90 ± 9.10
	mid	-	-	-	
	base	0	35.38	13.21 ± 8.46	
S0R	tip	7.75	56.62	24.23 ± 8.05	17.37 ± 10.71
	mid	0	16.80	7.75 ± 4.67	
	base	0	44.75	13.48 ± 10.21	
S-8R	tip	1.63	46.13	20.72 ± 10.45	20.17 ± 9.53
	mid	-	-	-	
	base	0.32	47.62	19.85 ± 8.99	
S+8R	tip	0	57.62	22.92 ± 11.27	19.71 ± 11.61
	mid	7.72	28.76	20.19 ± 5.39	
	base	0	43.95	14.47 ± 11.50	

[†] Identifies condition of three investigated design parameters; taper size, mismatch, and surface finish. L = large, S = small; -8 = -8' mismatch, 0 = 0 mismatch, +8 = +8' mismatch; R = rough, S = smooth.

significant, nor was the increase in the overall mean wear compared to S0R tapers. If mid-taper wear measurements were available for the S-8R tapers the overall mean wear would be expected to decrease.

S+8R (small, +8' mismatch, rough surface)

Tapers from the S+8R (tip engaged) test group had higher wear at the tip than elsewhere on the surface. Wear measurements obtained from the mid-taper zone were higher than those from the base, and were also higher than for any other test group in which mid-taper wear measurements were available.

Likewise, wear measurements from the tip of these tapers were higher than from the tip of S-8R (base engaged) tapers, but the base wear measurements were lower. Neither of these differences were statistically significant. Compared to the S0R tapers, wear at the tip was only slightly lower, and wear at the base was approximately equivalent. There was no statistically significant difference between the overall mean wear measurements for S+8R (tip engaged) tapers compared to the S-8R (base engaged) tapers, or the S0R tapers.

To summarize, taper mismatch affected the amount of wear observed in different zones, however, there was no statistically significant difference in overall mean wear measurements between ±8' mismatched and 0 mismatched tapers. Taper size had the greatest influence on the overall results, with statistically significant differences between large and small tapers. The overall linear wear values for the S0R and S-8R test groups were approximately twice as high as for the corresponding L0R and L-8R test groups. Taking into consideration dimensional differences between the two taper sizes, this increase in linear wear was equivalent to an overall volumetric increase of approximately 1.6-fold. As a final note, it was observed during testing that small tapers appeared to flex more than the large tapers during cyclic loading.

5 DISCUSSION

Modularity between the head and neck of total hip implants has greatly improved the efficacy of THR surgery because it allows more choice in implant fit and affords optimum adjustment of hip biomechanics. Furthermore, increased latitude in design features provides the potential for improved performance, and a longer operating life of the implants. Concern, however, about the generation of particulate debris from modular junctions generated by fretting and fretting induced corrosion has resulted in focused attention on design parameters that potentially affect the stability of the modular taper connections. This study investigated the effects of three design parameters on fretting at the Morse taper head/neck junction under simulated physiologic loading conditions: taper size, surface finish, and taper mismatch. The data strongly indicated that taper size had a profound influence on fretting. Damage to the small tapers visually appeared worse with distinct patches of discoloration indicative of fretting corrosion, and their overall linear wear values were significantly higher compared to large tapers. Surface finish had no obvious influence on the extent of fretting, although if wear were confined to regions of contact at the machining peaks on the male tapers, the smooth surface finish had the potential for less volumetric wear than the rough surface finish. Unexpectedly, within each taper size, mismatch in taper angle of +8' and/or -8' did not have any detectable or substantial effect on fretting at the taper junction.

5.1 ANALYSIS OF EXPERIMENTAL SET-UP

The experimental set-up for this study was designed to closely simulate *in-vivo* operating conditions of modular hip implants. Inevitably, there existed several limitations that necessitated deviations from these conditions.

The high cost of manufacturing actual implants to the required specifications rendered it necessary to use a simplified model of the Morse taper head/neck junction. Compared to an implanted femoral stem, the support of the

male taper by the cylindrical base of the test specimen fixed in the holding device was likely more rigid. Flexure of the femoral stem/femur would absorb some of the applied load at the hip, thus partially alleviating the bending moment acting directly on the head/neck junction. Consequently, it is speculated that stresses in, and deflection of, the male tapers under the *in-vitro* testing conditions in this study were higher than those experienced *in-vivo*, which, in turn, may have resulted in greater relative motion between the coupled components.

Loading conditions employed in this study were influenced by several factors. The 30° orientation used for the experimental load, which was selected from the orientation range of hip reaction forces identified by Davy et al,[12] was necessarily fixed due to the design of the specimen holding fixtures. As a consequence, the heaviest overall damage (including wear and corrosion) occurred at the base in quadrant 3 of the male tapers. This result is similar, however, to observations made on retrieved implants.[41,43,44]

With regard to load magnitude, initially the tapers were subjected to a maximum load of approximately 3 X BW. Based on the results of the tests, however, this was increased to approximately 5.5 X BW, which represents a worst case *in-vivo* loading scenario, to maximize the opportunity for detecting differences in wear between test groups.

Finally, the experimental load was applied at a frequency of 5 Hz; a value which may be considered high compared to realistic physiologic loading. This decision involved consideration of a feasible time frame for conducting the study, as well as of the effects of frequency and number of cycles on fretting wear. Theoretically, fretting wear, as measured by weight loss, decreases with increasing frequency up to approximately 10 Hz, but increases with the number of cycles up to steady state conditions believed to occur within the first million cycles.[50] Based on extrapolation from data presented by Waterhouse[50] the testing conditions of 5 Hz and 2 million cycles used in this study likely produced

greater wear than if testing were conducted at a more realistic frequency of 1 Hz for the same period of time (equating to only 400,000 cycles).

Despite these deviations from *in-vivo* operating conditions, since each test group was subjected to similar conditions the effects of the different taper design parameters on fretting wear can still be validly inferred from these results.

5.2 LIMITATIONS OF ANALYSIS

As demonstrated by the assembly test the damage to the machining peaks observed on the tapers was at least partially due to the initial locking of the two surfaces. If this initial deformation had been homogeneous over the entire contact area it may have been possible to account for the assembly damage in both the qualitative and quantitative results, however, evidence showed this was not the case. This outcome may have been the result of out-of-roundness circumferentially, and/or waviness of the surface longitudinally. Consequently, the analyses performed in this study necessarily assessed damage caused by both assembly and wear combined.

5.2.1 Qualitative Analysis

The wear classification results for the five test groups whose tapers had a rough surface finish (L0R, L-8R, S0R, S-8R, S+8R) were comparable based on the assumption that wear bands of similar widths represented approximately equivalent volumes of removed material. For the smooth tapers (L0S), however, the original machining marks were not volumetrically equivalent to those from the rough tapers, and because of this associated quantitative difference the wear classification results for the L0S test group could not be compared with the other test groups.

5.2.2 Quantitative Analysis

From the literature it had previously been reported that fretting wear of modular components manifested as small patches or scars randomly dispersed over the contact area of the tapers.[47] In anticipation of similar findings, profilometry was selected as the method for quantification analysis because it provided the advantage of direct physical measurement of material removal over other common quantification methods such as weight loss or particle counting. In this experiment, however, there were no well-defined localized fretting scars observed, but rather widespread damage of the machining peaks over the entire surface. Consequently, to get an accurate representation of the overall damage on the tapers would have required numerous scans randomly covering the entire contact area. In the current study, the number of scans obtained from each taper was limited to an average of five because of the time required to perform each scan. Due to this limitation, more data were collected from zones providing greater contrast in wear between test groups (i.e. base and tip), and less from the mid-taper zones that exhibited more homogeneous wear. With each scan contributing between 10 and 12 data points, the results were very sensitive to the location from which they were taken. Furthermore, since the reliability of statistical inference depends strongly on random sampling and the law of large numbers, neither of which criterion was strictly satisfied in this study, the statistics presented must be interpreted with caution. Consequently, while the quantitative results presented in this study are strongly suggestive of differences in wear between test groups, they probably should not be considered absolutely conclusive. One way to corroborate these findings would be to supplement the results using a second method of quantitative analysis such as particle counting of testing fluid surrounding the taper junction.

The presence of the black deposits believed to be oxides adherent to the taper surfaces presented some problems with regard to the measurement of

wear from these areas, however, it should be recognized that this is also a source of error for the other two common methods of fretting wear quantification. For example, oxidized wear debris adherent to components measured for weight loss would result in a lower weight loss value, and similarly this adherent debris would not be detected if particle counting of the testing fluid were the method used for quantifying wear. Fortunately, in this study uncontaminated surface profiles of the tapers exhibited a distinct pattern in the inter-peak recesses as seen in Figures 4.13 - 4.16, and deviations from this pattern revealed the presence of extraneous deposits. Any wear measurements believed to be erroneous were, therefore, discarded from the data.

5.3 ANALYSIS OF RESULTS

Damage to the machining peaks had three distinct appearances as shown in Figure 4.5. The majority of the damaged peaks had longitudinal striations running perpendicular to the original machining marks. Although similar striations were observed on some of the machining peaks deformed by the assembly test, the observed damage could have been caused by subsequent fretting as well. Since fretting wear is an adhesive wear mechanism whereby material is removed from the surface by a stick and slip process,[50] the appearance of longitudinal striations parallel to the direction of relative motion is not atypical for this type of wear. Consequently, it was impossible to ascertain what process caused the damage observed on the tested specimens. The presence of copious black deposits and apparent pitting was strong evidence indicating that fretting was partially responsible for some of the observed damage.

To explain the mechanism of damage causing the smooth appearance of several of the wear bands two possibilities were considered. The peaks may have been flattened by direct impact of the two surfaces due to toggling of the

female component, or may have undergone cyclic compressive stress in the absence of slip, a scenario which may occur on the lateral aspects of the tapers. No correlation was detected between the location where the described causative motion would likely occur and the region where the damage was observed.

The multidirectional scoring was also considered to be the result of toggling where relative motion of the two coupled components was not necessarily strictly longitudinal. This damage, however, was not exclusive to the mismatched tapers which would be more predisposed to this type of motion.

In addition to mechanical damage, SEM revealed possible evidence of corrosive activity. The dark cracked laminae adhered to the taper surface (Figure 5.1a) were reminiscent of the layers of oxide (a product of fretting corrosion) compacted to the taper surfaces of retrieved modular heads described by Gilbert et al.[42] (Figure 5.1b). Furthermore, energy dispersive x-ray spectra

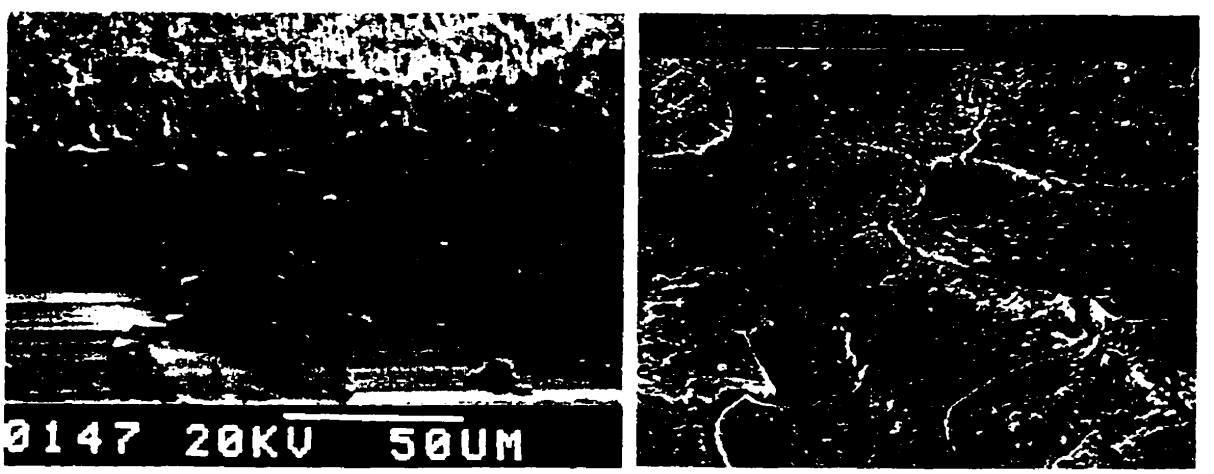

FIGURE 5.1 **a** Dark cracked lamina adherent to surface of male taper from S+8R test group of current study. **b** Compacted oxide layer observed on taper surface of retrieved modular head. (Reproduced from reference 42)

obtained from these laminae (Figure 5.2a) were comparable to spectra reported by Urban et al.[52] which were obtained from mixed oxides within the taper junction of retrieved specimens (Figure 5.2b). In the same study Urban also identified Co and Cr chlorides within the junction, and orthophosphate at the base of the contact junction, however, only one spectrum obtained in this study had a discernible Cl peak, and only small P peaks were seen on a few spectra.

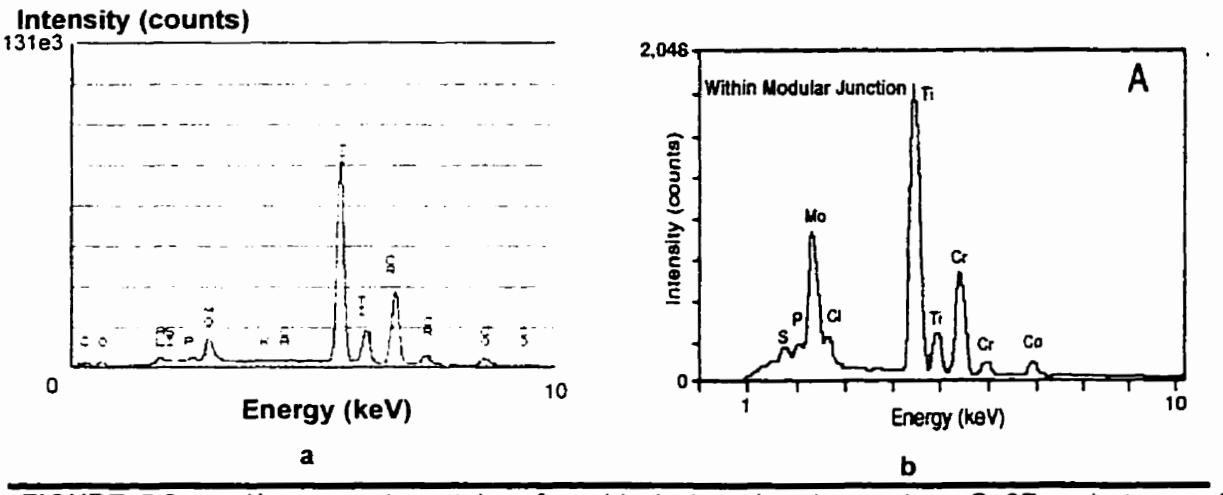

FIGURE 5.2 **a** X-ray spectrum taken from black deposits observed on S+8R male taper of current study. **b** X-ray spectrum of a black corrosion deposit taken from the modular junction of a retrieved implant. (Reproduced from reference 52)

Elongated micropits observed on some of the worn machining peaks (Figure 5.3a) strongly resembled damage to Ti alloy necks reported by other authors. The damage on a retrieved Ti alloy neck shown in Figure 5.3b, reported by Gilbert et al.,[46] was attributed to corrosive attack. Similar findings (Figure 5.3c) observed on the Ti alloy neck of *in-vitro* tested implants were reported by Bobyn et al.[47] In their study the head/neck junction was tested under dry conditions, suggesting that the pits were generated from a mechanical process rather than a chemical one. In the current study x-ray spectra taken

from within these pits revealed the presence of Cr and Co originating from the female component, which could result from either process.

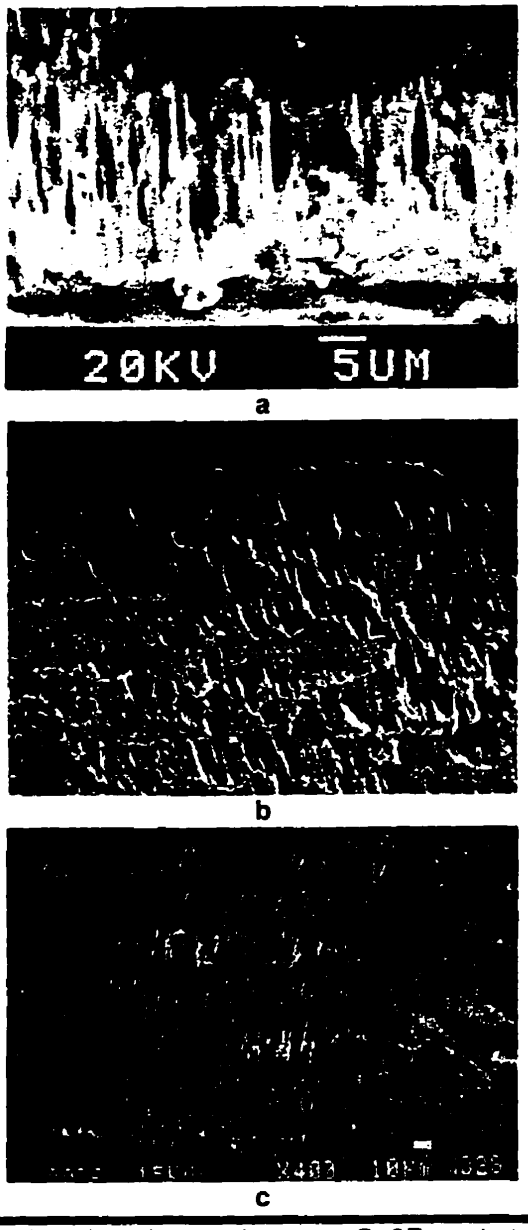

FIGURE 5.3 **a** Elongated micropits observed on an S+8R male taper from the current study. **b** Damage on a retrieved Ti alloy neck which was attributed to corrosive attack. (Reproduced from reference 46) **c** Similar micropitting observed on the Ti alloy neck of an implant tested *in-vitro* under dry conditions suggesting mechanical pitting. (Reproduced from reference 47)

5.3.1 Surface Finish

The effect of surface finish was only investigated on large tapers with 0 mismatch (L0S).

The high incidence of moderate and severe wear resulting from the qualitative analysis of these tapers seemed to indicate that fretting was worse with the smooth surface finish, however, as previously discussed in section 5.2.1 the wear classifications used for the smooth tapers were not equivalent in terms of debris generation to those used for the rough tapers. Comparing the non-contact surface profiles obtained from smooth and rough tapers (L0S vs L0R) shown in Figure 4.11 revealed that the volume of material that could potentially be removed from the machining marks of the smooth tapers was considerably less than from those of the rough tapers. For example, hypothetically, if the entire contact surface of a smooth taper were completely worn so that all original machining marks were totally obliterated (a worse scenario than that which occurred in this study) the volume of debris generated from the taper would be roughly equivalent to the volume generated if the tip 50% of the original machining peaks were worn from a rough taper with an equivalent contact area. Furthermore, this volume represents approximately only 25% of the total volume of material contained in the machining marks of the rough tapers. Since profilometry could not produce a quantitative measure of the wear sustained by the L0S tapers in this study no definite conclusion can be drawn with regard to the effect of surface finish on fretting wear. The indication that the potential for debris generation from smooth tapers was less compared to rough tapers certainly warrants further investigation.

5.3.2 Taper Mismatch

It has been postulated that taper mismatch resulting from loose design tolerances used for manufacturing the Morse taper connection of modular implants results in increased relative motion between components increasing the potential for fretting damage.

The incidental findings reported by Cook et al.[45] seemed to indicate that taper mismatch did affect particle debris generation, although taper mismatch was not one of the controlled variables in their study. Furthermore, greater amounts of debris were detected from tip engaged couplings compared to base engaged.

The investigation by Brown et al.[38] into the effect of taper mismatch on fretting current revealed higher fretting currents were produced with tip engaged tapers compared to base engaged, but the effect of increasing taper mismatch was desultory. A mismatch of +1' (base engaged) produced lower currents than either a 0 or a +2' mismatch, and greater fretting currents were obtained from a -1' (tip engaged) mismatch than from either a 0 or a -2' mismatch.

In the current study taper mismatch was investigated for both large (L-8R vs L0R) and small (both S+8R and S-8R vs S0R) tapers, and the results suggested no significant increase in fretting wear due to negative or positive mismatch for either large or small tapers. Compared to the L0R test group, the overall mean wear for the L-8R test group was less than 1.3 times higher which was not significant. Furthermore, this was considered to be an overestimate since data from the mid-taper zone, which would lower the overall mean value, were not included in the results for the L-8R tapers. A similar outcome was observed with the small tapers for both ±8' mismatch test groups (S+8 and S-8R). A maximum difference in overall mean wear of roughly 1.2-fold (not statistically significant) occurred between the S0R and S-8R test groups, and, again, data from the mid-

taper zone were not included in the latter results. Furthermore, the S-8R tapers were tested for three million cycles longer than the S0R tapers, and although the wear rate at this stage of the fretting wear process is believed to be low,[50] this would nevertheless likely contribute to the observed increase.

Although limitations of the quantitative analysis preclude drawing definitive conclusions, the fact that taper mismatch had no significant effect on fretting wear measurements in three different test groups (L-8R vs L0R, S-8R vs S0R, and S+8R vs S0R) in this study provided strong evidence supporting the conclusion that mismatch is not the predominant factor affecting fretting.

On the other hand, qualitative analysis revealed that taper mismatch did affect fluid ingress into the taper junction. Test specimens which engaged at the base of the tapers (L-8R and S-8R) seemed to substantially limit the amount of fluid penetrating the junction, whereas tip engaged tapers (S+8R) were partially covered with a flaky film indicative of fluid ingress. It was also noted that taper pairs with no mismatch (L0R and S0R) also allowed considerable fluid to permeate the junction indicating that these tapers engaged at the tip. These results may be important since fluid replenishment at the junction by a pumping action would possibly facilitate the release of wear particles, and/or corrosion.

Also demonstrated by the results of this study was the effect of taper mismatch on the distribution of wear which may also significantly affect the amount of debris liberated from the taper junction. Tapers from the L0R and S0R test groups produced greater wear at the tip of the male tapers (also suggesting tip engagement), whereas the L-8R (base engaged) tapers produced more wear in the base zone (this did not hold true for the S-8R tapers), the most severe wear occurring at the extreme edge of the taper junction. Since debris generated in this area can escape the junction more easily than that produced further up, base engaged tapers may potentially release greater amounts of

wear debris despite the absence of fluid ingress. Finally, wear measurements from the three longitudinal zones of the S+8R tapers were more equal, corroborating similar findings reported by Brown et al.[38] that tip engaged tapers appear to wear over the entire contact area as opposed to in localized regions.

5.3.3 Taper Size

The design parameter that appeared to have the greatest effect on fretting damage of the Morse taper head/neck junction was taper size. The overall mean wear measurements for the small tapers (S0R and S-8R) were almost double those of the analogous large tapers (L0R and L-8R), a statistically significant increase. The two taper sizes used in this study effected a change in two factors that could significantly influence fretting damage; a two-fold difference in contact area which, in turn, affects surface contact stresses, and a four-fold difference in flexural rigidity. It is surmised that the increased wear of the small tapers was due to the decrease in flexural rigidity compared to the large tapers (Appendix 1) which resulted in a noticeable difference in the amount of flexing of the tapers during testing. This suggests that flexing of the male component is the predominant factor contributing to fretting. In order to verify this, an investigation could be conducted on two tapers test designed so that the taper with a larger diameter, thus a greater flexural rigidity, had a decreased taper height but equivalent taper angle so that the contact area between the two sizes remained constant.

It was further noted in this study that even perfectly fit small tapers (S0R) had a greater overall mean wear value (>1.5 times higher) than the large tapers with a -8' mismatch (L-8R). These results imply that with small tapers, regardless of the fit of the coupled components, there is still considerable fretting

producing wear. Again, this might possibly have occurred because of flexure or interface shear during cyclic loading.

Interestingly, in the *in-vitro* study conducted by Barrack and Jani[63] comparing two commercially available femoral hip prostheses, the implants which produced obvious evidence of fretting wear and higher levels of corrosion products were those with the smaller diameter tapers, although other significant differences between the two test groups preclude a definitive attribution to this factor.

The most striking difference between large and small tapers observed in the current study was the presence of ostensible fretting corrosion manifested as adherent oxides on the majority of small tapers.

5.3.4 Relevance of Results to Fretting Corrosion

Several studies have been conducted in attempt to identify the mechanism responsible for corrosion at connection sites of modular components. It is now widely accepted that mechanical breakdown of the protective oxide layer covering the metals is key to its initiation, although there is still some question as to what promotes the corrosion process once started. Gilbert et al.[46] proposed a modification of classic crevice corrosion theory. They suggest that high local shear stresses at the modular interface are responsible for the initial breakdown of the oxide film, and subsequent reoxidation of exposed metal depletes the oxygen supply producing a high concentration of free metal ions in the crevice which, in turn, attracts chloride ions that form metal-chlorides. The metal chlorides subsequently react with water to form metal hydroxides and hydrochloric acid producing an aggressive environment with pH levels as low as 3[40] which accelerates the corrosion rate.

In the current study it is questionable whether the conditions within the taper junction were such that the oxygen supply was depleted, a key event in the crevice corrosion process. Since there was no tight seal on the fluid chamber, diffusion of oxygen from the atmosphere to the testing fluid was possible. Furthermore, vibration of the system prevented stagnation of the testing fluid, and the progressive formation of undulated flakes at the taper junction was considered evidence that fluid was being pumped in and out of the taper junction. Under these conditions it seems likely that the oxygen within the crevice was at least partially replenished during cyclic loading.

Detection of constant oxygen levels within the crevice of modular junctions has previously been reported by Gilbert et al.,[40] although they believed this observation to be due to a deficiency in the detection method. Monitoring the electrochemical conditions within the taper junction confirmed that pH and chlorine changes were consistent with crevice corrosion theory, but oxygen levels did not decrease as expected. The authors surmised that this was due to incomplete sealing of the monitoring electrodes as opposed to replenishment of oxygen from the testing fluid.

The influence of taper size on fretting corrosion has previously been suggested by Brown et al.[65] who demonstrated that male tapers with larger average diameters (larger root diameters and smaller taper angles) produced much lower fretting corrosion rates.

In the current study ostensible oxidation indicative of fretting corrosion was observed microscopically on all but one of the small tapers. None of the large tapers appeared to have any fretting corrosion products when examined under the stereomicroscope, although a limited number of very small patches were detected under the SEM at magnifications greater than 600X. Furthermore, the appearance of pitting, which was frequently observed in these same areas, was

confined to the worn surfaces and did not appear to attack the inter-peak valleys. If their genesis was chemical corrosive attack as suggested by Gilbert et al.[46] this finding gives credence to the theory that mechanical destruction of the passive oxide layer is a necessary antecedent for corrosion to occur.

On the other hand, the localization of fretting corrosion at the base in quadrant 3 of small tapers despite clear evidence of wear in conjunction with fluid ingress in other basal areas of both small and large tapers seemed to indicate that mere breakdown of the passive layer does not necessarily lead to corrosive attack. This was also suggested by Collier et al.[26] who reported that although other modular connection sites such as snap fit collars, sleeves, and bullet tips, frequently exhibited fretting wear, corrosion was generally limited to the head/neck junction.

One factor which may be implicated by these results are stresses within the taper due to loading. Finite element analysis has identified the base on the compressive side of the taper (corresponding to quadrant 3 in this study) as one region where the highest stresses occur under compressive and bending loads.[66] Using the parameters of the current study, theoretically it can be shown that in this region the compressive stress in the small tapers due to the axial load component could have been as high as twice that in the large tapers, and that stress due to the bending moment induced by the transverse load component could have been three times as high (Appendix 1). In addition, toggling of the female component may have also further increased the stresses in quadrant 3 of the tapers by radial compression.

It is hypothesized that the high accumulative compressive stresses in the distal portion in quadrant 3 of the small tapers generated a localized anodic stress concentration cell which enhanced corrosive attack[67] after breakdown of the protective oxide layer.

Finally, with regard to inducing corrosion, neither surface finish nor taper mismatch seemed to be a significant factor in this study. There was virtually no evidence of fretting corrosion or pitting on large tapers with either rough or smooth surface finishes, whereas small tapers with a rough surface finish exhibited considerable fretting corrosion and some pitting. Similarly, large tapers with a taper mismatch had no obvious fretting corrosion, unlike the small tapers with the same mismatch. All evidence from this study seemed to suggest that the most influential factor to fretting damage is related to the size of the tapers. In view of the high cost associated with manufacturing components to very high tolerances these results are very important to the implant manufacturing industry, but further investigation is necessary to corroborate these results.

5.4 SUGGESTIONS FOR FUTURE STUDIES

During the course of this investigation many issues were raised that warrant further investigation.

While profilometric analysis provided the advantage of direct measurement of wear over other analysis methods, the data were not sufficient to draw definitive conclusions. Conducting a study in which profilometric data is corroborated with particle counting data would give credence to the final conclusions.

There is some question as to whether pitting observed on tapers damaged by fretting is the result of a chemical or a mechanical process. Examination of the female tapers in conjunction with the male tapers may elucidate the genesis of pitting, providing valuable information to the corrosion issue.

It is believed that stresses play an important role in fretting damage, however, this is still purely conjectural. Microstructural examination of the surface and subsurface of both male and female components may reveal stress

induced changes that could be compared between regions within the taper, as well as between tapers with different design parameters.

The potential for a smooth surface finish to generate less volumetric wear needs to be reinvestigated using a more effective quantitative analysis method. Furthermore, the effect of a smooth surface finish on small tapers compared to large tapers still remains to be evaluated.

In order to isolate the effect of contact area (i.e. contact stress) from flexural rigidity a study should be conducted in which taper diameter and angle remain constant while changing the contact area between coupled components. Conversely, flexural rigidity could be investigated while maintaining a constant contact area. Quantification of the magnitude of flexing with tapers of different flexural rigidities would also add valuable information to the findings of such a study.

The current study revealed that taper roundness and surface waviness are likely factors affecting contact between coupled components and thus influence fretting. In subsequent studies these parameters should be controlled.

Finally, several *in-vivo* studies of retrieved implants have been conducted in which the implants are grouped according to various parameters such as material couplings, duration of implantation, neck extensions, manufacturers, etc. To date, no retrieval studies have been conducted to investigate the possible effects of taper size on fretting wear and fretting corrosion *in-vivo*.

6 CONCLUSION

Previous studies have demonstrated that the Morse taper connection between modular components of total hip implants are susceptible to fretting. This process can generate large amounts of particulate debris, and may play a significant role in the initiation and promotion of corrosion within the junction. In view of the potential problems associated with the release of particulate debris and corrosion products into the joint space this study investigated the effect of surface finish, taper mismatch, and taper size on the fretting behaviour of the Morse taper connection. In order to strictly control the engineering parameters under investigation a simplified model of a Morse taper femoral head/neck junction was designed and fabricated. After being subjected to simulated physiologic loading conditions, damage to the male taper surfaces was analysed qualitatively using microscopic methods and quantitatively using profilometric methods. Profilometric analysis was unsuccessful at quantifying damage to tapers with a 0.2 μm RMS surface finish, but it was instrumental in demonstrating that the volume of material in the original machining marks of these tapers was less than for those with a 1.6 μm RMS surface finish, leading to the conclusion that the smooth surface finish had the potential to generate less volumetric wear. This finding requires further investigation. Taper mismatches of +8' and -8' had no substantial effect on the fretting of these modular junctions. Finally, smaller tapers with half the contact area and one quarter the flexural rigidity produced significantly higher overall linear wear values, and exhibited surface damage indicative of fretting corrosion which was not apparent on the larger tapers. These results strongly suggested that the most influential factor with regard to fretting wear and fretting corrosion was taper size. Further investigation using more than one method of quantitative analysis is recommended to corroborate the findings of this study.

REFERENCES

1. Ahmed, A.H.: Class Notes, **Biomechanics of the Musculoskeletal System**, Montreal: McGill University, January 1996, p. 1.11.

2. Moore, K.L.: **Clinically Oriented Anatomy**, 3rd edition, Baltimore: Williams and Wilkins, 1992, pp. 373-477.

3. Palastanga, N., Field, D., Soames, R.: **Anatomy and Human Movement - Structure and Function**, 2nd edition, Oxford: Butterworth-Heinemann Ltd., 1994, pp. 414-441.

4. Agur, A.M.R.: **Grant's Atlas of Anatomy**, 9th edition, Baltimore: Williams and Wilkins, 1991, p. 259.

5. Shrive, N.G., and Frank, C.B.: **Joints**, in Nigg, B.M., and Herzog, W. (eds.), *Biomechanics of the Musculo-skeletal System*, New York: John Wiley and Sons Ltd., 1994, pp. 191-198.

6. Palastanga, N., Field, D., Soames, R.: **Anatomy and Human Movement - Structure and Function**, 2nd edition, Oxford: Butterworth-Heinemann Ltd., 1994, pp. 10-12.

7. McLeish, R.D., and Charnley, J.: **Abduction Forces in the One-Legged Stance**, *Journal of Biomechanics*, Vol. 3, 1970, pp. 191-209.

8. Paul, J.P.: **Loading on Normal Hip and Knee Joints and on Joint Replacements**, in Schaldach, M. and Hohmann, D. (eds.), *Advances in Artificial Hip and Knee Joint Technology*, Berlin: Springer-Verlag, 1976, pp. 53-70.

9. Patriarco, A.G., Mann, R.W., Simon, S.R., and Mansour, J.M.: **An Evaluation of the Approaches of Optimization Models in the Prediction of Muscle Forces During Human Gait**, *Journal of Biomechanics*, Vol. 14, No. 8, 1981, pp. 513-525.

10. Crowninshield, R.D., Johnston, R.C., Andrews, J.G., and Brand, R.A.: **A Biomechanical Investigation of the Human Hip**, *Journal of Biomechanics*, Vol. 11, 1978, pp. 75-85.

11. Seireg, A., and Arvikar, R.: **Biomechanical Analysis of the Musculoskeletal Structure for Medicine and Sports**, New York: Hemisphere Publishing Corp., 1989, pp. 155-229.

12. Davy, D.T., Kotzar, M.S., Brown, R.G., Heiple, K.G., Goldberg, V.M., Heiple Jr., K.G., Berilla, J., and Burstein, A.H.: **Telemetric Force Measurements Across the Hip After Total Arthroplasty**, *Journal of Bone and Joint Surgery*, Vol. 70-A, No. 1, 1988, pp. 45-50.

13. English, T.A., and Kilvington, M.: **In-Vivo Records of Hip Loads Using a Femoral Implant With Telemetric Output (A Preliminary Report)**, *Journal of Biomedical Engineering*, Vol. 1, No. 2, 1979, pp. 111-115.

14. Booth, R.E., Balderston, R.A., Rothman, R.H.: **Total Hip Arthroplasty**, Philadelphia: W.B. Saunders Co., 1988, pp. 279-280.

15. Kumar, V., Cotran, R.S., Robbins, S.L.: **Basic Pathology**, 5th edition, Philadelphia: W.B. Saunders Co., 1992, pp. 145-695.

16. Shands, A.R. Jr.: **Historical Milestones in the Development of Modern Surgery of the Hip Joint**, in Tronzo, R.G. (ed.), *Surgery of the Hip Joint*, Vol. 1, 2nd edition, New York: Springer-Verlag, 1984, pp. 1-26.

17. Waugh, W.: **John Charnley: The Man and the Hip**, London: Springer-Verlag Ltd., 1990, pp. 99-138.

18. Eftekhar, N.S.: **Principles of Total Hip Arthroplasty**, St. Louis: The C.V. Mosby Co., 1978, pp. 1-8.

19. Amstutz, H.C., Clarke, I.C.: **Evolution of Hip Arthroplasty**, in Amstutz, H.C. (ed.), *Hip Arthroplasty*, New York: Churchill Livingstone Inc., 1991, pp. 1-14.

20. Weber, B.G., and Stuhmer, G.: **The Trunnion Bearing Total Hip Prosthesis**, in Schaldach, M. and Hohmann, D. (eds.), *Advances in Artificial Hip and Knee Joint Technology*, Berlin: Springer-Verlag, 1976, pp. 203-209.

21. Weber, B.G.: **Total Hip Replacement with Rotation-Endoprosthesis [Trunnion-Bearing Prosthesis]**, *Clinical Orthopaedics and Related Research*, No. 72, 1970, pp. 79-84.

22. Christiansen, T.: **A Combined Endo- and Total Hip Prosthesis with Trunnion-Bearing**, *Acta Chirurgica Scandinavica*, No. 140, 1974, pp. 185-188.

23. Sundal, B., Kavlie, H., and Christiansen, T.: **Total Hip Replacement with a New Trunnion-Bearing Prosthesis (The Christiansen Prosthesis)**, *Acta Chirurgica Scandinavica*, No. 140, 1974, pp. 189-193.

24. Harris, W.H.: **A New Total Hip Implant**, *Clinical Orthopaedics and Related Research*, No. 81, 1971, pp. 105-113.

25. Oberg, E., Jones, F.D., and Horton, H.L., Ryffel, H.H.: **Machinery's Handbook**, 24th edition, New York: Industrial Press Inc., 1992, p. 926.

26 Collier, J.P., Mayor, M.B., Williams, I.R., Surprenant, V.A., Surprenant, H.P., and Currier, B.H.: **The Tradeoffs Associated With Modular Hip Prostheses**, *Clinical Orthopaedics and Related Research*, No. 311, 1995, pp. 91-101.

27. Pellicci, P.M., and Haas, S.B.: **Disassembly of a Modular Femoral Component During Closed Reduction of the Dislocated Femoral Component**, *Journal of Bone and Joint Surgery*, Vol. 72-A, No. 4, 1990, pp. 619-620.

28. Woolson, S.T., and Pottorff, G.T.: **Disassembly of a Modular Femoral Prosthesis After Dislocation of the Femoral Component**, *Journal of Bone and Joint Surgery*, Vol. 72-A, No. 4, 1990, pp. 624-625.

29. Barrack, R.L., Burke, D.W., Cook, S.D., Skinner, H.B., and Harris, W.H.: **Complications Related to Modularity of Total Hip Components**, *Journal of Bone and Joint Surgery*, Vol. 75-B, No. 5, 1993, pp. 688-692.

30. Boggan, R.S., Paxson, M.E.C., and Stiehl, J.B.: **The Effect of Assembly Environment on the Distraction Strength of Modular Taper Connections**, *Trans. Orthopaedic Research Society*, New Orleans, Louisiana, February 1994, p. 807.

31. Gilbert, J.L., Buckley, C.a., Jacobs, J.J., Bertin, K.C., and Zernich, M.R.: **Intergranular Corrosion-Fatigue Failure of Cobalt-Alloy Femoral Stems**, *Journal of Bone and Joint Surgery*, Vol. 76-A, No. 1, 1994, pp. 110-115.

32. Bobyn, J.D., Tanzer, M.D., Krygier, J.J., Dujovne, A.R. and Brooks, C.E.: **Concerns With Modularity in Total Hip Arthroplasty**, *Clinical Orthopaedics and Related Research*, No. 298, 1994, pp. 27-35.

33. Svensson, O., Mathiesen, E.B., Reinholt, F.P., and Blomgren, G.: **Formation of a Fulminant Soft-Tissue Pseudotumor after Uncemented Hip Arthroplasty**, *Journal of Bone and Joint Surgery*, Vol. 70-A, No. 8, 1988, pp. 1238-1242.

34. Mathiesen, E.B., Lindgren, J.U., Blomgren, G., and Reinholt, F.P.: **Corrosion of Modular Hip Prostheses**, *Journal of Bone and Joint Surgery*, Vol. 73-B, No. 4, 1991, pp. 569-575.

35. Kumar, P., Hickl, A.J., Asphahani, A.I., and Lawley, A.: **Properties and Characteristics of Cast, Wrought, and Powder Metallurgy (P/M) Processed Cobalt-Chromium-Molybdenum Implant Materials**, in Fraker, C. and Griffin, C.D. (eds.), *Corrosion and Degradation of Implant Materials*, 2nd Symposium, ASTM STP 859, Philadelphia: American Society for Testing and Materials, 1985, pp. 30-56.

36. Collier, J.P., Surprenant, V.A., Jensen, R.E., Mayor, M.B., and Surprenant, H.P.: **Corrosion Between the Components of Modular Femoral Hip Prostheses**, *Journal of Bone and Joint Surgery*, Vol. 74-B, No. 4, 1992, pp. 511-517.

37. Kummer,F.J., and Rose R.M.: **Corrosion of Titanium/Cobalt-Chromium Alloy Couples**, *Journal of Bone and Joint Surgery*, Vol. 65-A, No. 8, 1983, pp. 1125-1126.

38. Brown, S.A., Flemming, C.A.C., and Payer, J.H.: **Modifications of Head Neck Extension and Taper Angle Mismatch To Reduce Fretting Corrosion of Modular Total Hips**, *Trans. Orthopaedic Research Society*, New Orleans, Louisiana, February 1994, p. 593.

39. Humphrey, S., Levine, D.L., Merchant, K., and Shareef, N.H.: **An Examination of Modular Joints in Hip Replacement Prostheses**, *Trans. Society for Biomaterials*, Bermingham, Alabama, April 1993, p. 278.

40. Gilbert, J.L., Buckley, C.A., Jacobs, J.J., and Lautenschlager, E.P.: **In-Vitro Mechanical-Electrochemical Testing of the Fretting Corrosion Process in Modular Femoral Tapers**, *Trans. Orthopaedic Research Society*, Orlando, Florida, February 1995, p. 240-40.

41. Bauer, T.W., Brown, S.A., Jiang, M., Panigutti, M.A., and Flemming, C.A.C.: **Corrosion in Modular Hip Stems**, *Trans. Orthopaedic Research Society*, Washington, D.C., February 1992, p. 354.

42. Gilbert, J.L., Buckley, C.A., Jacobs, J.J., and Urban, R.M.: **Mechanically Assisted Corrosive Attack in the Morse Taper of Modular Hip Prostheses**, *Trans. World Biomaterials Congress*, Berlin, Germany, April 1992, p. 267.

43. Cook S.D., Barrack, R.L., and Clemow, A.J.T.: **Corrosion and Wear at the Modular Interface of Uncemented Femoral Stems**, *Journal of Bone and Joint Surgery*, Vol. 76-B, No. 1, 1994, pp. 68-72.

44. Brown, S.A., Flemming, C.A.C., Kawalec, J.S., Placko, H.E., Vassaux, C., Merritt, K., Payer, J.H., and Kraay, M.J.: **Fretting Corrosion Accelerates Crevice Corrosion of Modular Hip Tapers**, *Journal of Applied Biomaterials*, Vol. 6, 1995, pp. 19-26.

45. Cook, S.D., Barrack, R.L., Baffes, G.C., Clemow, A.J.T., Serekian, P., Dong, N., and Kester, M.A.: **Wear and Corrosion of Modular Interfaces in Total Hip Replacements**, *Clinical Orthopaedics and Related Research*, No. 298, 1994, pp. 80-88.

46. Gilbert, G.L., Buckley, C.A., and Jacobs, J.J.: ***In Vivo* Corrosion of Modular Hip Prosthesis Components in Mixed and Similar Metal Combinations. The Effect of Crevice, Stress, Motion, and Alloy Coupling**, *Journal of Biomedical Materials Research*, Vol. 27, 1993, pp. 1533-1544.

47. Bobyn, J.D., Dujovne, A.R., Krygier, J.J., and Young, D.L.: **Surface Analysis of the Taper Junctions of Retrieved and *In Vitro* Tested Modular Hip Prostheses**, in Morrey, B.F. (ed.), *Biological, Material, and Mechanical Considerations of Joint Replacement*, New York: Raven Press, Ltd., 1993, pp. 287-301.

48. Lieberman, J.R., Rimnac, C.M., Garvin, K.L., Klein, R.W., and Salvati, E.A.: **An Analysis of the Head-Neck Taper Interface in Retrieved Hip Prostheses**, *Clinical Orthopaedics and Related Research*, No. 300, 1994, pp. 162-167.

49. Boggan, R.S., Lemons, J.E., Rigney, E.D., Chillag, K.C. and Kim W.C.: **Clinical and Laboratory Investigations of Fretting and Corrosion of a**

Modular Femoral Stem Design, *Trans. Society for Biomaterials*, Boston, Massachusetts, April 1994, p. 322.

50. Waterhouse, R.B. **Fretting Wear**, in *Friction, Lubrication, and Wear Technology*, ASM Handbook, Vol. 18, ASM International, 1992, pp. 242-256.

51. Krygier J.J., Bobyn J.D., Dujovne, A.R., Young, D.L., and Brooks, C.E.: **Strength, Stability, and Wear Analysis of a Modular Titanium Femoral Hip Prosthesis Tested in Fatigue**, *Trans. Fourth World Biomaterials Congress*, Berlin, Germany, April 1992, p.626.

52. Urban, R.M., Jacobs, J.J., Gilbert, J.L., and Galante, J.O.: **Migration of Corrosion Products From Modular Hip Prostheses**, *Journal of Bone and Joint Surgery*, Vol. 76-A, No. 9, 1994, pp. 1345-1359.

53. Jacobs, J.J., Urban, R.M., Gilbert, J.L., Skipor, A.K., Black, J., Jasty, M., Galante, J.O.: **Local and Distant Products From Modularity**, *Clinical Orthopaedics and Related Research*, No. 319, 1995, pp. 94-105.

54. Urban, R.M., Jacobs, J.J., Tomlinson, M.J., Black, J., Turner, T.M., and Galante, J.O.: **Particles of Metal Alloys and Their Corrosion Products in the Liver, Spleen, and Para-aortic Lymph Nodes of Patients with Total Hip Replacement Prostheses**, *Trans. Orthopaedic Research Society*, Orlando, Florida, February 1995, p. 241-40.

55. Dowd, J.E., Schwendeman, L.E., Doyle, S., Wilson, S., Larkin, L., Rubash, H.E., Evans, R., and Herndon, J.H.: **Aseptic Loosening: A Histologic and Biochemical Analysis in a Canine Model**, *Trans. Orthopaedic Research Society*, New Orleans, Louisiana, February 1994, p. 805.

56. Theiss, S.M., Luchetti, W., Baker, D.G., Cuckler, J.M., Ducheyne, P.: **A Quantitative, *In-Vivo*, Comparison of the Inflammatory Response to Submicron Ti64 and CoCr Particulates**, *Trans. Orthopaedic Research Society*, San Francisco, California, February 1993, p. 85.

57. Goldring, S.R., Bennett, N.E., Jasty, M.J., and Wang, J.T.: ***In Vitro* Activation of Monocyte Macrophages and Fibroblasts by Metal Particles**, in St. John, K.R. (ed.), *Particulate Debris from Medical Implants. Mechanisms of Formation and Biological Consequences*,

ASTM STP 1144, Philadelphia: American Society for Testing and Materials, 1992, pp. 136-142.

58. Shanbhag, A.S., Black, J., Jacobs, J.J., Galante, J.O., and Glant, T.T.: **Human Monocyte Response to Submicron Fabricated and Retrieved Polyethylene, Ti-6Al-4V and Ti Particles**, *Trans. Orthopaedic Research Society*, New Orleans, Louisiana, February 1994, p. 849.

59. Ohta, S., Graves, S., Rogers, S., Haynes, D., Hay, S., Pearcy, M., and Howie, D.: **Osteoblasts Release Il-6 and PGE_2 in Response to $TiCl_3$ and Conditioned Media from Macrophages exposed to TiAlV Wear Particles**, *Trans. Orthopaedic Research Society*, New Orleans, Louisiana, February 1994, p. 149-26.

60. Harada, Y., Brown, S., Merritt, K., Wang, J.T., Doppalapudi, V.A., Willis, A.A., Jasty, M., Harris, W.H., and Goldring, S.R.: **Effects of Metal Particles and Their Corrosion Products on Human Monocyte/Macrophages *In Vitro***, *Trans. Orthopaedic Research Society*, Orlando, Florida, February 1995, p. 776.

61. Jasty, J., Bragdon, C.R., Lee, K., Hanson, A., and Harris, W.H.: **Surface Damage to Cobalt-Chrome Femoral Head Prostheses**, *Journal of Bone and Joint Surgery*, Vol. 76-B, No. 1, 1994, pp. 73-77.

62. Isaac, G.H., Atkinson, J.R., Dowson, D., Wroblewski, B.M.: **The Role of Cement in Long-term Performance and Premature Failure of Charnley Low Friction Arthroplasties**, *Engineering in Medicine*, Vol. 15(1), 1986, pp. 19-22.

63. Barrack, R.L., and Jani, S.C.: **Effect of Taper Design Parameters on the Presence and Severity of Fretting Corrosion**, *Trans. Orthopaedic Research Society*, Atlanta, Georgia, February 1996, p. 488.

64. Brown, S. A., and Merritt, K.: **Fretting Corrosion in Saline and Serum**, *Journal of Biomedical Materials Research*, Vol. 15, 1981, pp. 479-488

65. Brown, S.A., Flemming, C.A.C., Merritt, K., and Payer, J.H.: **Fretting Corrosion Testing of Modular Hip Designs**, *Trans. World Biomaterials Congress*, Berlin, Germany, April 1992, p. 268.

66. Chao, E.Y., Kwak, B.M., and Kasman, R.: **Stress Analysis of Conical Coupling Joint in Modular Prosthetic System Design**, Trans. Orthopaedic Research society, Atlanta, Georgia, February 1984, p. 103.

67. Askeland, D.R.: **The Science and Engineering of Materials**, alternate edition, Boston: PWS Publishers, 1985, pp.501-502.

APPENDIX 1

EQUATIONS

(1) Flexural rigidity
(2) Compressive stress due to axial load
(3) Compressive stress due to bending moment

Flexural rigidity

Flexural rigidity of a mechanical component is a function of the material property, as well as the geometry of the component. For a cylindrical component the flexural rigidity is defined as follows:

$$flexural\ rigidity = EI = E\pi r^4 \quad (1)$$

where E = modulus of elasticity
I = moment of inertia
r = radius

In the current study the flexural rigidity (calculated at the taper base) of the large male taper was approximately four times that of the small taper.

$$flexural\ rigidity_{sm\ vs\ lg} = \frac{r_{lg}^4}{r_{sm}^4} \approx \frac{(\frac{0.653}{2})^4}{(\frac{0.472}{2})^4} = 3.7$$

where r_{lg} = radius at base of large taper
r_{sm} = radius at base of small taper

Compressive stress due to axial load

The compressive stress within a mechanical component due to an axial load is proportional to the load magnitude, and inversely proportional to the cross sectional area. For a component with a circular cross section the compressive stress is defined as follows:

$$\sigma_{(axial)} = \frac{F}{A} = \frac{F}{\pi r^2} \quad (2)$$

where F = axial load
A = cross sectional area
r = radius

In the current study, theoretically, the compressive stress in the small taper due to the axial load component could have been as much as twice that in the large taper, assuming rigid locking (i.e. negligible slip) between the coupled components.

$$\frac{\sigma_{(axial)_{sm}}}{\sigma_{(axial)_{lg}}} = \frac{r_{lg}^2}{r_{sm}^2} \approx \frac{(\frac{0.653}{2})^2}{(\frac{0.472}{2})^2} = 1.9$$

where r_{lg} = radius at base of large taper
r_{sm} = radius at base of small taper

Compressive stress due to bending moment

Transverse loads on a mechanical component cause bending moments which generate stress within the component. For a component with circular cross section the stress is defined as follows:

$$\sigma_{(bend)} = \frac{Mr}{I} = \frac{Mr}{\frac{1}{4}\pi r^4} \quad \textbf{(3)}$$

where M = bending moment due to transverse load
I = moment of inertia
r = radius

Given the situation in the current study the compressive stress on the side of the taper opposite the load caused by the transverse load component, theoretically, could have been more than 2.5 times as high in the small taper compared to the large taper. (Note: The following does not take into account the tensile stress in the taper at this location due to the counteracting moment generated by the offset axial component of the load.)

$$\frac{\sigma_{(bend)_{sm}}}{\sigma_{(bend)_{lg}}} = \frac{r_{lg}^3}{r_{sm}^3} \approx \frac{(\frac{0.653}{2})^3}{(\frac{0.472}{2})^3} = 2.6$$

where r_{lg} = radius at base of large taper
r_{sm} = radius at base of small taper

APPENDIX 2

DRAWINGS

A2.1 Wear test specimen - female component

A2.2 Wear test specimen - male component

Specimen Numbers	Dimensions (inches) D	H	Taper Angle A	Qty
1 - 5	0.632	0.654	5°56'	5
6 - 15	0.632	0.654	6°0'	10
16 - 20	0.451	0.428	5°56'	5
21 - 25	0.451	0.428	6°0'	5
26 - 30	0.451	0.428	6°4'	5

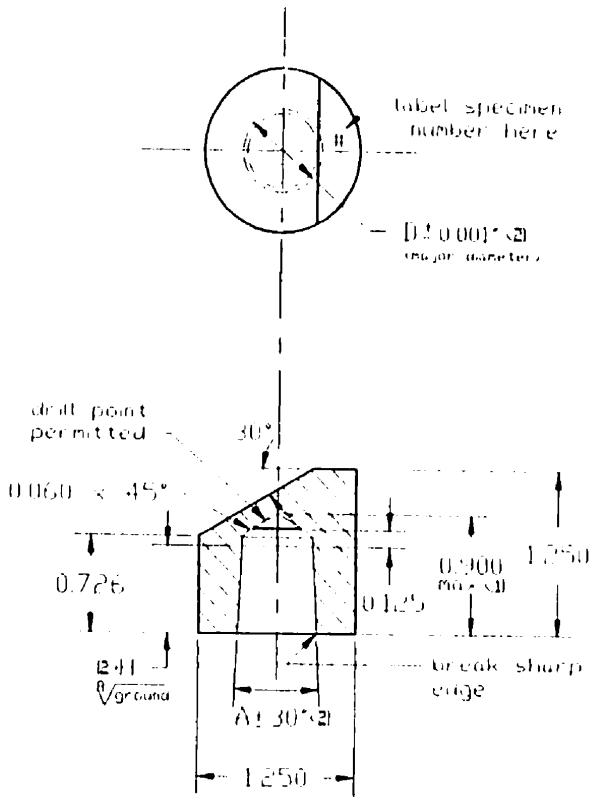

(1) Based on maximum draft tip point angle of 118 degrees

(2) Refer to table above

TITLE: Wear Test Specimen Female	MATERIAL: Co Cr Mo (as per ASTM F799-87)	
	DIMENSIONS IN INCHES	DATE: July 16th, 1993
SCALE: NTS	APPROVED BY:	DRAWN BY: D. Young
TOLERANCES: ±.001" unless other wise specified		REVISED: Sept. 16, 1993
ORTHOPAEDIC RESEARCH LAB MGH		DRAWING NUMBER: A2.1

Specimen Numbers	Dimensions (inches) D	Dimensions (inches) H	Taper Angle A	Surface Finish (RMS) B	Qty
1 - 5	0.653	0.854	6°4'	63 μin	5
6 - 10	0.653	0.854	6°0'	63 μin	5
11 - 15	0.653	0.854	6°0'	8 μin	5
16 - 20	0.472	0.628	6°0'	63 μin	5
21 - 25	0.472	0.628	6°4'	63 μin	5
25 - 30	0.472	0.628	5°56'	63 μin	5

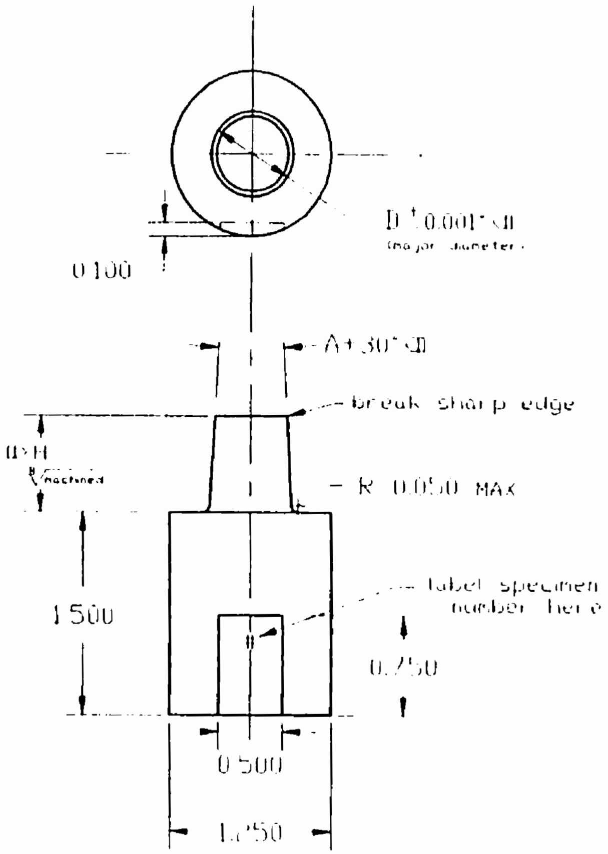

(1) Refer to table above

TITLE: Wear Test Specimen Male	MATERIAL: Ti6Al4V ELI (as per ASTM 136-84)	
	DIMENSIONS IN INCHES	DATE: July 16th 1993
SCALE: NBS	APPROVED BY:	DRAWN BY: DL Young
TOLERANCES: ±0.001" unless otherwise specified		REVISED: Sept. 15, 1993
ORTHOPAEDIC RESEARCH LAB - MGH		DRAWING NUMBER A22

APPENDIX 3

DRAWINGS

A3.1 CMM measurement locations - female component

A3.2 CMM measurement locations - male component

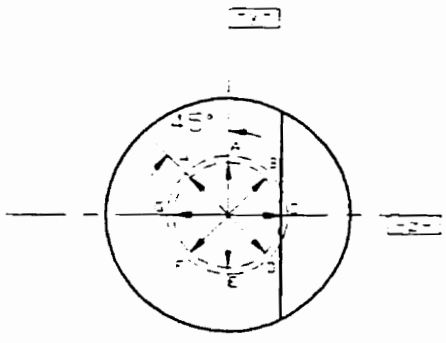

Dimensions to be measured at eight points around the circumference of the taper (see top view) at each of the three locations indicated in the front view.

Dimensions to be taken with respect to reference point at intersection of lines 1 and 2 on surface 3.

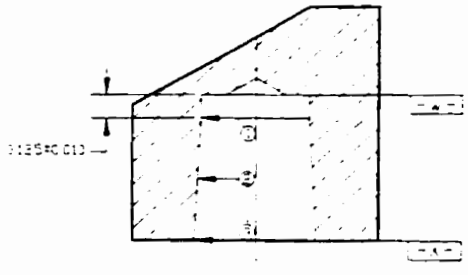

1. Tip of taper at 0.135" below M.
2. Midpoint
3. Baseline

TITLE Taper Measurements Female	MATERIAL Co-Cr-Mo	
	DIMENSIONS IN INCHES	DATE Aug 31 1993
SCALE NTS	APPROVED BY	DRAWN BY D.L. Young
TOLERANCES not applicable		REVISED Sept 29 1993
ORTHOPAEDIC RESEARCH LAB - MCH		DRAWING NUMBER A31

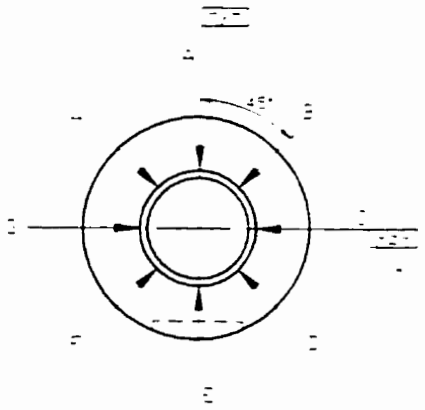

Dimensions to be measured at eight points around the circumference of the tube. See top view at the three heights indicated in the front view.

Dimensions to be given with respect to reference point at intersection of rear wall and the surface

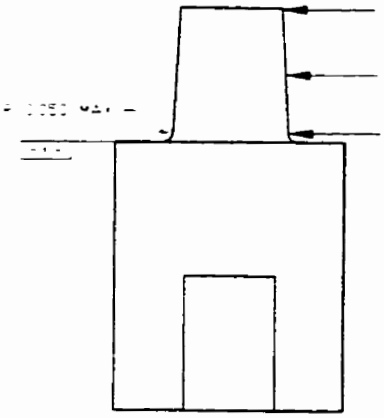

Top

Middle

Base at 1.180" min. above surface

TITLE: Tube Measurements		MATERIAL: 304 SS	
Value		DIMENSIONS IN INCHES	DATE: Aug 31 1993
SCALE: NTS	APPROVED BY:		DRAWN BY: DL Young
TOLERANCES: not specified			REVISED: Sept 29 1993
BIOTECHNOLOGY RESEARCH LAB - WSU			DRAWING NUMBER: A32

APPENDIX 4

DRAWINGS

A4.1 Holding fixture 1 - inclined plate

A4.2 Holding fixture 1 - base plate

A4.3 Holding fixture 1 - vertical plate

A4.4 Holding fixture 1 - assembly

A4.5 Specimen holding plate

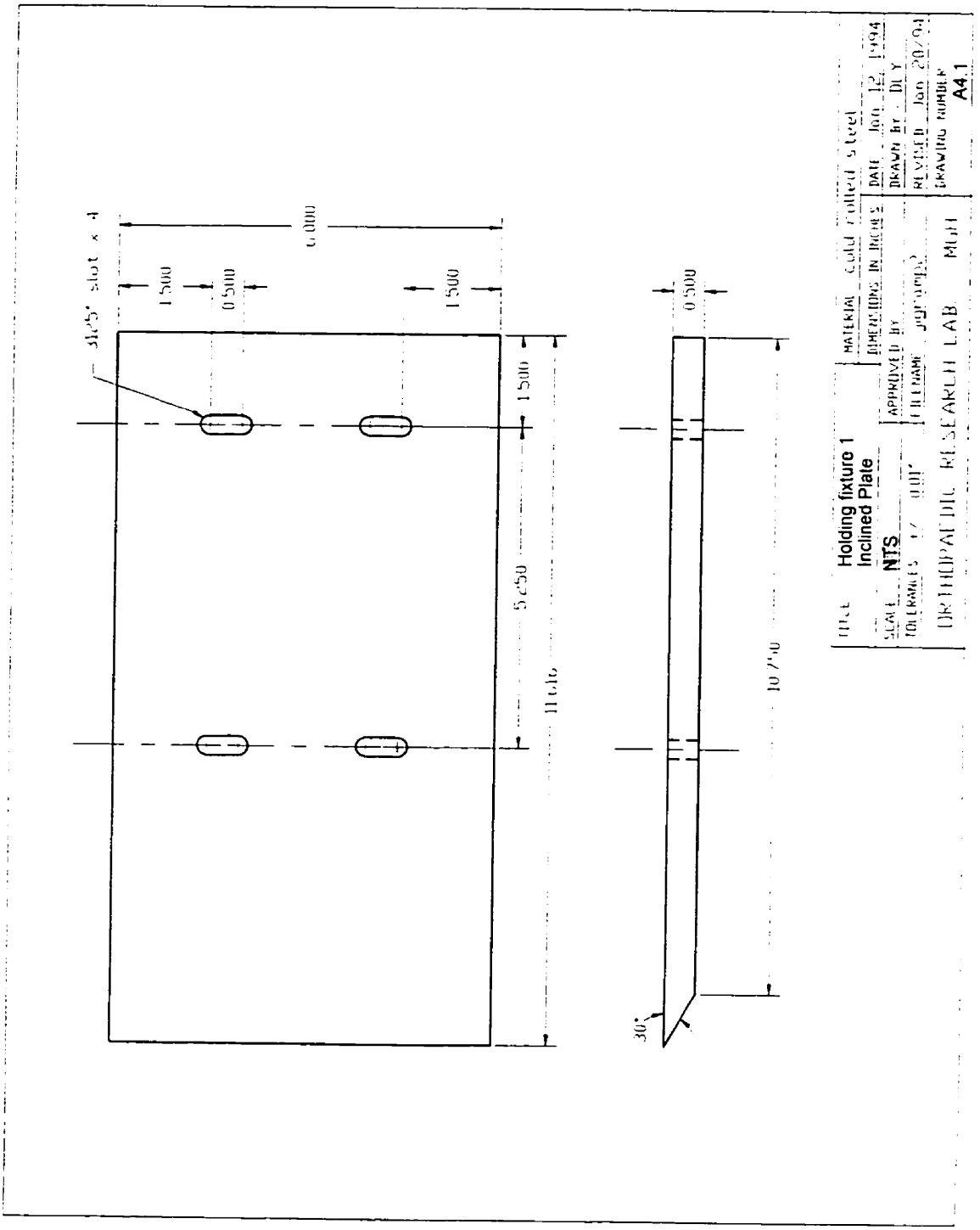
Holding fixture 1
Inclined Plate
NTS
A4.1
1500
1500
1500
0500
0500
5250
30°

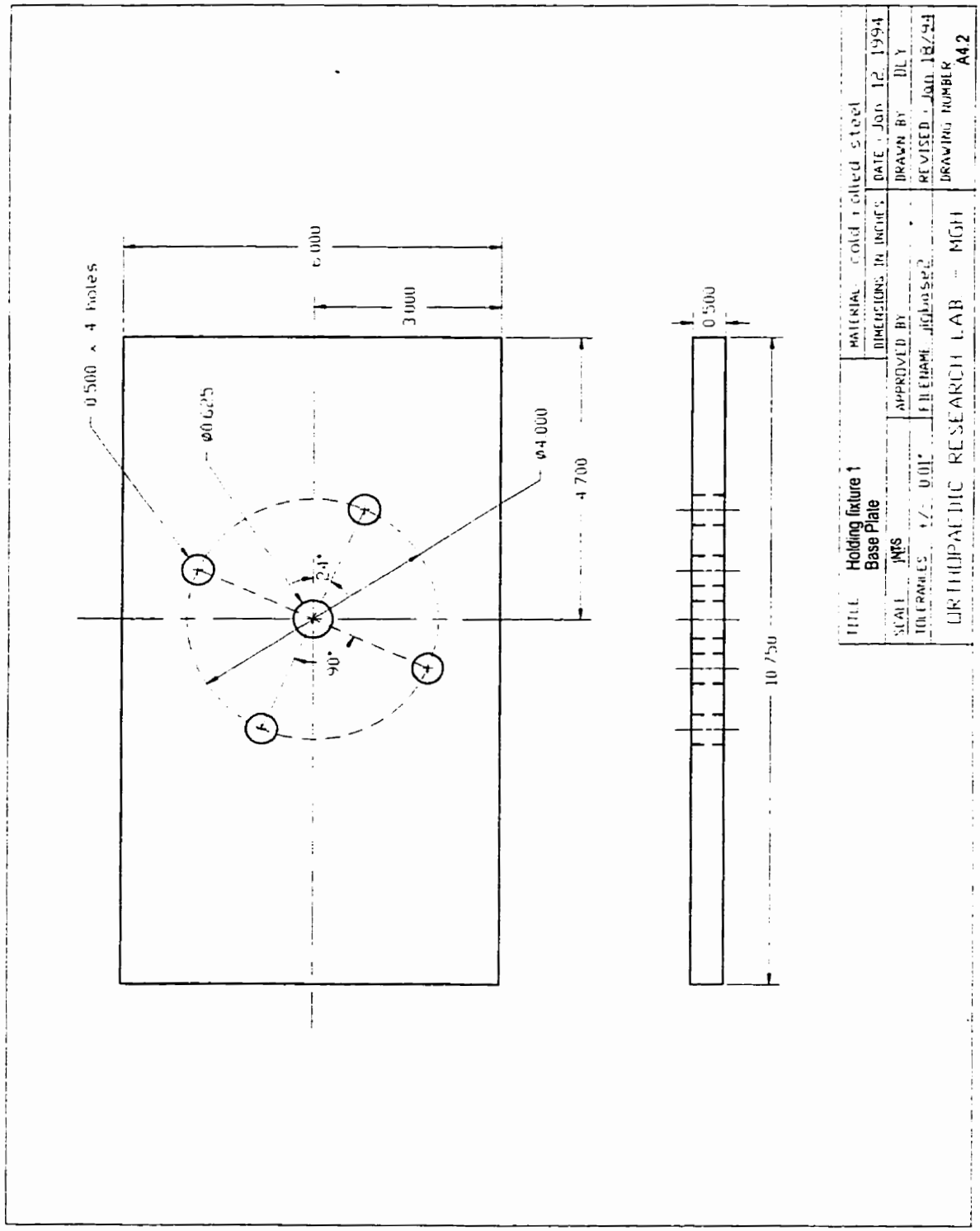
0.500 x 4 holes
Ø0.625
6.000
3.000
Ø4.000
4.700
24°
90°
0.500
10.750
TITLE Holding fixture 1 Base Plate
MATERIAL cold rolled steel
DIMENSIONS IN INCHES
SCALE NTS
APPROVED BY
TOLERANCES +/- 0.01"
DRAWN BY DLY
DATE : Jan 12 1994
REVISED : Jan 12/94
DRAWING NUMBER A4.2
UNIVERSITY RESEARCH LAB - MGH

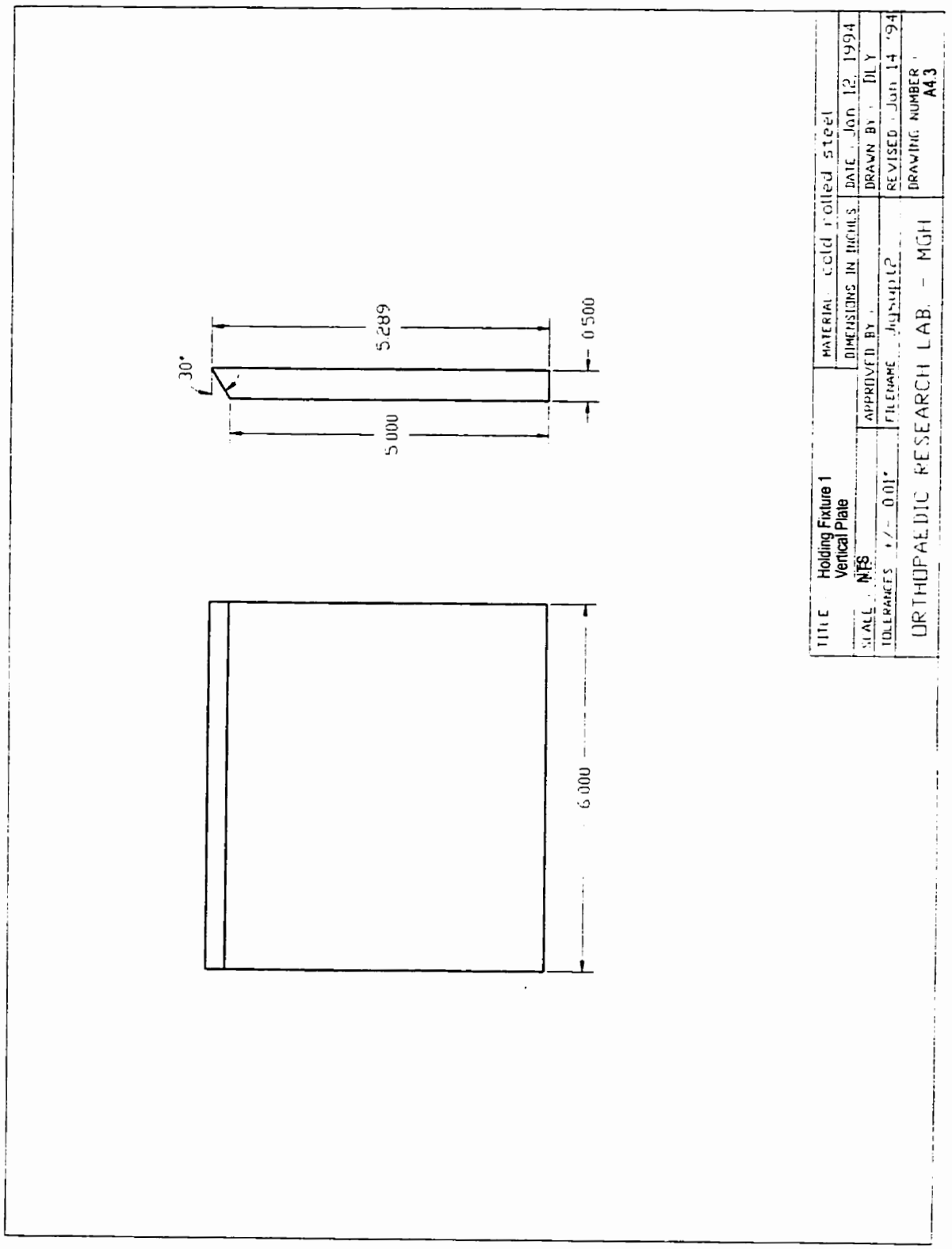
30°
5.289
0.500
5.000
6.000
TITLE: Holding Fixture 1
Vertical Plate
SCALE: NTS
TOLERANCES: +/- 0.01"
MATERIAL: cold rolled steel
DIMENSIONS IN INCHES
APPROVED BY:
FILENAME: fixture2
DATE: Jan 12, 1994
DRAWN BY: DLY
REVISED: Jan 14 '94
DRAWING NUMBER: A43
ORTHOPAEDIC RESEARCH LAB. - MGH

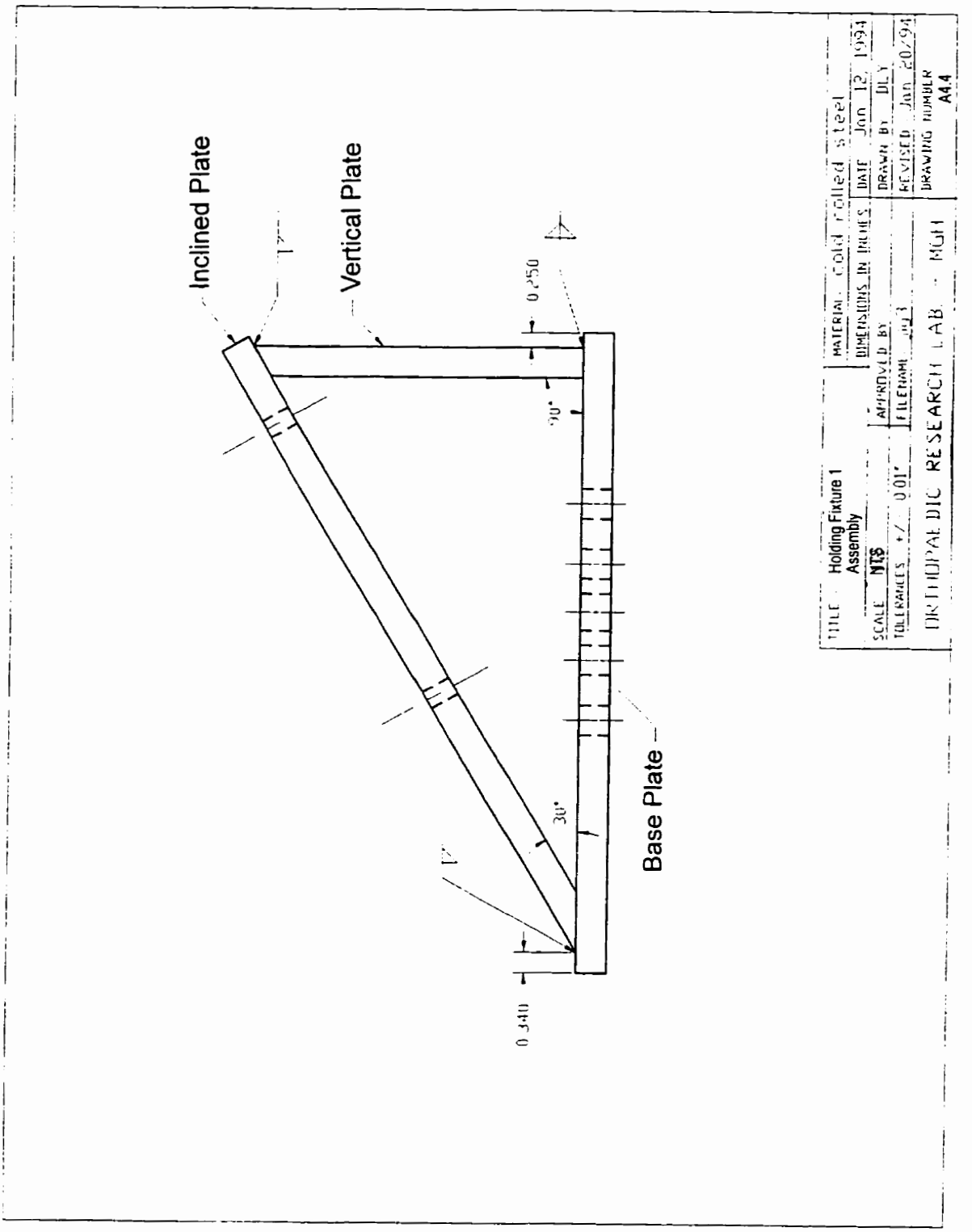
Inclined Plate
Vertical Plate
Base Plate
0.250
90°
30°
0.340
TITLE Holding Fixture 1 Assembly
MATERIAL Cold rolled steel
DIMENSIONS IN INCHES
DATE Jan 12, 1994
SCALE NTS
APPROVED BY
DRAWN BY DLY
TOLERANCES +/- 0.01"
FILENAME
REVISED Jan 20/94
DRAWING NUMBER A4.4
DR THEOPHILUS RESEARCH LAB - MGH

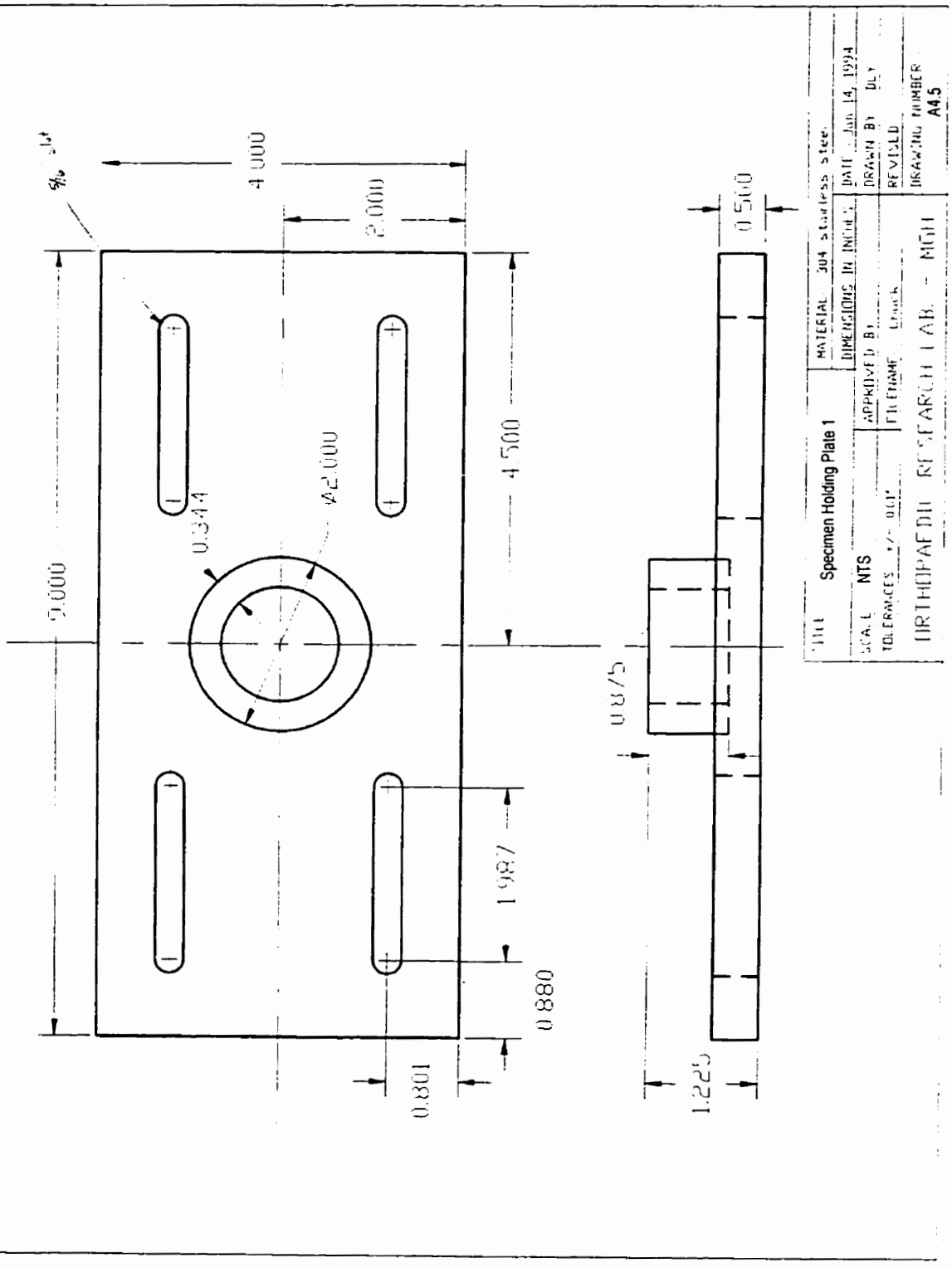
4.000
2.000
5.000
4.500
0.344
Ø2.000
0.880
1.987
0.801
0.875
1.225
0.500
Specimen Holding Plate 1
MATERIAL 304 stainless steel
DIMENSIONS IN INCHES
DATE Jan 14, 1994
SCALE NTS
DRAWN BY DLY
REVISED
DRAWING NUMBER
A4.5

APPENDIX 5

DRAWINGS

A5.1 Holding fixture 2 - base

A5.2 Specimen holding plate 2 - base plate

A5.3 Specimen holding plate 2 - receptacle

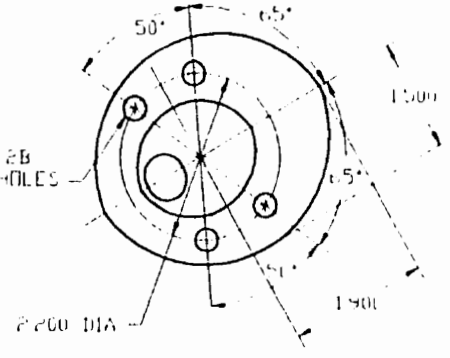

VIEW B B

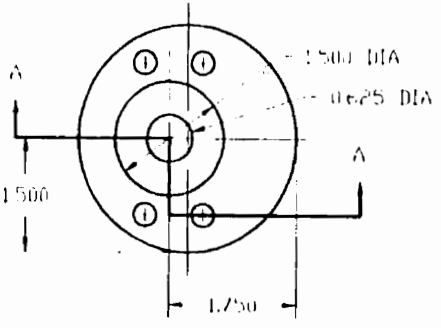

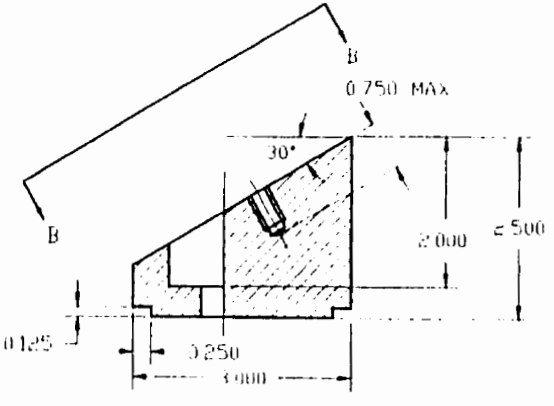

SECTION A A

TITLE: Holding Fixture 2 Base		MATERIAL: Aluminum	
		DIMENSIONS IN INCHES	DATE: Aug 21 1994
SCALE: NTS		APPROVED BY:	DRAWN BY: Dr. Young
TOLERANCES: +/- .005"		FILENAME: jig2a	REVISED: Aug 15 1994
ORTHOPAEDIC RESEARCH LAB - MGH			DRAWING NUMBER: A5 1

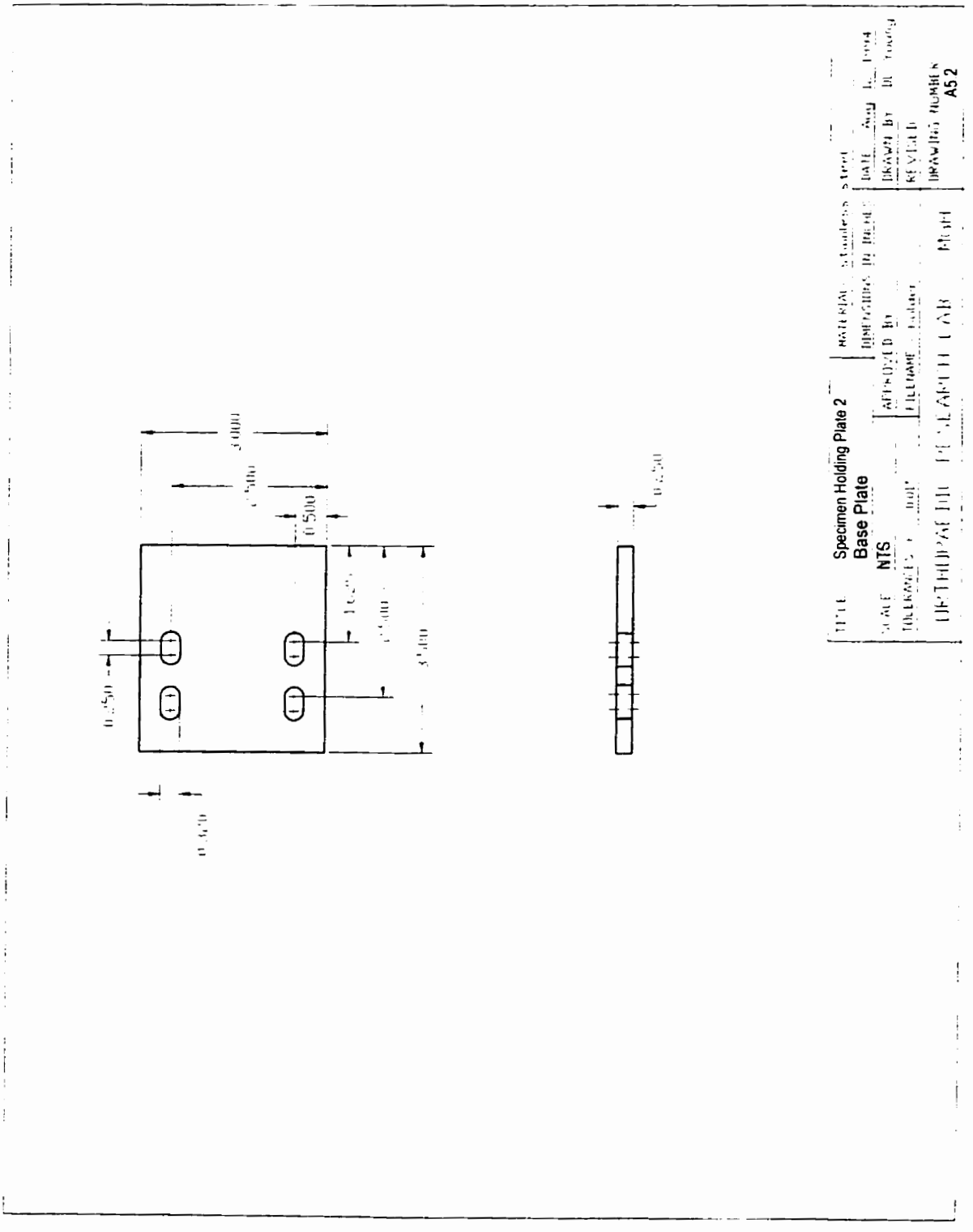
Specimen Holding Plate 2
Base Plate
NTS
A52

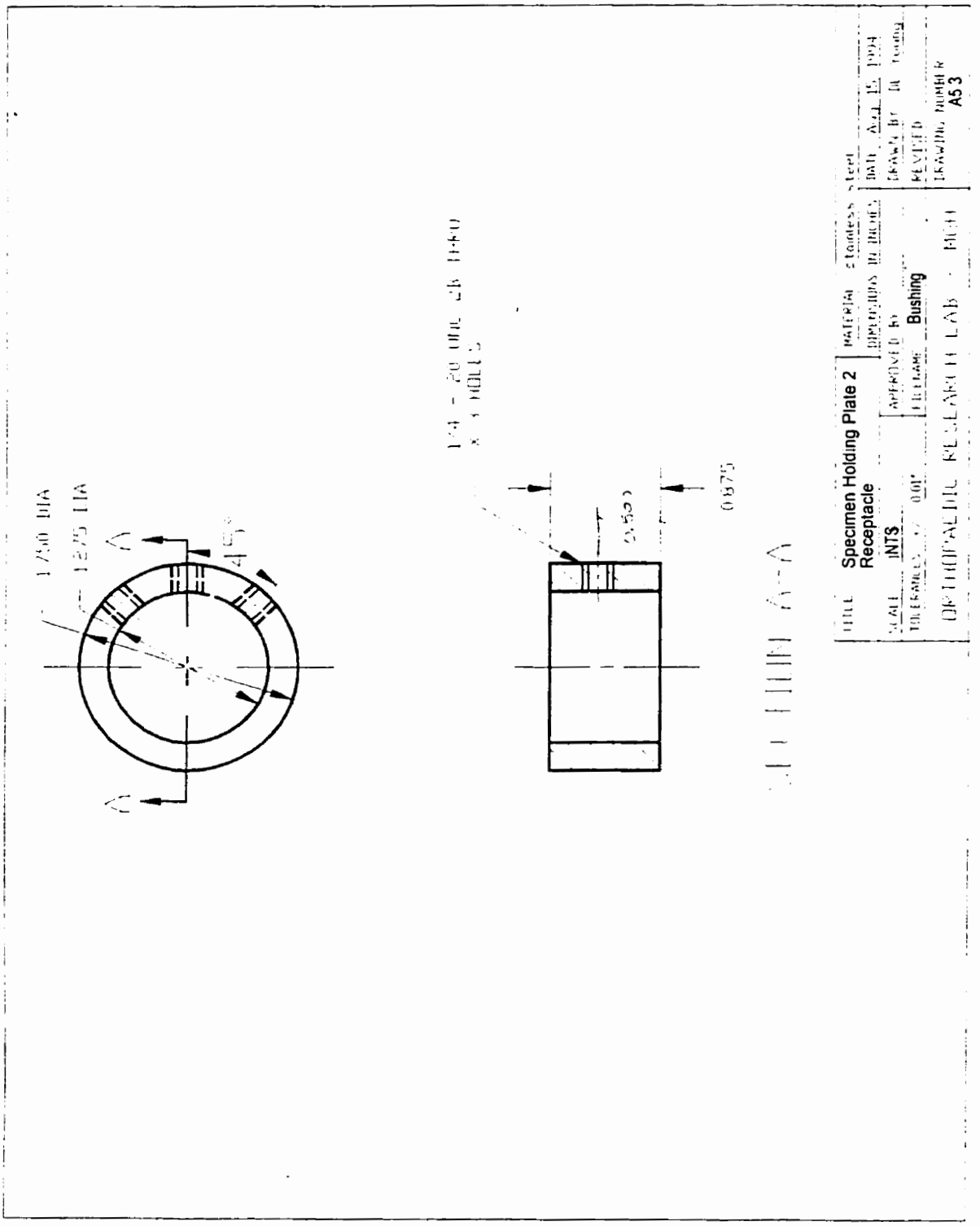
Specimen Holding Plate 2
Receptacle
iNTS
Bushing
A53

APPENDIX 6

DRAWINGS

A6.1 Fluid chamber 1 - container wall

A6.2 Fluid chamber 1 - base

A6.3 Fluid chamber 1 - lid

A6.4 Fluid chamber 1 - assembly

A6.5 Fluid chamber 2

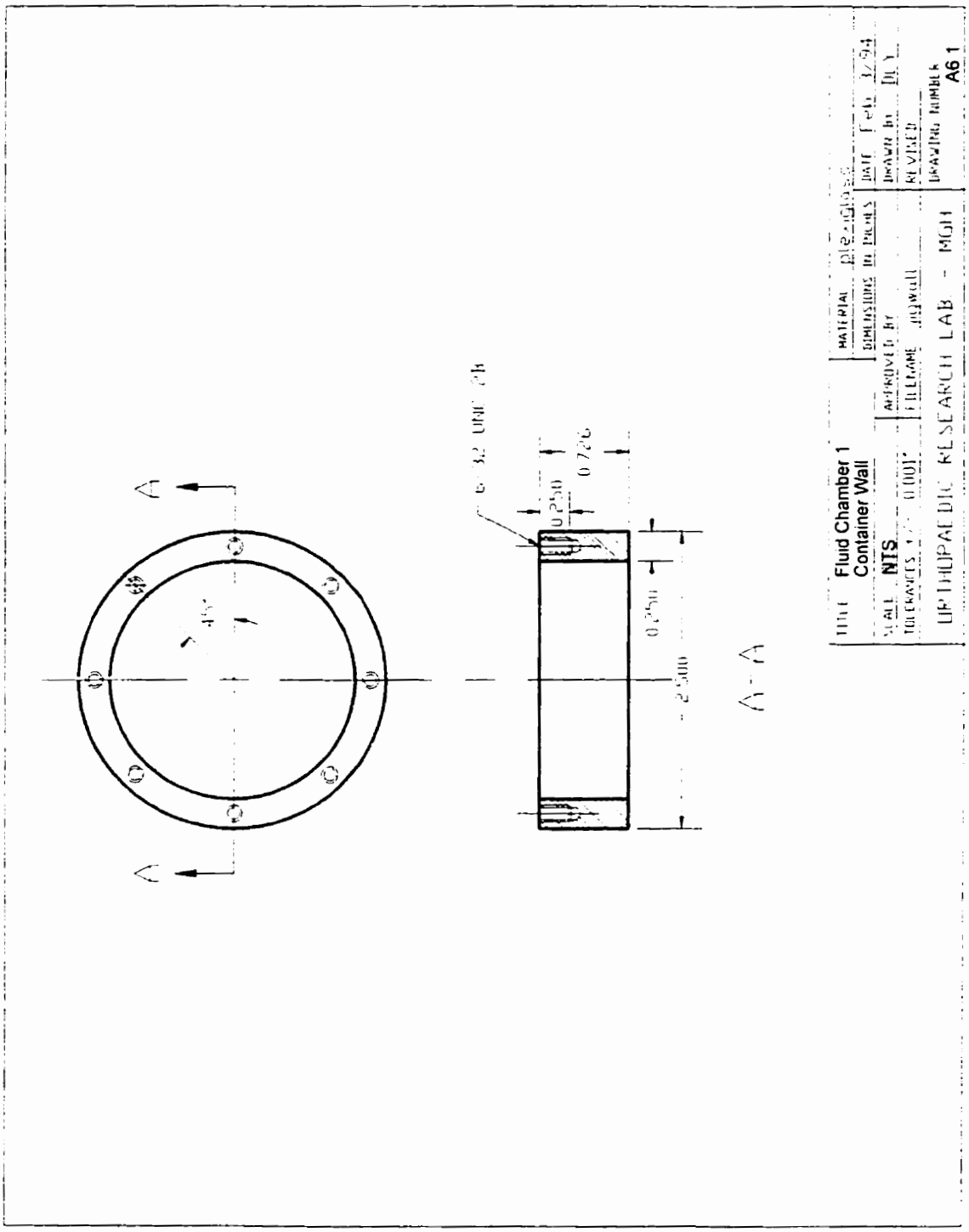
A
A
A - A
0.250
0.726
2.500
Fluid Chamber 1
Container Wall
NTS
UNIVERSITY OF CALGARY RESEARCH LAB - MGH
A6 1

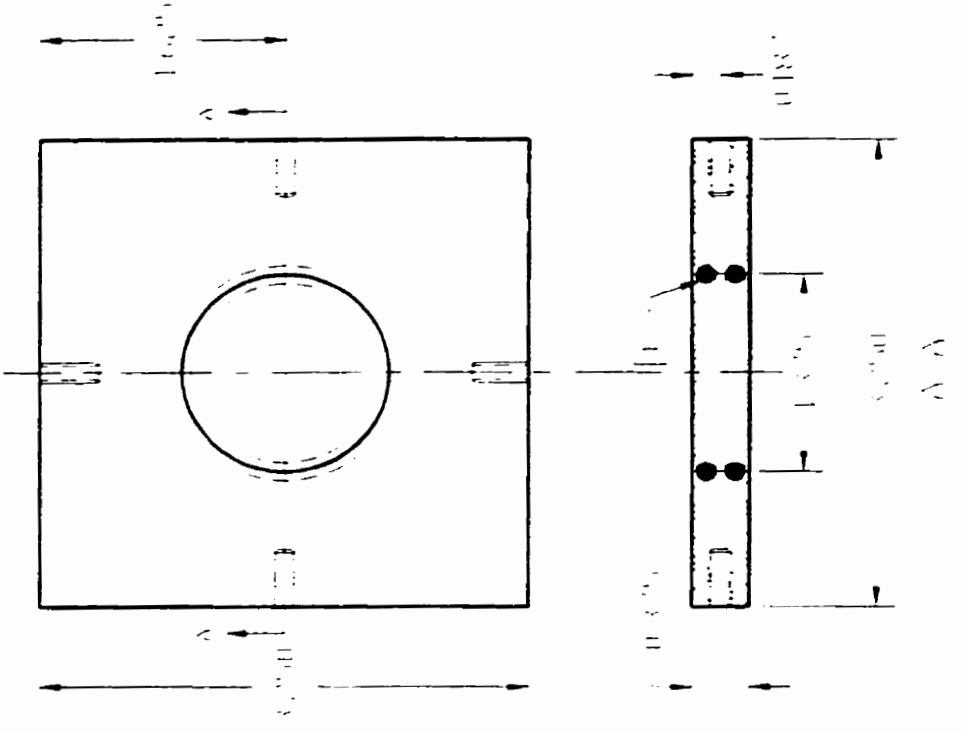

Fluid Chamber 1
Base
NTS
A6.2

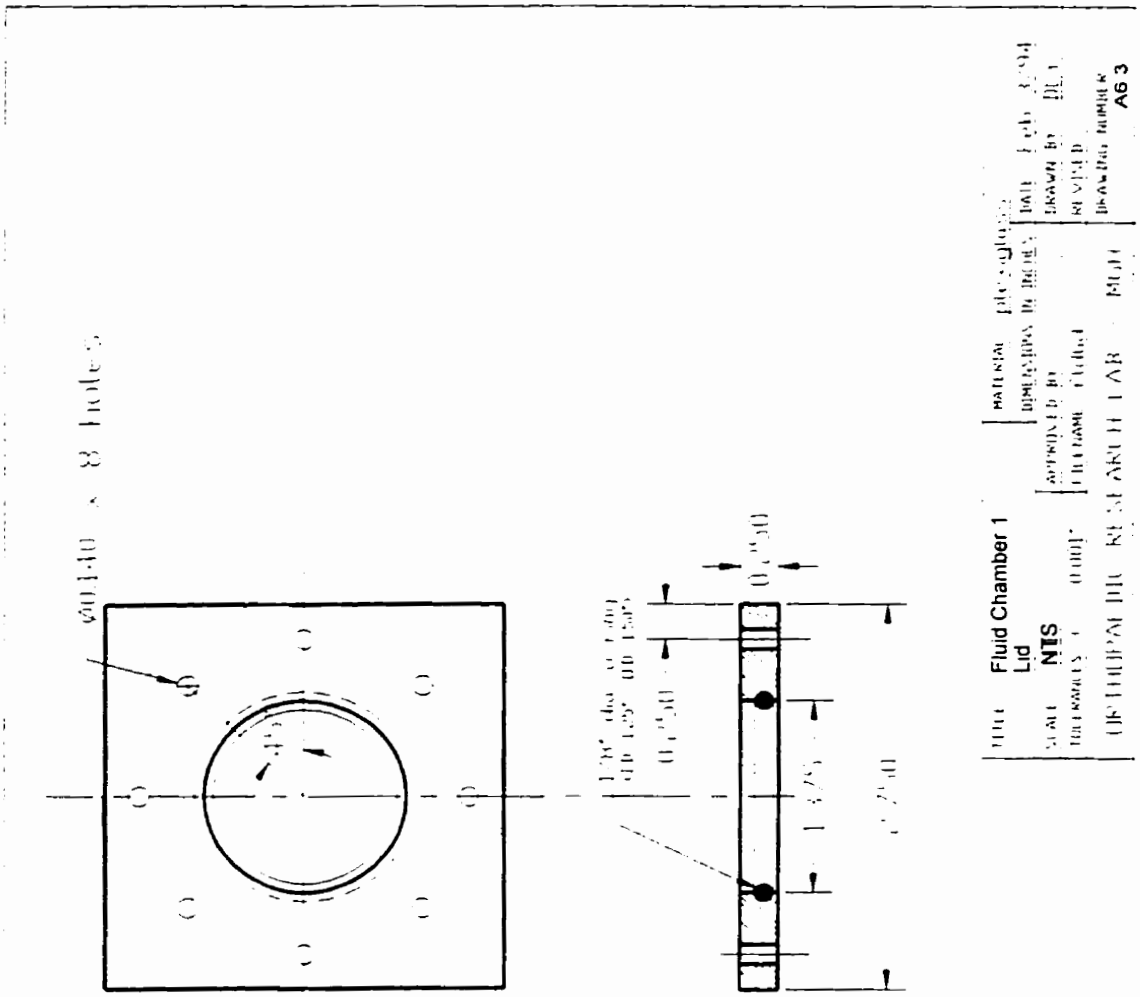
Fluid Chamber 1
Lid
NTS
A6 3

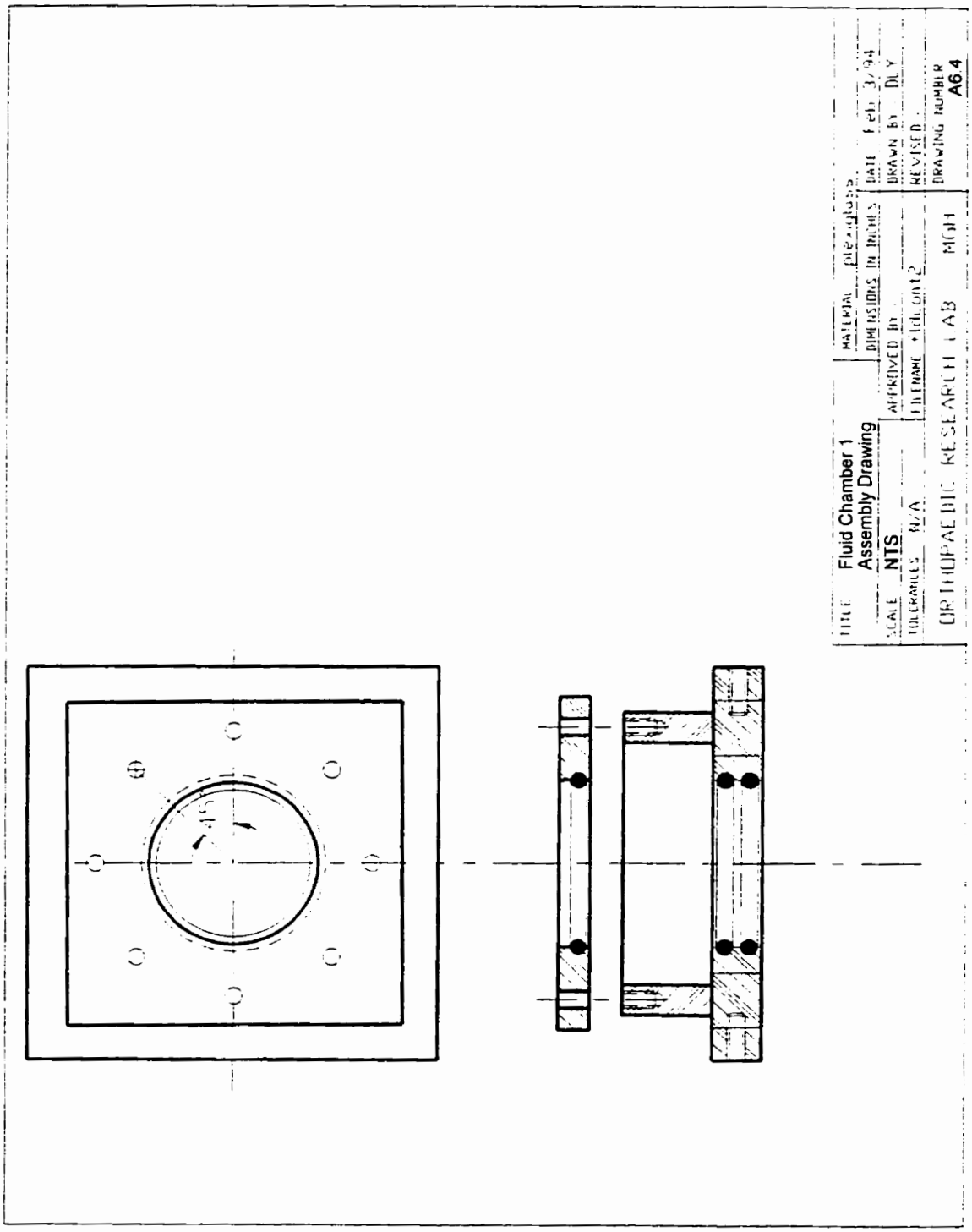
Fluid Chamber 1
Assembly Drawing
SCALE NTS
TOLERANCES N/A
MATERIAL
DIMENSIONS IN INCHES
APPROVED BY
FILENAME
DATE Feb 3/94
DRAWN BY DLY
REVISED
DRAWING NUMBER
A64
ORTHOPAEDIC RESEARCH LAB MGH

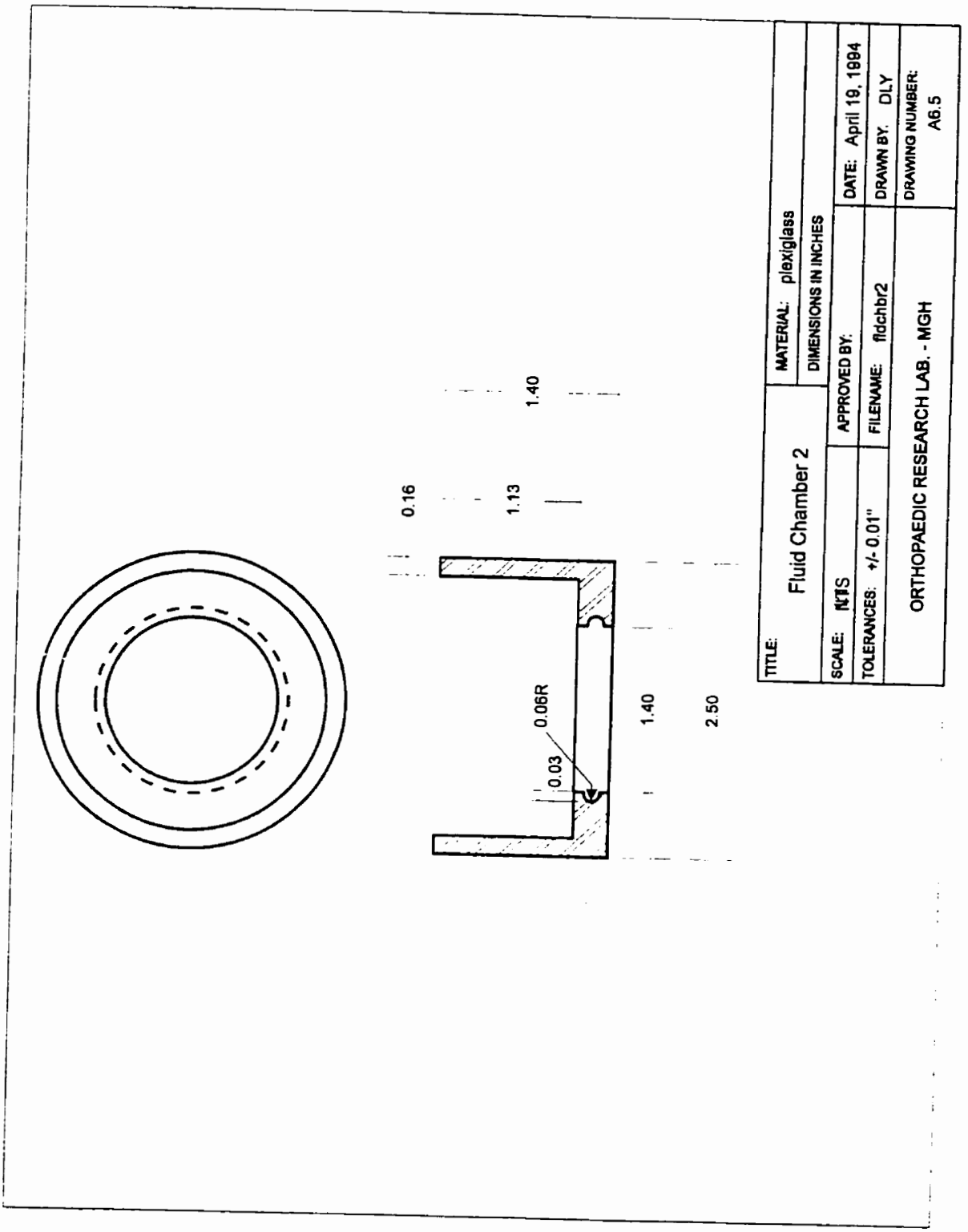
0.16
1.13
1.40
0.06R
0.03
1.40
2.50
TITLE:
Fluid Chamber 2
MATERIAL: plexiglass
DIMENSIONS IN INCHES
SCALE: NTS
APPROVED BY:
DATE: April 19, 1984
TOLERANCES: +/- 0.01"
FILENAME: fldchbr2
DRAWN BY: DLY
ORTHOPAEDIC RESEARCH LAB. - MGH
DRAWING NUMBER:
A6.5

APPENDIX 7

MATLAB Programs and User Defined Functions

MAIN.M
DATARRAY.M
PKVALLEY.M
PRETST.M
WEAR.M

Program: MAIN.M

```
% This program, through the use of user defined functions,
% formats an ascii file of data (representing a surface profile) into
% a single array (function 'datarray'), determines the peak-to-
% valley measurements for each machining mark in the profile
% (function 'pkvalley'), and calculates the mean and the standard
% deviation of these peak-to-valley measurements.

% Load profilometric data for specimen

load c:\profdata\spec11b.txt;

% Format the data into a single array for analysis and plotting.
% Save data in an ascii file and plot the profile.

[data11b]=datarray(spec11b);

save c:\profdata\data11b -ascii

figure(1)
plot(data11b)
xlabel('data points')
ylabel('profile height (angstroms)')
title('PROFILE FROM SPEC11b')
print

% Determine the peak to valley measure for each machining
% mark (one cycle of data) and plot each height value.

[pv11b]=pkvalley(data11b);

figure(2)
plot(pv11b);
ylabel('peak to valley measure (angstroms)');
xlabel('cycle number')
title('PEAK TO VALLEY MEASURES FROM SPEC11b')
grid
print

% Determine the mean peak height measure and the standard
% deviation.

mn11b=mean(pv11b)
sd11b=std(pv11b)

save spec11bvar
```

User defined function: DATARRAY.M

```
% This function takes the data points from the
% ascii data file generated from the profilometer
% and rearranges them into a single array so that
% they can be plotted and analysed.


function[datas]=datarray(specdata);

% Determine the number of rows in the data file
% (the first entry in variable 's' below).

s=size(specdata);

% Generate one long data array (variable 'data') by adding subsequent
% rows onto the previous row.

data=specdata(1,:);
for m=2:s(1);
   data=[data,specdata(m,:)];
end

% Shift data so that the profile is centered about a zero mean.

shft=(max(data)+min(data))/2;
datas=data-shft;
```

User defined function: PKVALLEY.M

```
% This function determines where the profile crosses the
% reference axis in order to define each machining mark.
% Reference crossings caused by small perturbations in
% the profile are identified. The peak-to-valley measurements
% for each machining mark, defined as one cycle of data
% in the profile, are determined from the maximum
% and minimum values of each cycle.

function[pv]=pkvalley(data);

% One machining mark is defined as one cycle in the profile
% data, identified by determining where the profile crosses
% the reference axis. By multiply adjacent entries in the data
% array, a negative product indicates an axis crossing.

for n=1:(length(data)-1);
    c(n)=data(n)*data(n+1);
end

% Find the axis crossings (negative entries) and enter the indices
% in the variable 'crosss'.

crosss=find(c<=0);
sze=size(crosss);

% Check if each reference crossing is a true crossing or
% if it is just a small perturbation in the
% profile. If it is a small perturbation the
% difference between indices is less than 10
% for a 1000 data point scan (arbitrarily chosen based
% on fact that there should be approximately
% 20-30 data points for each half cycle) or less
% than 65 for a 4000 data point scan (based on half cycle
% of approximately 100-150 points). The indices of true
% reference crossings are entered into the variable
% 'cross', and crossings caused by perturbations are given
% an entry value of 0.

for m=1:sze(2)-1;
 if max(size(data))==1000;
  if (crosss(m+1)-crosss(m))<10;
    cross(m)=0;
  else
    cross(m)=crosss(m+1);
  end
```

```
elseif max(size(data))==4000;
  if (crosss(m+1)-crosss(m))<65;
    cross(m)=0;
  else
    cross(m)=crosss(m+1);
  end
 end
end

% The above routine eliminates the first entry in the
% variable "crosss", therefore it is added here.

cross=[crosss(1),cross];

% The following assigns all the zero indices in
% the variable cross so it now contains only
% the true zero crossings.

keep=find(cross~=0);
cross=cross(keep);

% For the purpose of determining the peak-to-valley measurements,
% for consistency each cycle of data defining a machining mark
% always starts with a positive slope.

% Determine if the initial slope in the data is positive or negative.

slp=data((cross(1))+10)-data(cross(1));

% Determine if the last cycle of data is complete (even number
% of zero crossings) or incomplete (odd number of zero
% crossings). For each completely defined machining mark
% (one complete cycle of data) find the maximum (variable 'd')
% and minimum (variable 'e') values.

sz=size(cross);
num_cross=sz(2);
rmdr=rem(num_cross,2);

if rmdr==0;
  if slp>0;
    for m=1:((num_cross-2)/2);
      d(m)=max(data(cross(2*m-1):cross(2*m+1)));
   e(m)=min(data(cross(2*m-1):cross(2*m+1)));
    end
  elseif slp<0;
    for m=1:(num_cross/2-1);
      d(m)=max(data(cross(2*m):cross(2*m+2)));
   e(m)=min(data(cross(2*m):cross(2*m+2)));
    end
```

```
   end
elseif rmdr~=0;
   if slp>0;
    for m=1:((num_cross-1)/2);
      d(m)=max(data(cross(2*m-1):cross(2*m+1)));
    e(m)=min(data(cross(2*m-1):cross(2*m+1)));
    end
   elseif slp<0;
    for m=1:((num_cross-1)/2-1);
      d(m)=max(data(cross(2*m):cross(2*m+2)));
    e(m)=min(data(cross(2*m):cross(2*m+2)));
    end
   end
end

% Determine the peak-to-valley measure of each machining
% mark by subtracting the minimum and maximum value for
% each cycle.

pv=d-e;
```

Program: PRETST.M

```
% This program calculates the mean and standard deviation
% of the peak-to-valley measurements of the non-contact profiles
% (which are all in one single array 'pretst#'). The three
% variables pretst#, mnpre#, and stdpre# are saved in the matlab
% file 'pre#.mat' to be used when calculating the percent wear
% of the contact profiles (using program 'wear.m').

% Determine the mean and standard deviation of the peak-to-valley
% measurements.

mnpre22=mean(pretst22);
stdpre22=std(pretst22);

save pre22.mat pretst22 mnpre22 stdpre22;

% Create variables containing the mean, the mean plus one standard
% deviation, and the mean minus one standard deviation. All variables
% are of the same size as 'pretst#' so they can be superimposed
% on a plot of peak-to-valley measurements of the non-contact profiles.

mean22=ones(size(pretst22));
mean22=mean22*mnpre22;
plustd22=mean22+stdpre22;
minusstd22=mean22-stdpre22;

plot(pretst22);
hold on
plot(mean22, '-')
plot(plustd22, ' ');
plot(minusstd22, '.');
title('PRETEST PEAK-VALLEY MEASUREMENTS FOR SPECIMEN 22')
xlabel('data points')
ylabel('pretest peak-valley measurements (angstroms)')
print
```

Program: WEAR.M

```
% This program determines the percent
% wear of each machining mark in the contact profiles.

% Determine the percentage of wear based on
% the following formula

%    mean non-contact peak height  - worn peak height
%    ------------------------------------------------------ X 100
%                mean non-contact peak height
wear_pv23g=(mnpre23-pv23g)*100/mnpre23;

% Plot the percentage of wear for each peak in the
% contact profile.

plot(wear_pv23g)
xlabel('data point')
ylabel('percent wear (%)')
title('PERCENT WEAR FOR EACH PEAK FROM SPEC23g')
grid
print
```

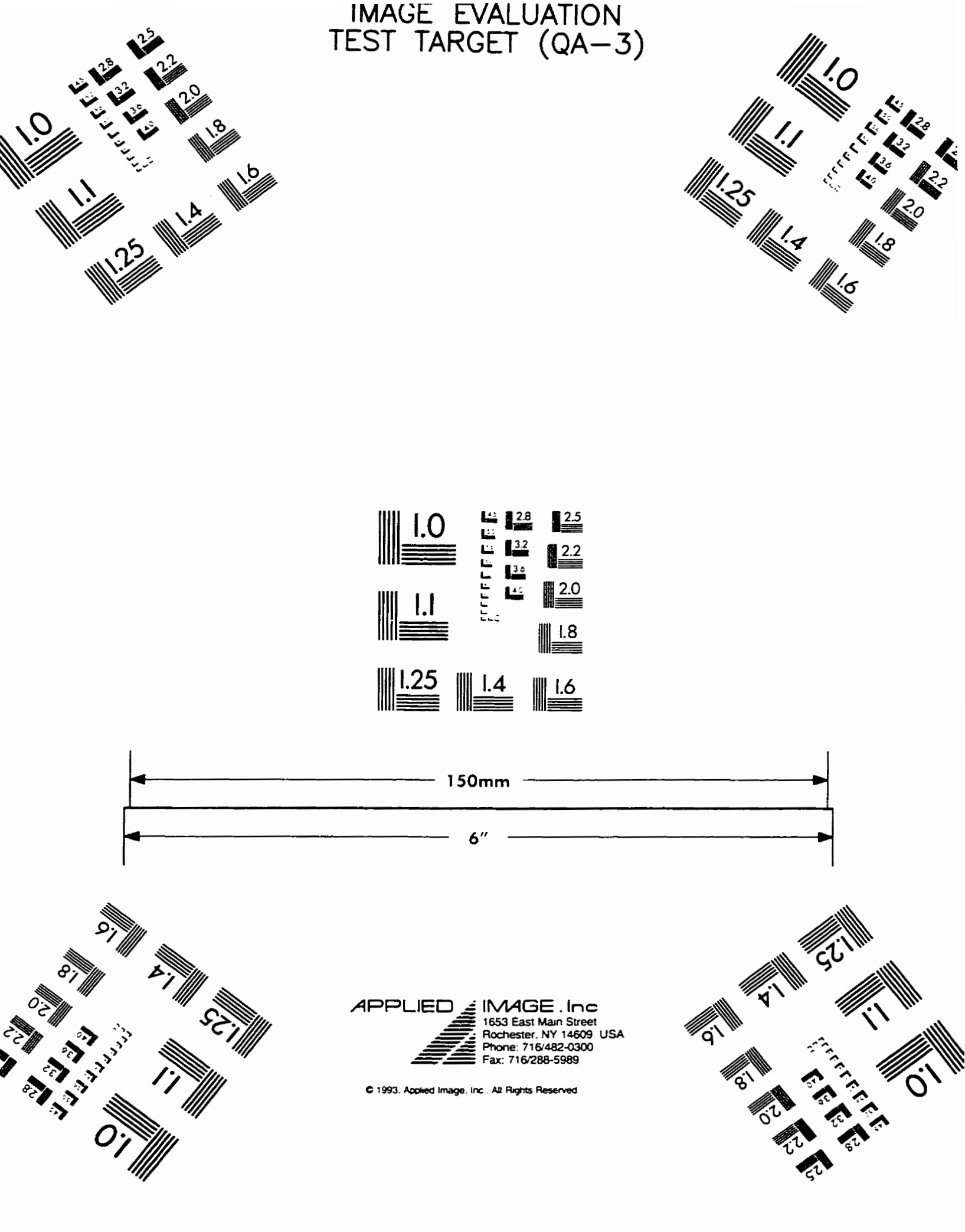
IMAGE EVALUATION
TEST TARGET (QA-3)
1.0
1.1
1.25
1.4
1.6
1.8
2.0
2.2
2.5
2.8
3.2
3.6
4.0
150mm
6"
APPLIED IMAGE, Inc
1653 East Main Street
Rochester, NY 14609 USA
Phone: 716/482-0300
Fax: 716/288-5989
© 1993, Applied Image, Inc., All Rights Reserved